Novel Poly(propylene thiophenoimine)-co-Poly(ethylenedioxythiophene) Composites of Naphthalene Diimide for Applications in Organic Photovoltaic Cells

By

Anne Lutgarde Djoumessi Yonkeu

(BSc Honours, ***Cum Laude***)

A thesis submitted in partial fulfilment of the requirements for the degree of
Magister Scientiae in Nanoscience
Faculty of Science
University of the Western Cape
Cape Town / South Africa

Supervisor: Prof. Emmanuel I. Iwuoha

November, 2013

ABSTRACT

Solar energy generation arises as a result of direct conversion of sunlight into electricity a by solar cell; which is mainly made up of a semiconducting material incorporated into a system. It is emerging as one of the most reliable and cost efficient renewable energy sources. Within the solar field, organic bulk heterojunction photovoltaic cells have proved of being able to have a great impact in the future years; mainly due to the easy processability of the active layer and substrate, their cost effectiveness and above all, a good power conversion efficiency associated to the close 3-dimensional interpenetrating network that is generated from blending donor and acceptor semiconducting materials together in a bulk heterojunction active layer. In this research work, we therefore report on the study of a newly developed organic bulk heterojunction active layer based on a blend of a star-copolymer generation 1 poly(propylenethiophenoimine)-co-poly(ethylenedioxythiophene) (G1PPT-co-PEDOT) as donor material with N,N-diisopropylnaphthalene diimide (NDI) as acceptor material. Both materials were chemically synthesized. The synthesis of G1PPT-co-PEDOT started first by the functionalization of generation 1 poly(propyleneimine) tetramine, G1PPI into G1PPT by condensation reaction in the presence of 2-thiophene carboxaldehyde under Nitrogen gas followed by the copolymerization of G1PPT with ethylene dioxythiophene (EDOT) monomer in the presence of ammonium persulfate, $(NH_4)_2S_2O_8$ as oxidant. On the other hand, NDI was also synthesized via condensation reaction of 1,4,5,8-naphthalene tetracarboxylic dianhydride in the presence of two (2) equivalences of N,N-diisopropylamine at 110 ^{o}C overnight in DMF. Both materials were characterized using FT-IR, UV-Vis spectroscopy, Fluorescence spectroscopy, Voltammetry, HRSEM microscopy and XRD. Based on the cyclic voltammetry and UV-Vis results, we were able to calculate the HOMO, LUMO and band gap energy (E_g) values of both the donor and acceptor to be -4.03 eV, -6.287 eV and 2.25 eV for the donor G1PPT-co-PEDOT respectively and -4.302 eV, -7.572 eV and 3.27 eV for the acceptor respectively. From these results, the energy diagram for both donor and acceptor was drawn and it comes out that the separation between the HOMO of the donor and the LUMO of the acceptor ΔE_g = 1.985 eV, the ideal value for a good donor-acceptor combination. Also the offset energy that is, the energy difference between the LUMO of the donor and the LUMO of the acceptor is 0.302 eV.

KEYS WORDS

- Solar energy
- Organic Photovoltaics
- Bulk heterojunction cell.
- Star copolymer
- G1PPT-co-PEDOT
- Naphthalene diimide
- HOMO
- LUMO
- Energy band gap, E_g

DECLARATION

I, hereby declare that "**Novel Poly(propylenethiophenoimine)-co-poly(ethylenedioxythiophene) Composites of Naphthalene Diimide for Applications in Organic Photovoltaic Cells**" is my own work; that it has not been previously submitted for any degree or examination in any other university or higher education; and that all the sources and quotations have been indicated and acknowledged by complete references

Anne Lutgarde Djoumessi Yonkeu

Signed: ____________ Date:

DEDICATION

I dedicate this work to God, my Lord and Saviour and to my parents in Cameroon.

ACKNOWLEDGMENTS

To God the Almighty be the Glory for He showed me Love and He gave me His peace, strength and courage during the course of these past two years.

I will like to acknowledge my parents, Mr Binjamen Djoumessi and Mrs Melanie Tchounke Djoumessi for their unconditional love and support. They have been role models and source of inspiration all my life. This is just the result of their hardwork and perseverance.

To my brothers and sisters, B.G. Djoumessi, A.G. Ngatat, M.D. Djoumessi, D.D. Djoumessi; my uncles and aunties, J-B. and R. Donguitsop, H. Dongmo, H. Ndonguissop, J. Takougang, C. Bideu Essindi, C. Tchounkeu; my grandmother, Anne Yonkeu and particularly to my elder sister Clark Vanessa Djoumessi, I say a big thank you for your love, support, care and perpetual encouragement.

To my beloved Dr B. Hollong, Estelle Tshouongang, Nina Afonge Ngwah, Gertrude Fomo, Olivier Ngadjou, Judith Donang, Carole Kodjou, Sandrine Kuimo, your love, care and support led me through. Thank you.

To all my SensorLab colleagues particularly Dr Abdul, Dr Chinwe, Dr Tesfaye, Sara Hamid, G. Mbambisa and all my Nanoscience friends, your help was always a blessing for me and I will like you to receive my gratitude.

To all the Chemistry Department, especially to Prof. F. Ameer, Prof P. Baker and Mrs W. Jackson, I expand my gratitude.

I will also like to acknowledge the Department of Science and Technology for funding this project and the National Nanotechnology Teaching and Training Platform, especially V. Jamalie and C. Abrahams for being there to make things go smooth for us.

At last and not least, my greatest acknowledgement goes to my supervisor Prof. E. Iwuoha; first, for the opportunity he gave me to be part of his research group but mostly for his great guidance not only as a mentor and supervisor but as an elder, parent and father.

TABLE OF CONTENTS

LIST OF ABBREVIATIONS

BHJ: Bulk Heterojunction

CdTe: Cadmium Telluride

c-Si: crystalline Silicon

$CuInGaSe_2$: Copper Indium Gallium selenide

CV: Cyclic Voltammetry

DCM: Dichloromethane

DMF: N, N-dimethylformamide

DMSO: N, N-dimethylsulfoxide

DSSC: Dye-sensitized solar cell

EDOT: Ethylene dioxythiophene

EDX: Energy Dispersive Spectroscopy

FT-IR: Fourrier Transform Infrared

G1PPI: Generation 1 poly(propyleneimine) tetramine

G1PPT: Generation 1 poly(propylenethiophenoimine)

G1PPT-co-PEDOT: Generation 1 poly(propylenethiophenoimine)-co-poly(ethylenedioxythiophene)

HOMO: Highest Occupied Molecular Orbital

HRSEM: High Resolution Scanning Electron microscopy

ITO: Indium Tin Oxide

LUMO: lowest Unoccupied Molecular Orbital

NDI: N, N-diisopropylnaphthalene diimide

NTCDA: 1,4,5,8-naphthalene tetracarboxylic dianhydride

OPV: Organic Photovoltaic

PEDOT: Poly(ethylenedioxythiophene)

SWV: Square Wave Voltammetry

TiO_2: Titanium dioxide

UV-Vis: Ultraviolet-Visible

XRD: X-Ray Diffraction

LIST OF SYMBOLS

A: absorbance

c: speed of light

E_g: energy band gap

E_g^A: acceptor band gap

E_g^D: donor band gap.

E_{ox}: oxidation potential

E_p: peak potential

E_{pa}: anodic peak potential

E_{pc}: cathodic peak potential

E_{red}: reduction potential

h: planck's constant

I_p; peak current

I_{pa}: anodic peak current

I_{pc}: cathodic peak current

ΔE_p: change in potential

λ: wavelength

μ_e: electron mobility.

υ: scan rate

LIST OF FIGURES

LIST OF SCHEMES

LIST OF TABLES

CHAPTER ONE

Introduction

1.1 Fossil fuel depletion and environmental impact

“Fossil fuels” is the generic term used to refer to the group of non-renewable energy sources that are constituted by oil, coal and natural gas. They have been so-called because they are formed from organic remains of prehistoric plants and animals. Over the past centuries, the world energy consumption has been majorly based on these three and has been increasing in an exponential way - considering the increase in the world population. Since fossil fuels are not re-usable, it is expected as a consequence that the world will reach a point at which fossil fuel reserves will have been completely extracted. Indeed, according to a research carried out in 2009 using a specific calculation method, it was shown that the fossil fuel depletion time was 35, 107 and 37 years for oil, coal and gas respectively; therefore showing that oil will be the first depleted and coal will still last about three (3) times more than oil and gas (Shafiee and Topal, 2009). Thus, there is an indisputable need to look for alternative clean, environmental friendly and renewable sources of energy. Over the past decennia, a lot of researches have been done to develop these new energy carriers and it came out that biomass, biofuel, wind energy, hydrothermal power and solar energy could be potential replacements for fossil fuels.

Among all these renewable energy sources, solar energy has attracted much attention; not only due to the fact that it is renewable but mostly due to the continuous availability of sunlight throughout the year and on almost all the surface of earth. Over generations, solar energy has therefore been able to contribute considerably to the decrease in fossil fuel dependency.

1.2 Solar Cells: an evolution from one generation to another

After the discovery of the *Photovoltaic effect* in 1839, it is only in 1954 many decades after that the possibility of practical photovoltaic power became a reality. Indeed, Chapman, Fuller, and Pearson reported the first silicon solar cell (Assender and Barkhouse, 2010). And this first generation of solar cells comprised p-n junctions in crystalline Silicon (c-Si) with a typical conversion efficiency of about 6%. It was reported that the maximum efficiency c-Si could reach at that time was 24%, which could then only be achieved in materials with very high purity (Spanggaard and Krebs, 2004). Silicon material was thus used as the solar cell material of choice due to his advantages such as non-toxicity, abundance and its availability - silicon being the second most abundant element on earth after oxygen. This early technology was prohibitively expensive, but developments during the 1950s and 1960s led to the use of silicon photovoltaic technology in applications ranging from satellites to rooftops. c-Si solar cells till to date are regarded as the most efficient type of solar cells due to its wide absorption spectrum and the high mobility of generating charge carriers (Assender and Barkhouse, 2010). But c-Si solar cells still encounter challenging disadvantages such as the high fabrication cost of large-area c-Si wafers, higher recombination rates which indicate the ease with which photogenerated electrons and holes recombine, and the fact that a significant part of the energy of high-energy photons (with ultraviolet and blue wavelengths) is lost as heat. This therefore led to the need for developing new types of solar cells; and came out the second generation of solar cells which includes thin-film solar cells (based on Si, CdTe, $CuInGaSe_2$ (CIGS), etc.); and the Grätzel cells also called Dye-sensitized solar cells (DSSC) based on the sensitized absorption of nanocrystalline TiO_2 and other nanocrystalline molecules (Hoppe and Sariftcci, 2004; Kerp *et al.*, 1998; Savanjie *et al.*, 1998;). In this second category of solar cells, although the production cost could be reduced and the thin-films can be fabricated on all substrates, including flexible substrates and textiles, the main issue is that their conversion efficiency remains far lower than what could be achieved by silicon cells. This therefore led to the third generation of solar cells: the Organic photovoltaic cells denoted OPVs.

Although conventional materials used for photovoltaics are inorganic, an important effort has been put to develop organic solar cells within the past three decades. The field started by the application of small organic molecules such as pigments (Chamberlain, 1983; Wöhrle, 1991) and since the development of semiconducting polymers, these materials have been incorporated in OPVs resulting in outstanding improvement. Organic semiconductor materials have a great potential of transporting electric current and absorbing light in the ultraviolet – visible (UV-Vis) region of the solar spectrum due to the sp^2-hybridization of their carbon atoms. An important feature which differentiates organic semiconducting materials from their inorganic counterparts is generally the poor (order of magnitude lower) charge-carrier mobility in organic materials (Dimitrakopoulos and Mascaro, 2001) which therefore has a large effect on OPVs' design and efficiency. Nevertheless, the relatively strong absorption coefficients (usually 10^5 cm^{-1}) partly balances the low mobility therefore giving rise to high absorption even with thin devices with dimensions less than 100 nm (Hoppe and Sariftcci, 2004). Another important difference to crystalline, inorganic semiconductors is the relatively small diffusion length of primary photoexcitations (called excitons) in these rather amorphous and disordered organic materials (Peumans *et al*., 2003; Haugeneder *et al*., 1999). These excitons are an important intermediate in the solar energy conversion process, and usually strong electric fields are required to dissociate them into free charge carriers, which are the desired final products for photovoltaic conversion. This is a consequence of exciton binding energies usually exceeding those of inorganic semiconductors (Gregg and Hanna, 2003; Sariftci, 1997). These features of organic semiconducting materials generally lead to devices with very small layer thicknesses of the order 100 nm. Most of the organic semiconductors are hole-conductors and have an optical band gap around 2 eV, which is considerably higher than that of silicon and thus limits the harvesting of the solar spectrum to a great extent. Nevertheless, the chemical flexibility for modifications on organic semiconductors via chemical synthesis methods as well as the perspective of low cost, large-scale production drives the research in this field in academia and industry (Hoppe and Sariftci, 2004). .

Altogether, organic photovoltaic cells have many attractive features, amongst which are:

- The potential to be flexible and semi-transparent,
- Potential to be manufactured in a continuous printing process,
- Large area coating,
- Easy integration in different devices,
- Significant cost reduction compared to traditional solutions,
- Substantial ecological and economic advantages (Brabec, 2004).

1.3 Rationale and Motivation

Organic Photovoltaics (OPVs) are emerging as a promising development of low cost solar energy conversion technologies (Ahmed *et al.*, 2011). Among all the OPV device architectures explored to date, going from single layer to bilayer solar cells and including the Schotcky barrier solar cells, the Bulk Heterojunction (BHJ) cell, with an active layer consisting of a blend of donor polymer and an acceptor material, provides the most efficient example of excitonic solar cells. Indeed, once the photons contained in the solar light are absorbed in the BHJ active layer, strongly bound excitons (Gregg, 2003), instead of free electron-hole pairs as produced in organic materials are generated; an efficient electron donor-acceptor interface with suitable HOMO/LUMO energy level offsets is therefore of first importance for efficient charge photogeneration (Chen *et al.*, 2009). One of the peculiar properties of BHJ devices is their sensitivity to the morphology of the blend. The crystalline ordering for both donor and acceptor along their nanometer length scales was proven to be beneficial to carrier transport and device efficiency (Green *et al.*, 2006; Hoppe and Sariftci, 2006; Yang *et al.*, 2005; Li *et al.*, 2005; Shaheen *et al.*, 2001). Thus the idea to use a star-copolymer which consists of a dendrimer copolymerised to PEDOT.

On the other side, among all the classes of acceptor materials which have been studied, fullerene-based acceptor materials have demonstrated excellent electron-accepting and electron-transporting properties and still dominate in OPV technologies. However, fullerene acceptor material exhibit considerable drawbacks in organic photovoltaic cells: (i) they have negligible light absorption in the visible-near infrared region (Wienk *et al.*, 2003); (ii) they have relatively poor photochemical, photothermal and chemical stability, requiring extensive encapsulation for the use of OPVs in the air (Reese *et al.*, 2010); (iii) Controlling their phase-separation kinetics and their BHJ film morphology faces challenges due to their much higher rates of molecular diffusion and crystallization compared to those of the donor polymer material component (Chen *et al.*, 2009; Thompson and Frechet, 2008); (iv) their accessible photovoltage is limited by the very narrow range in which their accessible LUMO energy levels lies; (v) the available chemistry of the synthesis of fullerenes derivatives is limited (Hummelen *et al*., 1995; Wudl, 1992); (vi) the synthesis and purification cost of fullerenes is very high (Sonar *et al.*, 2011). Considering all the disadvantages encountered with fullerene-based acceptor materials, it is of prior importance to consider other n-type organic semiconductors. Other acceptor materials which have been studied in OPV cells include inorganic nanocrystals (CdSe, PbS, TiO_2, etc.), grapheme sheets, carbon nanotubes, n-type conjugated small molecules and n-type polymer semiconductors. In the latter category of acceptor materials, fall cyano-poly (phenylenevinylene) (CN-PPV), Poly(benzo-bis-imidazobenzophenanthroline) (BBL), Polyfluorene(benzothiadazole) (F8TBT), vinazene derivatives, cyanopentacenes, bifluoronylidenes, diketonepyrrolopyrrole derivatives, perylene diimides and naphthalene diimides among others, which have already been investigated.

In this project, we will therefore focus on using N, N-dialkylnaphthalene diimides considering they constitute an electron-deficient class of six-membered aromatic compound and thus have a high tendency of forming n-type (electron-accepting) semiconductor materials.

1.4 Aim of the study

To fabricate an organic Bulk Heterojunction cell based on a blend of a star-copolymer donor material: generation 1 poly(propylenethiophenoimine)-co-poly(ethylenedioxythiophene) and N, N- diisopropylnaphthalene diimide as the acceptor material and study the photovoltaic properties of the fabricated cell.

1.5 Objectives of the study

The focus of this study lies in preparing an electron donating material based on generation 1 Poly(propylenethiophenoimine)-co-poly(ethylenedioxythiophene), a star copolymer, blending it at different ratio with N, N-diisopropylnaphthalene diimide which constitutes the electron acceptor material and study its applicability towards the conversion of solar energy into electrical current.

To achieve this, the following must be met:

(i) Functionalization of generation 1 Poly(propyleneimine) tetramine (G1PPI) by condensation reaction with 2-thiophene carbaldehyde in methanol under Nitrogen gas to produce generation 1 Poly(propylenethiophenoimine) (G1PPT).

(ii) To characterize G1PPT using FTIR, UV-Vis, Fluorescence, Voltammetry, HRSEM and X-ray Diffraction.

(iii) Chemical copolymerization of EDOT on G1PPT to form G1PPT-co-PEDOT.

(iv) To characterize G1PPT-co-PEDOT using FTIR, UV-Vis spectroscopy, Fluorescence, Voltammetry, HRSEM and X-ray Diffraction.

(v) Synthesis of N, N-diisopropylnaphthalene diimide by condensation reaction of 1;4,5,8-naphthalene tetracarboxylic dianhydride with two (2) equivalences of isopropylamine in N, N-dimethylformaldehyde (DMF).

(vi) To characterize N, N-diisopropylnaphthalene diimide using FTIR, UV-Vis, Fluorescence, Voltammetry, HRSEM and X-Ray Diffraction.

(vii) Blending of G1PPT-co-PEDOT and N, N-diisopropylnaphthalene diimide and investigate the properties of the newly formed material using UV-Vis and Fluorescence.

(viii) Fabrication of the Organic Bulk heterojunction cell and study the photovoltaic properties.

1.6 Thesis Structure

This thesis comprises six (6) chapters and is structured as follows:

Chapter 1 – Introduction

Chapter 1 gives an introduction on the origin of solar energy, starting with the depletion of non-renewable energies and their impact on the environment and thus the need for a new kind of energy sources; and also discusses the evolution in solar cell technologies. The rationale and motivation of this project are also given; as well as the aim and objectives that need to be met.

Chapter 2 - Literature review

Chapter 2 presents a review of the literature, which covers a short review on the *Photovoltaic effect*, presents the general structure of photovoltaic devices as well as the different types of active layer architectures going from single layer cells to Bulk heterojunction cells and finally discusses the application of dendrimers and polymers as donor materials in OPVs and the application of naphthalene diimides as acceptor materials.

Chapter 3 - Experimental

Chapter 3 gives an account of the specific reagents and equipment used in the analysis, before explaining in details the protocols involved in the synthesis, characterization, electrode preparation and electrochemical analysis.

Chapter 4 and 5 - Results and discussion

Chapter 4 and 5 present the results and discussion with relevant references to literature. The main trends of the results are discussed, connecting the results with the literature and any correlation that has emerged in the data are highlighted.

Chapter 6 - Conclusion and Recommendations

Chapter 6 ends this thesis by summarizing the key points, highlights the novelty of the research and, provides conclusions and recommendations as well as future work.

References

This section lists the references that were consulted during this project.

CHAPTER TWO

Literature Review

2.1 The "Photovoltaic Effect"

A French physicist, E. Becquerel in 1839 during an experiment realized that certain materials when immersed in an electrolyte between two metal electrodes were able to generate electrical current when exposed to light (Spanggaard and Krebs, 2004). This discovery will have an important impact in the world. Indeed in 1905, Einstein first used the term "*photoelectric effect*" which established the foundation for a theoretical understanding of the "*photovoltaic effect*" (Kim, 2009). When photons in the UV range are absorbed by a metal surface, due to the excitation energy from the incident light free electrons escape from the metal surface. These electrons are then ejected into the atmosphere. In most cases, when absorbed photons in a material pump ground state electrons to the excited state, the excited electrons promptly relax to the ground state. However, in photovoltaic devices, excited electrons and the produced holes in the ground state are collected separately at the negative and positive electrodes respectively to generate electric power (Kim, 2009), see scheme 2.1 respectively (a) and (b) below.

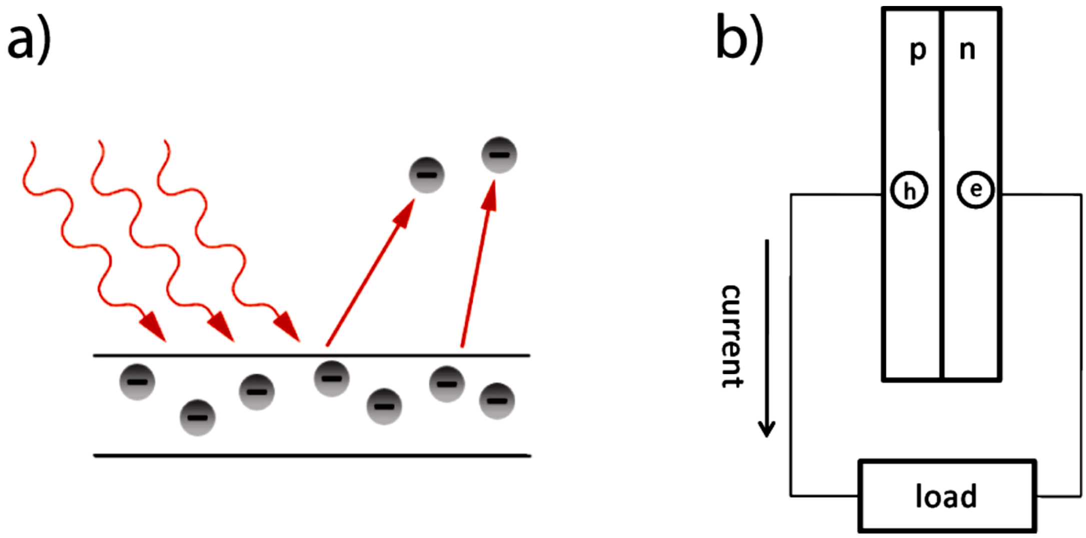

***Scheme 2.1:* *(a)* The photoelectric effect and *(b)* The photovoltaic effect (Kim, 2009)**

The four main steps characterizing the photovoltaic process are summarized in scheme 2.2 below: a) light absorption and excitation, b) exciton formation and diffusion c) exciton dissociation/ separation and d) charges transport and collection (Forrest, 2009).

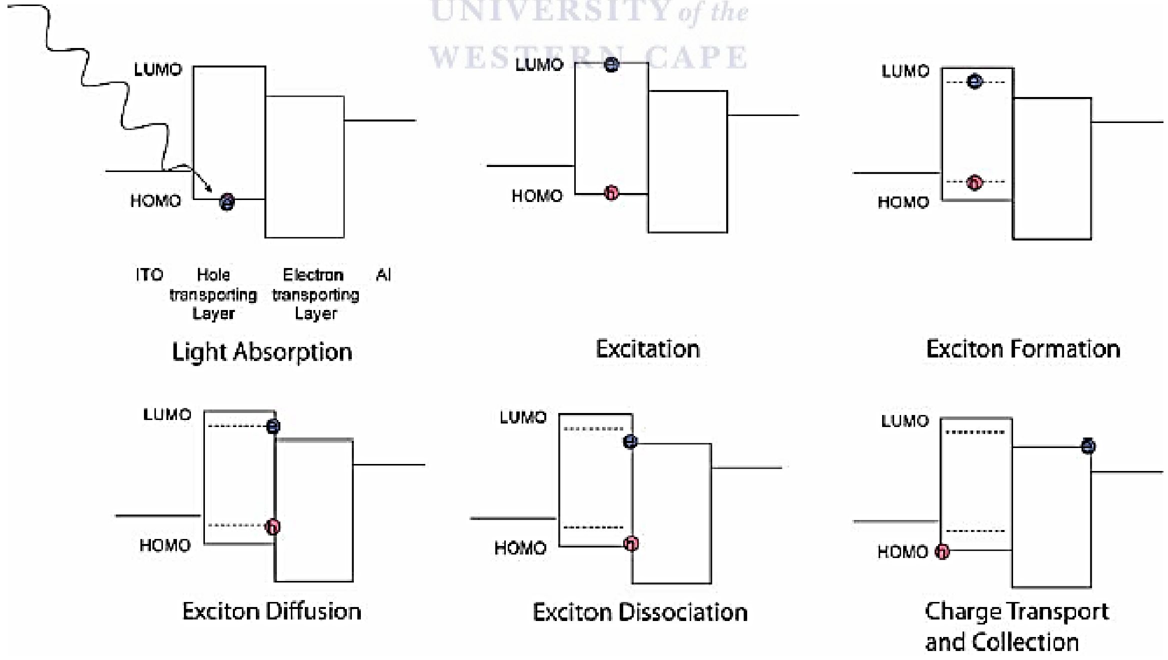

Scheme 2.2: *Steps in the Photovoltaic process (Kim, 2009).*

Light absorption occurs when the material has a semiconducting property that responds to incident waves. When the incident photon hits electrons in the ground state, inorganic semiconductors generate free carriers. However, in organic semiconductors, excited electrons slightly relax and then form an exciton, a bounded electron and hole pair (Knupfer, 2003). The electron-hole pair then diffuses to the interface between the donor and acceptor materials and dissociates into a free electron and a free hole which are then transported and collected at the negative and positive electrodes respectively.

2.2 Organic Photovoltaic Cells

2.2.1 Structure of photovoltaic devices

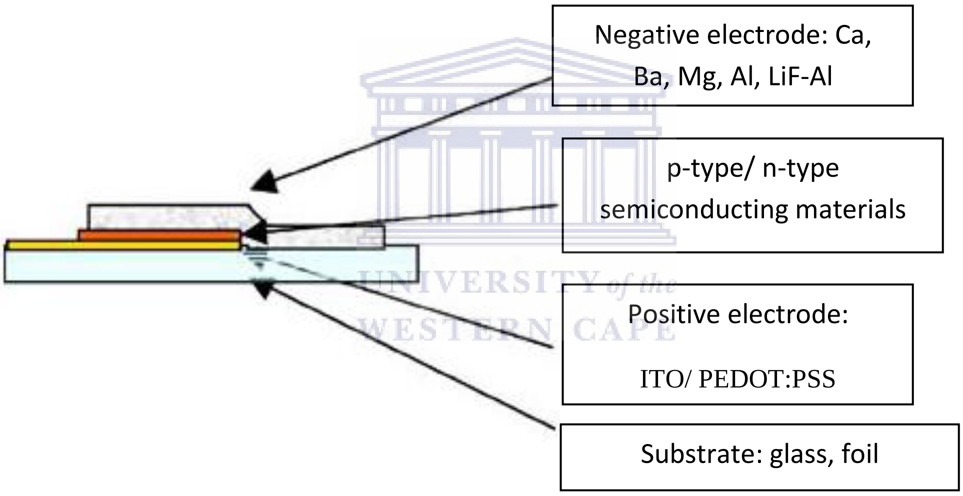

Scheme 2.3: *Structure of an organic photovoltaic cell*

The architecture of organic solar cells is depicted in scheme 2.3 above. Indium-doped tin oxide (ITO) glasses which constitute the positive electrode are typically used as semi-transparent substrates with a transimissivity of B90 % in the visible range and a conductivity of B20O/square. Poly(ethylenedioxythiophene) doped with polystyrene sulphonic acid (PEDOT:PSS) is spin-coated on top of the ITO from a water solution, giving a conductive (typically B103 S cm^{-1}) layer which prevents shorts and allows to increase the shunt resistivity of the thin film devices. The photoactive layer consisting of the donor/acceptor composites again is coated on top of the PEDOT: PSS. The negative electrode, the cathode, typically Ca/Al, Ba/Al or LiF/Al is then thermally deposited through a shadow mask. The geometrical overlap between the positive electrode and the negative electrode defines the active area.

2.2.2 Different types of photovoltaic active layer architectures

2.2.2.1 Single-layer cells

The first reported organic solar cells consisted of a single layer of photoactive material sandwiched between two metallic electrodes of different work functions (Wöhrle and Meissner, 1991; Chamberlain, 1983). These metals were primarily used due to their ability to generate an electric field as well as asymmetric carrier extraction required for a photovoltaic device. Unlike silicon, the higher optical density associated with conjugated polymers means that only approximately 100 nm are required to absorb more light at the polymer's absorption maximum. For a typical work-function difference of 1 eV between the electrodes, a yield of the order of 10^5 V cm^{-1} will be produced. Due to the low dielectric constant typical of most conjugated polymers, the primary photoexcitations are not free electrons and holes but rather bound electron-hole pairs known as excitons (Snaith and Gratzel, 2006). These excitons have a binding energy of a few tenths of electron-volts (eV) and a radius of about 1 nm, thus requiring a field of 10^6 V cm^{-1} to dissociate (Gregg and Hanna, 2003). As a consequence, only very few excitons are separated by thermal fluctuations and most likely recombine before being dissociated. On the other hand, those free electrons and holes move towards opposite electrodes under the influence of the built-in field provided by the contacts. However, the low hole and electron mobilities in conjugated polymers make the transit times to the electrodes long, so that charge transport and collection must compete with recombination. As a result, the separation of the photogenerated charge carriers was so inefficient that single-layer polymer solar cell power conversion efficiency was far less than 1% achievement (Mark *et al.*, 1994).

2.2.2.2 Bilayer cells

In organic bilayer solar cells, a second semiconducting material is added in order to increase the photogenerated excitons separation. The relevance of the added semiconductor lies in the fact that its conduction band (or LUMO) or valence band (or HOMO) differs from that of the polymer by an amount higher than the exciton binding energy in the polymer. The energetic field at the interface between the two semiconductors favours exciton dissociation into an electron in the material with a lower LUMO level i.e. electron acceptor material and a hole in the other material i.e. electron donating material. Adding a second semiconducting material doesn't only improve exciton separation but actually has two significant advantages over single-layer devices; indeed the fact that electrons and holes are localized in different materials after the exciton is separated implies that each material needs to transport only one type of charge, therefore reducing design constraint on the materials. Secondly, since the electrons and holes are already partially separated upon photogeneration, there is therefore a large amount of holes in the donor and electrons in the acceptor, giving rise to a chemical potential that promotes that photovoltaic effect (Assender and Barkhouse, 2010).

The simplest structure of an organic bilayer solar cell appears to be the superposition of a donor and an acceptor material on top of each other as represented in scheme 2.4 below, providing the interface needed to achieve charge transfer. The schematic energy diagram of such an organic bilayer solar cell is also presented in scheme 2.4. The excitons photogenerated in the donor or in the acceptor can diffuse to the interface where they will separate. According to the Onsager theory (Onsager, 1938) that can be evoked as a first approximation in organic semiconductors, photoexcited electrons and holes are coulombically bound by virtue of the low dielectric constant proper to conjugated polymers. Due to the related exciton binding energy, around 0.5 eV which is much higher than the thermal energy, the photoexcitons are not easily dissociated (Yumusak and Egbe, 2011). Once the excitons are generated by absorption of photons by the donor and/or acceptor, they can diffuse over an approximate length of 5-15 nm (Haugeneder *et al.*, 1999). Since the exciton diffusion lengths in conjugated polymers are less than the photon absorption length, the efficiency of a bilayer cell is limited by the numbers of photons that can be absorbed within the effective exciton diffusion range at the polymer/electron interface. Also, there is a poor spectral match because the optical band gap of most conjugated polymers is too high to use the IR regions of the solar spectrum. This drastically limits the photocurrent and hence the overall efficiency of the organic bilayer solar cell (Yumusak and Egbe, 2011).

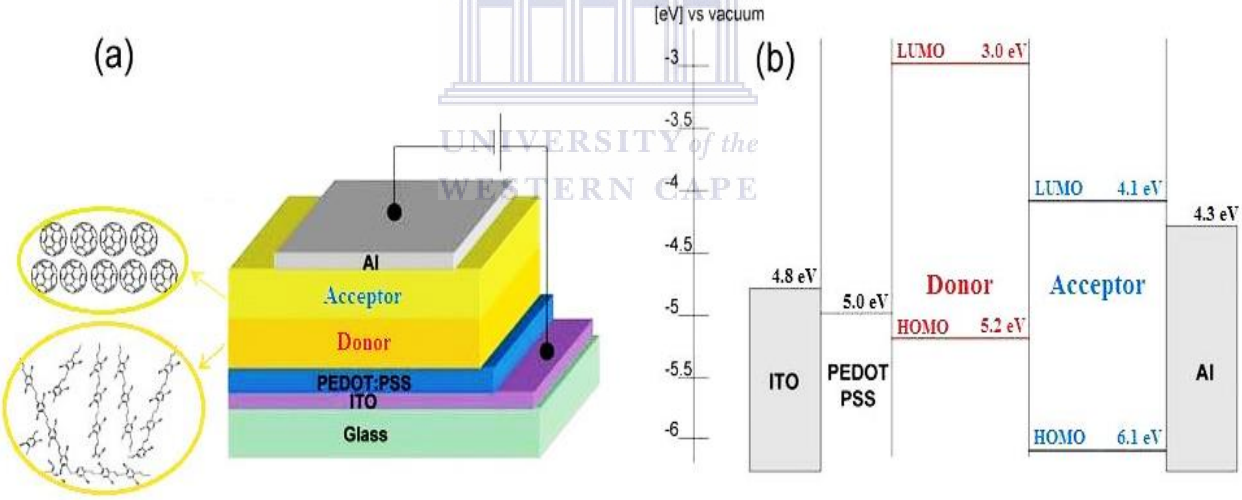

***Scheme 2 4: (a)** Schematic device structure and **(b)** Energy diagram for an organic bilayer solar cell*

(Yumusak and Egbe, 2011)

The first reported organic bilayer solar cell consisted of a light-absorbing copper-phthalocyanine layer combined with an electronegative perylene carboxylic derivative. The exciton dissociation in this bilayer cell was mainly as a result of the difference between the electron affinities of the two materials which generated an energy offset at their interface (Tang, 1986).

2.2.2.3 Bulk Heterojunction layer

The organic bulk heterojunction layer was created to overcome the high diffusion length problem encountered in organic bilayer solar cell. Indeed, here the surface area of the donor/acceptor interface is increased. This has been achieved by creating a mixture of donor and acceptor materials with a nanoscale phase separation resulting in a three-dimensional interpenetrating network: the “bulk heterojunction solar cells” (Assener and Barkhouse, 2010) whose picture is depicted in scheme 2.5 below.

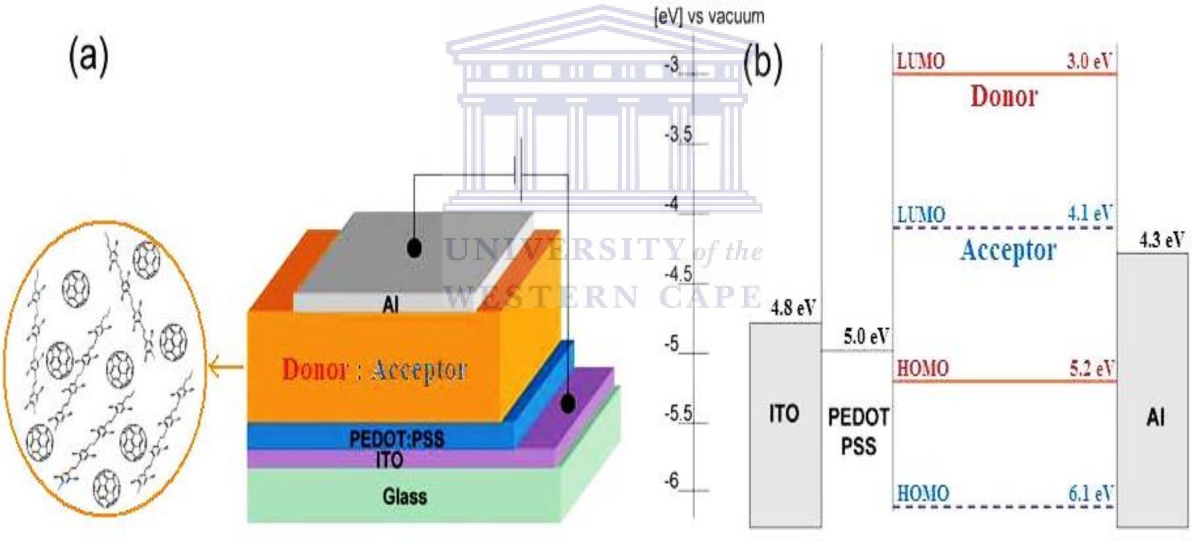

Scheme 2.5: (a) *Schematic device structure and* ***(b)*** *Energy diagram for an organic bulk hetero junction solar cell* (Yumusak and Egbe, 2011)

The first organic bulk heterojunction solar cell was fabricated in 1995 by blending of 1-(3-methoxycarbonyl)propyl-1-phenyl [6] C_{61} (PCBM) a soluble and processable derivative of fullerene C_{60} with poly(2-methoxy-5-(2’-ethyl-hexoxy)-1,4-phenylene-vinylene) (MEH-PPV) (Yu et al., 1998). In 2001, power conversion efficiency for bulk heterojunction organic solar cells of 2.5% was achieved when blending the conjugated polymer poly(2-methoxy-5-(3’,7’-

dimethyl-octyloxy)-p-phenylenevinylene) (MDMO-PPV) with methanofullerene [6,6]-phenyl C_{61}-butyric acid methyl ester (PCBM) (Shabeen *et al.*, 2001). In 2003, Padinger *et al*., presented a further increase in the power conversion efficiency by using a blend, poly(3-hexylthiophene) donor (P3HT) in conjunction with PCBM. It was shown that annealing at a temperature above the glass transition of the polymer enabled an enhancement of the efficiency from 0.4% to 3.5% (Padinger *et al.*, 2003). To allow an increased control of the phase segregation during film formation of a copolymer-fullerene blend, additives were used, enabling efficiency yields of about 6% (Park *et al.*, 2009). Up to 8% power conversion efficiency has also been reported in organic bulk heterojunction solar cells (Green *et al.*, 2010).

Solar cells based on solution-processable organic semiconductors have demonstrated an important performance increase in recent years; and a lot of improvement has been achieved as far as the understanding of the elementary processes for photogeneration is concerned (Gunes et al., 2007; Mozer and Sariftci, 2006; Hoppe and Sariftci, 2004). Indeed Organic BHJ solar cells with almost 100% internal quantum yield were proven, resulting in up to approximately 8 % power conversion efficiency (Green *et al.*, 2010; Park *et al.*, 2009). This device concept showed to be compatible with solution-processing at room temperature, at the instar of high-throughput printing techniques. Processing on flexible substrates is possible, therefore enabling roll-to-roll manufacturing as well as affecting the properties of the finished electronic devices.

2.3 Dendritic molecules and polymers: their applications as donor material in Organic Photovoltaic cells

2.3.1 Properties of polymers and dendrimers

Since the discovery of electrical conductivity in chemically doped polyacetylene, tremendous effort has been put in the modelling, fabrication and detailed studies of the properties and applications of π-conjugated polymers (Yu *et al.*, 1998). Indeed, the award of the Novel price in chemistry in 2000 to Allan J. Heeger, Alan G. MacDiarmid and Hideki Shirakawa for the discovery of π-conjugated polymers and development of semiconducting polymers prove of the enormous work which has been going on in this field (Shirakwa, 2001). Polymers have attracted more attention nowadays compared to inorganic semiconductors due to their low production cost, ease of processability, flexibility as well as the tunability of their optical and electronic properties through chemical modifications. These superior properties therefore make them outstanding candidates as advanced materials in the field of photonics and electronics (Shinar and Shinar, 2009; Nalwa, 2008). Four main classes of conjugated polymers, classified according to the structure of their conjugated backbone, have been studied for optoelectronic device applications. These include: poly(para-phenylene)s (PPPs), poly(paraphenylenevinylene)s (PPVs), polythiophenes (PTs) and polyfluorenes (PFs). Insertion of side-chains in these polymers decreases backbone rigidity, increases their solubility and enables the preparation of films through inexpensive, solution-based methods such as spin-coating (Akcelrud, 2003). These ramifications also account for the tunability of the photophysical and electrochemical properties of these polymers using various routes. Table 2.1 below summarises some conducting polymers often use in OPVs.

Table 2.1: Summary of some conducting polymers and their chemical structures.

Name	Structure	Conductivity (S cm^{-2})	Type of doping
Polyacetylene	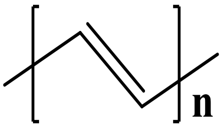	200 – 1000	n, p
Polypyrole	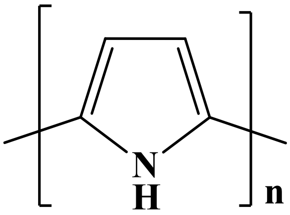	40 – 200	p
Polythiophene	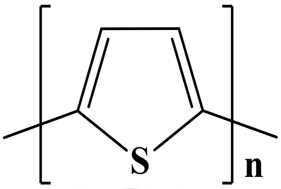	10 – 100	p
Poly(ethylenedioxythiophene)	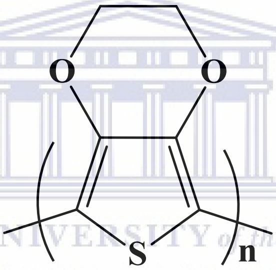	10 – 600	p
Poly(para-phenylene)	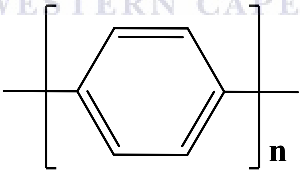	500	n, p
Poly(para-phenylene sulphide)	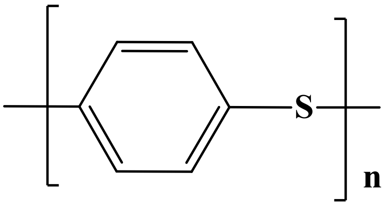	3 -500	p
Polyaniline	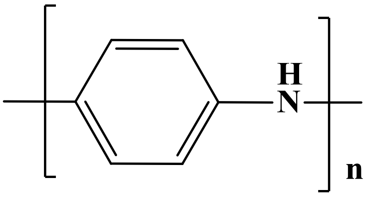	5 – 200	n, p

Considerable scientific interest has been put on polythiophenes and its derivatives for their attractive and superior chemical and physical properties (Roncali, 1992). Among the polythiophene derivatives, poly(ethylenedioxythiophene) (PEDOT) is one of the most successful conducting polymers because of its low band gap, excellent environmental stability, high electrical conductivity and transparency in thin oxidized films which confer PEDOT good properties towards applications in organic photovoltaics.

On the other hand, dendrimers constitute an interesting class of molecules which have found sound use in organic optoelectronic applications (Kopidakis *et al.*, 2005). Just like polymers, they are built from smaller repeating subunits, but instead of generating linear chains, the subunit branches out in a well-defined pattern from a central point. Synthesis of dendrimers can be achieved with high regularity and controlled molecular weight via either divergent or convergent methods (Miller *et al.*, 1997). As such, the non-linear and accurately controlled covalent structure of this class of polymers induced a wide range of studies (Miller *et al.*, 1997). π-conjugated dendrimers have shown to be efficient charge transporters in organic light-emitting diodes which was attributed to the high-quality films formed by the dendrimers (Anthopoulos et al., 2003).

2.3.2 Dendrimers as good donor materials

Due to their strong π-π cofacial interactions, these molecules exhibit an extremely high degree of molecular ordering. The film morphology of dendrimers is aided by their monodisperse nature which provides them a potential advantage over common polymers (Kopidakis *et al.*, 2006). They can also be easily purified to a great extent using simple techniques such as column chromatography. Taking into account all the good properties of dendrimers, they outstand as good candidates in light-absorbing, charge-transporting and electron donating agents in efficient organic photovoltaic devices.

2.4 Naphthalene diimides as acceptor materials

2.4.1 Properties of Naphthalene diimides

1,4,5,8-naphthalene diimides (NDIs) also called naphthalene carbodiimides are among six-membered aromatic compounds that have found applicability in many fields, particularly in the design of conducting materials (Bhosale *et al.*, 2008). The chemistry of the NDIs was pioneered back in the early 1970s by *Hung et al.* (Hung *et al.*, 1973) but more deeper researches started to be done on them in the 1990s as their potential as useful precursors and the geometries associated with some analogues in the field of supramolecular chemistry were revealed (Bhosale *et al*., 2008). Indeed, they attracted much attraction due to their tendency to form more n-type over p-type semiconductors (Katz *et al*., 2000). Also, they are known to be compact, electron-deficient and capable of self-organisation (Mukhopadhyay *et al.*, 2006) and they can also be easily incorporated in larger multicomponent assemblies through intercalations (Stewart, 1981). 1,4,5,8-naphthalene diimides are neutral, planar, chemically robust, redox-active compounds with high melting points (Bhosale *et al.*, 2008). When looking at their absorption and emission properties, the N, N- dialkyl-substituted NDIs exhibit strong, structured absorption peaks below 400 nm in many solvents. Naphthalene diimides are also able to undergo two (2) single reversible one-electron reductions at modest potentials, chemically or electrochemically, to form stable radical anions in high yield (Andric *et al.*, 2004). NDIs have a lipophilic naphthyl core and four polar carbonyl groups and as a result can easily dissolve in low polarity lipophilic solvents such as toluene, dichloromethane, chloroform; and in polar aprotic solvents such as acetonitrile, DMF, DMSO, depending on the imide substituents (Bhosale *et al.*, 2008). As such they can be better fabricated compare to perylene diimides dyes because of their enhanced solubility properties. In addition, NDIs are able to exhibit stacking in the solid state with distances commensurate with π-π stabilisation due to their planar aromatic structure. This property finds use when formation of continuous stacks is necessary (Erten *et al.*, 2005). Because NDIs have desirable electronic and spectroscopic properties over pyromellitic diimides, they appear as ideal components for the creation of supramolecular functional materials (Fallon *et al.*, 2004; Hansen *et al.*, 2000). Other properties of NDIs include their tunable fluorescence properties. Indeed, when aromatic units are bonded to the diimide nitrogens, non-fluorecent or weakly fluorescent compounds are produced while alkyl group at this same positions produce the typical white-blue colour characteristic of this compounds. On the other hand, core-substituted NDIs (cNDIs) are fastly emerging as a class of highly colourful, conducting functional materials with much different photophysical properties than their core-unsubstituted counterparts (Wurthmer *et al.*, 2002).

2.4.2 Naphthalene diimides in Photovoltaics

Naphthalene carbodiimides great potential as n-type (electron-transporting) semiconductors in organic photovoltaics lies in their compact and electron deficient cores (Yuan *et al.*, 2010). But the main reason for an up-growing interest in these six-membered ring diimides comes not only from their electron acceptor ability but also from their photochemical stability as well as their air and thermal stabilities.

2.4.3 Design criteria of good acceptor material

Towards the design of n-type semiconductors for use as efficient electron acceptors and electron-conducting materials in OPVs, the following major considerations and design criteria must be considered:

(1) The HOMO/LUMO energy levels of the acceptor material relative to those of the donor polymer semiconductor should offer sufficient offsets to facilitate photoinduced electron charge transfer and efficient charge separation while maximizing the photovoltage.

(2) To facilitate good charge transport and efficient charge collection at the electrodes, the acceptor material should have high electron mobility ($\mu_e > 10^4$ - 10^3 cm^2 (V s)$^{-1}$).

(3) The absorption band and optical band gap (E_g^A) of the acceptor material should contribute to light harvesting and exciton generation, and ideally, they should be complementary to those of the donor polymer (E_g^D) in the visible-near IR spectral range.

(4) To facilitate favourable acceptor material/donor polymer blend phase separation, thermodynamics and kinetics in forming the BHJ active layer film, the acceptor material should have a sufficiently large molar mass.

(5) The solubility of the acceptor material in common organic solvents is essential to realize solution-based processing and the fabrication of OPVs.

(6) The purity of the acceptor material should be sufficiently high (electronic grade) to enable high performance OPVs (Eilaf *et al.*, 2011).

2.5 Characterization techniques in Organic photovoltaic devices

2.5.1 UV-Vis Spectroscopy

UV-Vis spectroscopy is a technique used to study the electronic transitions of materials with transition energy in the approximate range $10^2 – 10^3$ kJ mol^{-1}, which is found within the IR through UV region of the electromagnetic spectrum. For most semiconductors, the required energy for an electron to jump from the valence band to the conduction band is in the same energy region, and thus UV-Vis spectroscopy is a powerful way to study the inter-band electronic transition in semiconductors. Studying the optical absorption of semiconducting materials is therefore important to understand their behaviour in OPVs. Indeed a fundamental feature in semiconductors is the band gap – the energy separation between the filled valence band and the empty or partially filled conduction band. In semiconductors, optical excitation of electrons across the bang gap is strongly allowed, resulting in an abrupt increase in absorbance of light at the wavelength corresponding to the band gap energy. The absorption of light at a specific wavelength is determined by the ratio of transmitted light and incident light (I_t/I_i). Absorbance can therefore be expressed as:

$$A = -\log \frac{I_t}{I_i}$$

Each molecule in solution absorbs a certain amount of light. Using the Beer's law, it is possible to express the correlation of the absorbance of each molecule at a specific wavelength to its concentration and the length of the light path.

$$A= \varepsilon_{\lambda}cl$$

Where,

A: light absorbance, ε_{λ}: the extinction coefficient, c: the concentration of the molecule and l: the length of the pathway of the sample holder.

2.5.2 Fluorescence Spectroscopy

Fluorescence is the emission of light by a molecule (fluorophore) after the absorption of light (excitation) of shorter wavelength; it usually occurs within microseconds (Litchman and Conchello, 2005). Semiconductors in general and polymers in particular contain a conduction band, a band gap, as well as a valence band. And the interaction of all these three components imparts their optical properties. Under normal conditions of room temperature, the electronic state of any semiconductor will be in its lowest possible energy state, known as the ground state (S_0). But once exposed to a visible or ultraviolet light, a semiconductor will absorb a photon and one or more of his electrons will jump from the valence band to the conduction band. This therefore leaves a hole in the valence band where the electron originally was found and an electron-hole pair known as an exciton is produced. An excited polymer acquires several energy levels known as singlet states, denoted as S_1, S_2, S_n. In the a singlet excited state, the electron in the higher energy orbital has the opposite spin orientation relative to electron in the lower orbital as depicted in the scheme below:

Scheme 2.6: *A singlet excited state*

From the excited state, the hole and the electron recombine bringing the polymer back to the ground state. This process may take place via non-radiative transition or a radiative decay from a singlet excited state to the ground state. When radiative electron-hole recombination occurs, it results in the direct transition from a singlet excited state to the ground state. This produces a photon emission spectrum and the process is called fluorescence. Typically, fluorescence results from a transition between the lowest energy level of the first excited singlet state and some vibrational level of the ground state. The delay between absorption and emission in fluorescence is of the order of 10^{-8} seconds or less (Taylor and Salmon, 1999).

2.5.3 Fourrier-Transform Infrared Spectroscopy (FT-IR)

Fourier-Transform infrared spectroscopy (FT-IR) is more generally applicable towards many samples, since it does not require a UV chromophore, but rather requires infrared light which is absorbed by the molecular bonds to cause transitions between molecular vibrational states (Vakkasoglu, 2009). So, it is the absorption measurement of different infrared frequencies by a sample positioned in the path of an infrared beam. The main goal of FT-IR spectroscopic analysis is to determine the chemical functional groups in the sample. The IR spectrum refers to electromagnetic waves whose wavelengths range from 0.78 µm to 1000 µm. However the more manageable, the wavenumber unit (cm^{-1}) is generally used instead of microns thus the total IR spectrum ranges from 14,286 cm^{-1} to 28.5 cm^{-1}. The advantages of FT-IR are its superior speed, sensitivity and have been applied to many areas that are very difficult or nearly impossible to analyse by IR-dispersive instruments. Instead of viewing each component frequency sequentially as in a dispersive IR-spectrometer, all frequencies are examined simultaneously in Fourier transform infrared (FT-IR) spectroscopy (Hallam, Online 2010).

2.5.4 X-Ray Diffraction Spectroscopy (XRD)

X-ray Diffraction (XRD) is a versatile, non-destructive technique which provides detailed information about the chemical composition and crystallographic structure of many kind of materials; natural and manufactured. It is therefore an indispensable technique in material characterization. X-ray diffraction working process is based on the assumption that x-ray radiations with wavelengths in the order of Angstroms elastically scatter off the electronic structure of a crystal (scheme 2.7). The periodicity of the crystal will cause this scattering of the x-ray plane-wave to constructively interfere at certain scattering directions while destructively interfering at other scattering directions (Weisstein, Online 2005). The diffraction of X-rays by matter results from combinations of different phenomena namely, the scattering by each atom and interference between the waves scattered by these atoms. This interference occurs because the wave scattered by the individual atoms are coherent with the incident wave, and therefore between themselves (Guinier, 1994).

There exist two types of X-ray diffraction methods: the spectroscopic and the photographic methods. The spectroscopic technique now known as the X-ray powder diffractometry or simply X-ray diffractometry is the most widely used. An example of x-ray diffraction system is illustrated below.

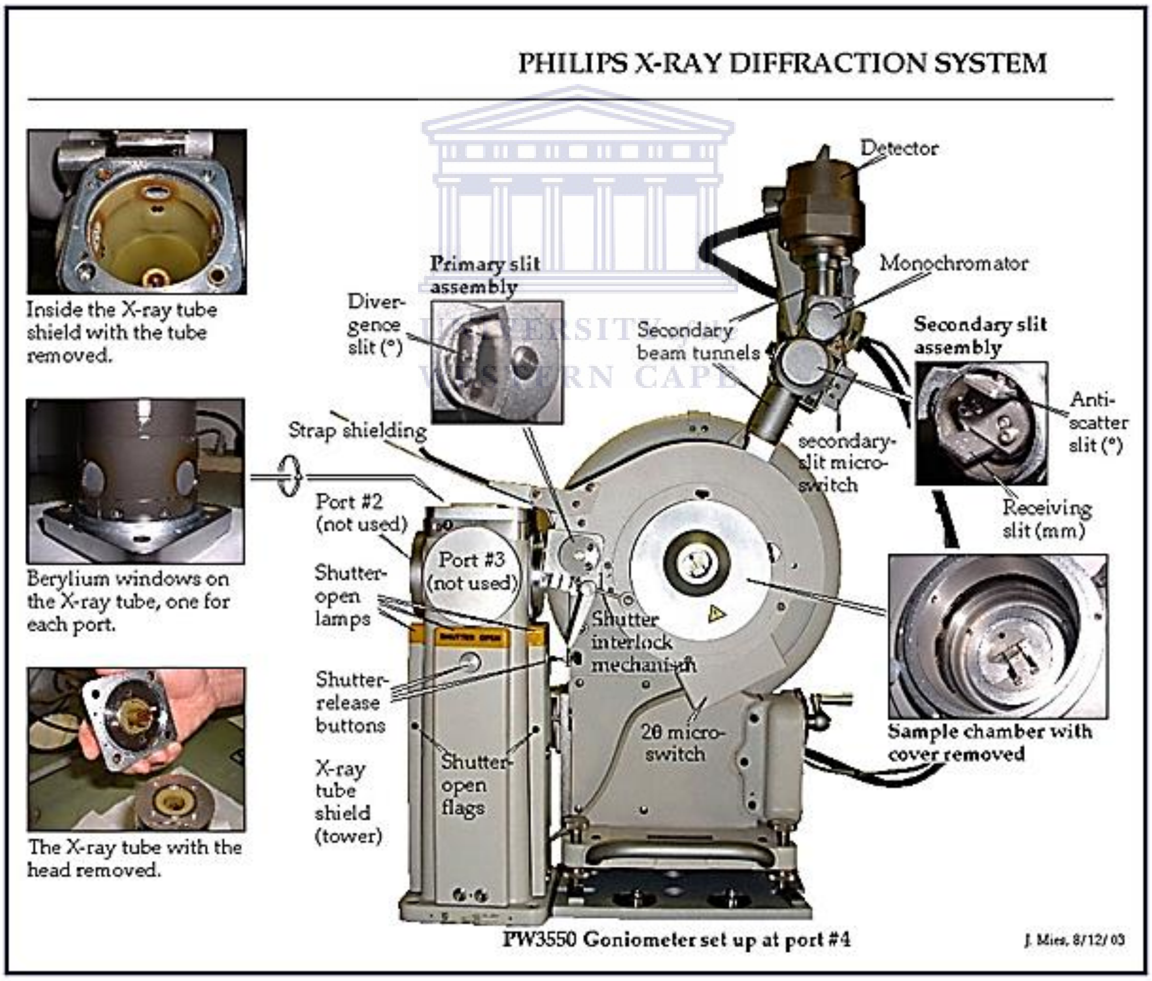

Scheme 2.7: *X-ray Diffraction System*

2.5.5 High Resolution Scanning Electrode Microscopy (HRSEM)

High Resolution Scanning electron microscopy (HRSEM) is a versatile imaging technique capable of producing three-dimensional images of material surfaces. And nowadays, it is one of the most frequently used instruments in material sciences research because of the combination of high magnification, large depth of focus, greater resolution and ease of sample observation. Indeed, over the past years the scanning electron microscope (SEM) has grown from a specialized research device to a universal industrial tool considering that SEM imaging was first characterized to be used as a benchmark. The scanning electron microscope has two main parts, see scheme 2.8. The electronics are used to control electron beam on the specimen, identify and analyse signals, form image and do other functions to control the microscope. Whereas the electron column creates electrons including the group of lenses that focus the electron beam exactly to the specimen (Lyman *et al.*, 1990). The focused electron beam is scanned over a specimen such that the interaction between the beam and the specimen excites various forms of radiations including backscattered electrons, secondary electrons, and x-rays. These radiations are then detected and analysed to reveal information concerning the specimen's composition and topography. SEM has the advantages in detecting impurities, ruptures, folds, voids and discontinuities of the analysed materials. A requirement for effective performance is that the surface of the samples should be electrically conductive. During operation, electrons are deposited onto the sample. These electrons must be conducted away to earth, thus conductive materials such as metals and carbon can be placed directly into the HRSEM whereas non-metallic samples have to be coated with a gold metal layer to be observed. Many scanning electron microscopes have an energy dispersive spectrometer (EDX) detection system, which detects and displays most of the spectra of the elements contributing to the sample composition.

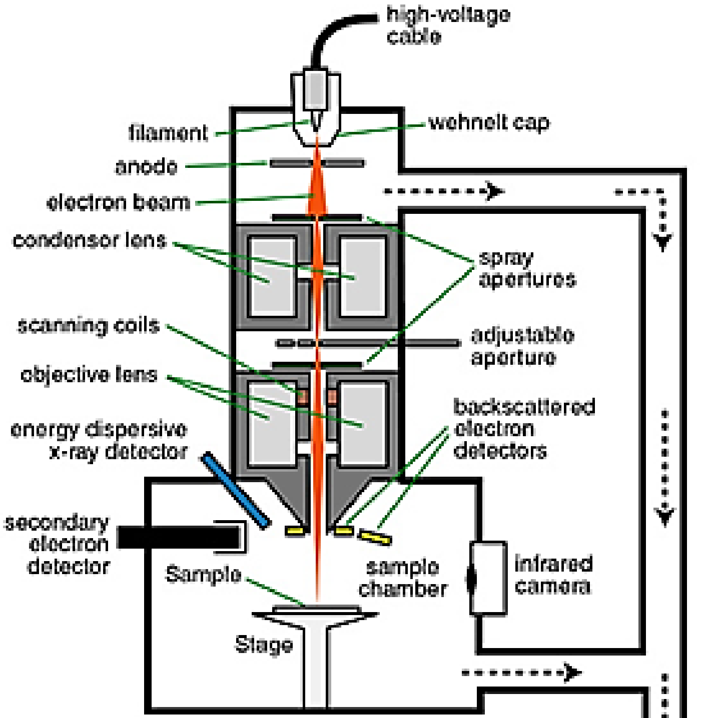

Scheme 2.8: *Scanning electron microscopy system*

2.5.6 Electrochemical techniques

Generally, electrochemical techniques give information on the reduction and/or oxidation processes taking place when an electric potential is applied to the system under study. The basic components of a modern electrochemical system for voltammetric and impedimetric measurements comprise of a potentiostat, a computer and an electrochemical cell as shown in the scheme 2.9 below.

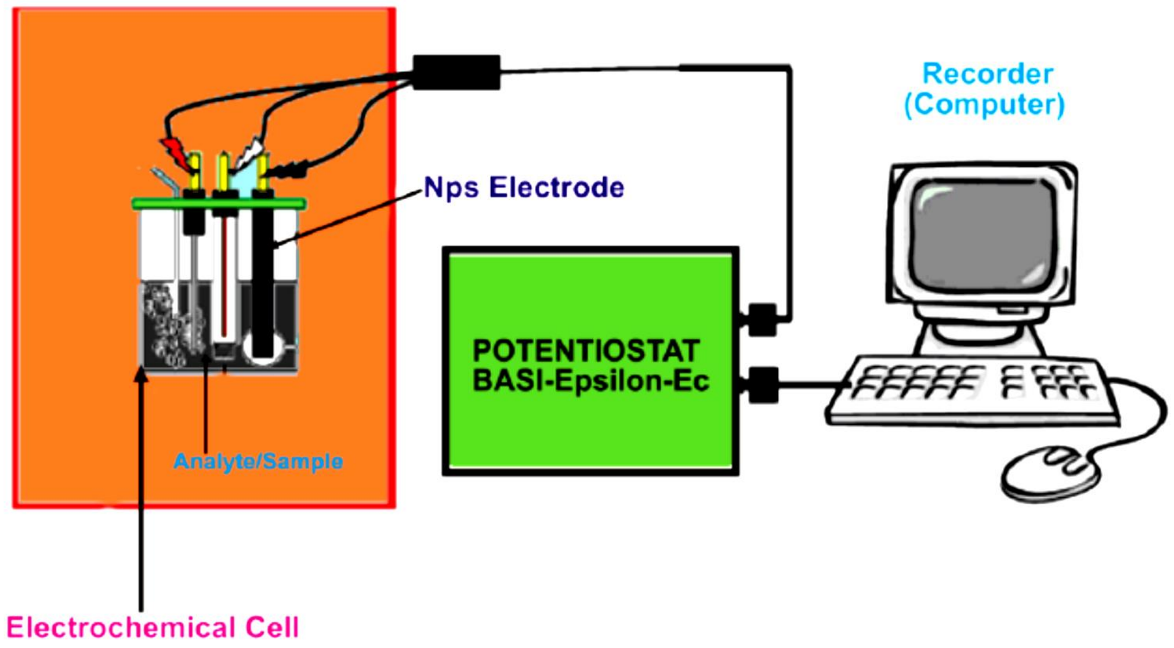

Scheme.2.9: *Major components of the electroanalytical system used for electrochemical analysis*

A potentiostat is an electronic device that controls the difference of voltage between the working electrode (WE) and the reference electrode (RE). Both electrodes are immersed in an electrolyte contained in an electrochemical cell. The potentiostat implements this control by injecting current into the cell through an auxiliary electrode (AE). In almost all applications, the potentiostat measures the current flow between the working and auxiliary electrodes. The controlled variable in a potentiostat is the cell potential and the measured variable is the cell current. A potentiostat typically functions with an electrochemical cell containing three electrodes; the working, reference and the auxiliary or counter electrodes, which are described below.

The *working electrode*: this is the electrode at which the redox reaction of the analyte or the electrochemical phenomena being investigated occurs. The most commonly used materials for working electrodes include solid disk glassy carbon, platinum, gold electrodes, etc. Screen printed electrodes of each of these materials are also used as working electrodes. Whereas solid disk working electrodes can be used over and over again with standard cleaning before and after use, screen printed electrodes are mainly “single use” electrodes.

The *reference electrode*: this is the electrode against which the potential of the working electrode is measured. A reference electrode has a known and constant electrochemical potential as long as no current flows through it. Commonly used reference electrodes for electrochemical measurements in aqueous solutions are the silver/silver chloride (Ag/AgCl) and the saturated calomel electrodes (SCE).

The *auxiliary or counter electrode*: this is a conductor that completes the cell circuit, acting as a sink for electrons so that current can be passed from the external circuit through the cell. Reactions occurring at this electrode surface are unimportant as long as it continues to conduct current well. To maintain the observed current, this electrode will often oxidize or reduce the solvent or bulk electrolyte though the reactions occur over short periods of time and rarely produce any appreciable changes in bulk concentrations. Most often the auxiliary electrode consists of a metallic foil or thin platinum wire, although gold and sometimes graphite have also been used.

The main target of an electrochemical experiment is to study in details the electron transfer process of a material and an understanding of the redox behaviour of the material requires the study of the kinetic aspects of the electron transfer processes exhibited by that material as well as the thermodynamic aspects of such electron transfer processes.

2.5.6.1 Cyclic Voltammetry

Cyclic voltammetry, also known as linear scan voltammetry, is an electrochemical technique that is classified under sweep techniques. Within the electrochemistry field, cyclic voltammetry is known to be a simple, easy and effective technique for elucidating the electroactivity of polymers and to measure the oxidation and reduction potentials. These potential values allow the determination the Highest occupied Molecular orbital (HOMO) and the Lowest unoccupied Molecular Level (LUMO). Therefore when an organic material shows an electron reversible reduction and oxidation cycle, cyclic voltammetry appears to be an important tool for the calculations of ionisation potentials, I_p (HOMO), electron affinities, E_a (LUMO) and therefore energy band gaps (E_g). Here, the oxidation step constitutes the removal of an electron from HOMO energy level and the addition of an electron to LUMO level is associated to the reduction step (Bernède, 2010).

Calculations of HOMO, LUMO and energy band gaps can therefore be achieved using the following equations:

E_a (LUMO) = $- e(E'_{red} + 4.8)$ V

I_p (HOMO) = $- e(E'_{ox} + 4.8)$ V

E_g = LUMO - HOMO (Dong *et al*., 2009)

2.5.6.2 Square Wave Voltammetry

Square wave voltammetry is a type of pulse voltammetry that offers the advantage of speed and high sensitivity. An entire voltammogram is obtained in a few seconds or less. In addition, square wave voltammetry (SWV) has proved to be a suitable method to investigate redox reactions with overlapping waves. The excitation signal in SWV consists of a symmetrical square wave pulse of amplitude superimposed on staircase wave form of step height ΔE. The forward pulse coincides with the staircase step. A typical square wave voltammogram is shown in the scheme 2.10 below.

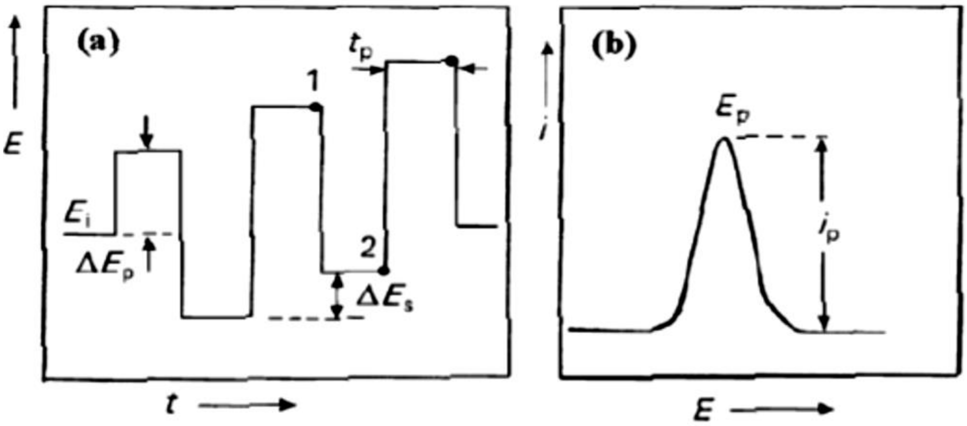

Scheme 2.10: ***(a)*** *Excitation waveform of square wave voltammetry and* ***(b)*** *response obtained by square wave voltammetry*

In SWV, the peak height is directly proportional to the concentration of the electroactive species. Excellent sensitivity is achieved from the fact that the net current is larger than either the forward or the reverse components, since it is the difference between them and direct detection limits as low as 10^{-8} M are possible. It presents some advantages over cyclic voltammetry, including excellent sensitivity and rejection of background currents. The scanning speed in SWV is also high and, coupled with computer control and signal averaging experiments, can be performed repetitively with increases in the signal to noise ratio. It is also applied in study of electrode kinetics with regard to preceding, following or catalytic homogeneous chemical reactions and determination of some species at trace levels.

CHAPTER THREE

Experimental

3.1 Reagents used

Table 3.1: Reagents Used

Name and percentage	**Purchasing Company**
DAB-Am4, Poly(propyleneimine) tetramine dendrimer, Generation 1	Sigma Aldrich – South Africa
1, 4, 5, 8-Naphthalene tetracarboxylic dianhydride	Sigma Aldrich – South Africa
2-Thiophene carboxaldhyde, 98%	Sigma Aldrich – South Africa
Tetrabutylammonium hexafluorophosphate, ≥ 99.0 %	Fluka – South Africa
3, 4-ethylenedioxythiophene, 97 %	Sigma Aldrich – South Africa
Ammonium persulfate	Sigma Aldrich – South Africa
Lithium perchlorate anhydrous	Sigma Aldrich – South Africa
Chloroform, 99.9 % HPLC Grade	Sigma Aldrich – South Africa
N,N-dimethylsulfoxide, Analytical Grade	Sigma Aldrich – South Africa
N,N-dimethylformamide anhydrous, 99.8%	Sigma Aldrich – South Africa
Dichloromethane Chromasolv Plus HPLC, ≥ 99.9 %	Sigma Aldrich – South Africa
Mehanol, Analytical Grade	Sigma Aldrich – South Africa

3.2 Synthetic Methods

3.2.1 Generation 1 Poly(propyleneimine) tetramine (G1PPI) functionalization

Prior to the functionalization of the dendrimer, a 250 mL 2-neck round bottom flask was washed, rinsed then dried for two (2) hours in order to remove all moisture. Then the glassware was cleaned with nitrogen (N_2) gas.

In order to functionalize the dendrimer, 0.3863 g (1.2205 mmol) of Generation 1 Poly(propyleneimine) tetramine dendrimer, G1PPI was dissolved in 25 mL of Methanol (MeOH), then 472.55 µL (4.8821 mmol) of 2-thiophene carbaldehyde was added and the mixture was allowed to stir for 48 hours under N_2 gas. G1PPT was thus functionalized into Generation 1 Poly(propylenethiophenoimine) G1PPT.

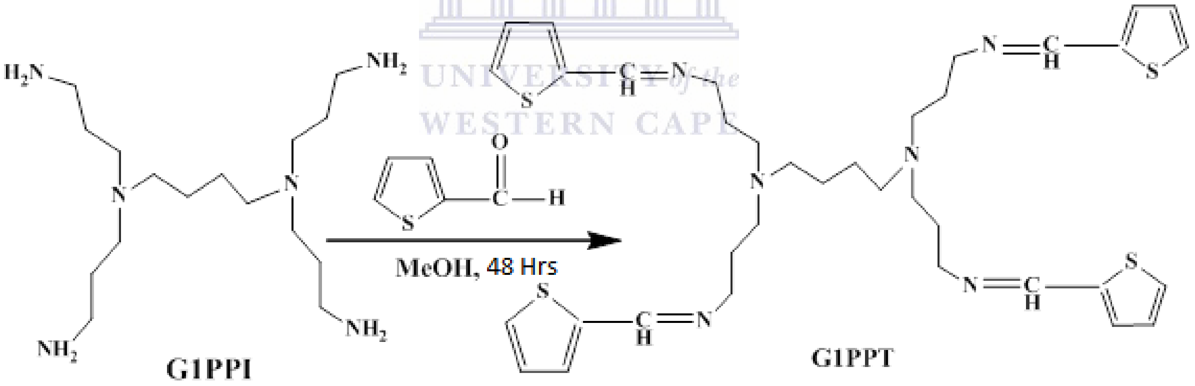

Scheme 3.1: Functionalization of G1PPI

Upon completion of functionalization, the methanol solvent was completely removed using a rotary evaporator for 10-15 min, then came the washing step whereby 25 mL of dichloromethane and 25 mL of water was added to the functionalized dendrimer and transferred into a separation funnel, shaken for 10-15 min and then the mixture was allowed to rest in order to separate the organic phase from the aqueous phase. This was repeated 5 times to ensure complete removal of any excess of 2-thiophene carbaldehyde. The final step was the evaporation of the dichloromethane.

G1PPT was then characterized by FTIR, UV-Vis Spectroscopy, Cyclic Voltammetry (CV), SEM and XRD.

3.2.2 Copolymerization of ethylenedioxythiophene (EDOT) monomer to G1PPT to form the star copolymer G1PPT-co-PEDOT.

Again, prior to the synthesis of NDI, a 250 mL one-neck round bottom flask was washed, rinsed then dried for two (2) hours in order to remove all moisture. Then the glassware was cleaned with nitrogen (N_2) gas.

495 mg (0.71424 mmol) of G1PPT was dissolved in 10 mL of chloroform. Then 318 µL (2.8570 mmol) of the monomer EDOT was added with 29.75 mL of 0.1 M $(NH_4)_2S_2O_8$ and the mixture was allowed to stir for 2 hours at room temperature. Then the reaction was stopped and the solvents, chloroform and water were evaporated; the material was then left overnight for polymerization to continue.

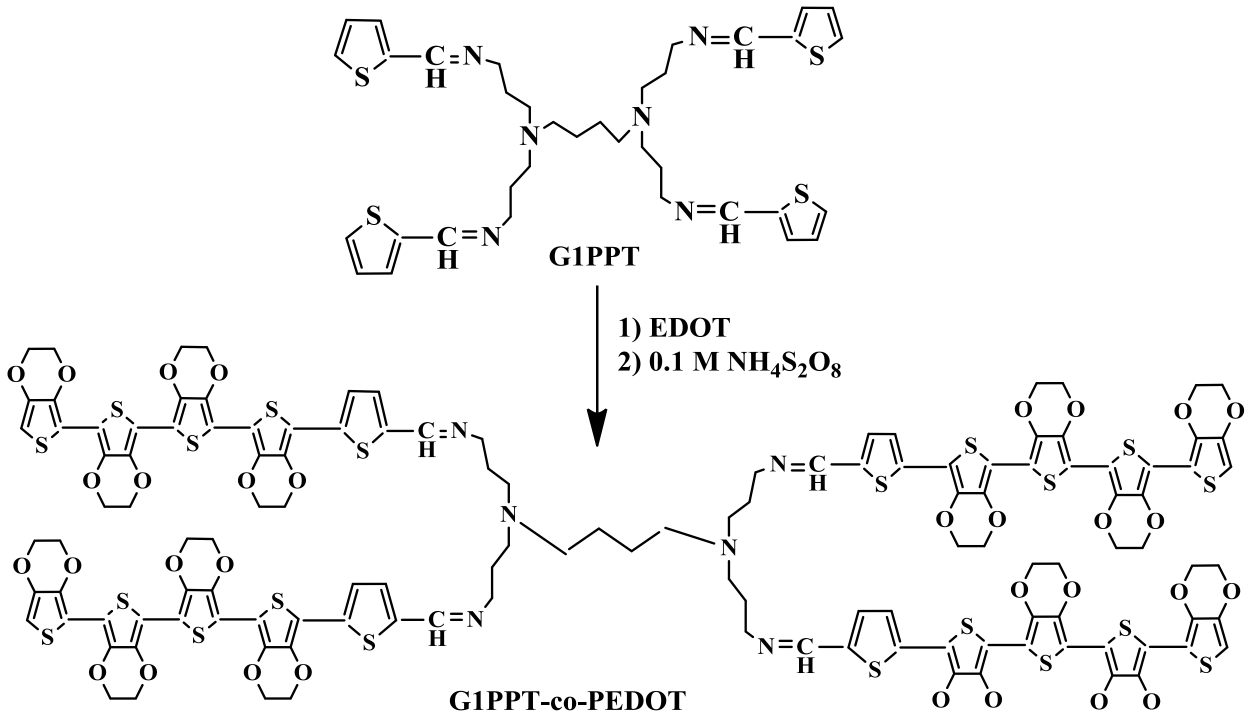

Scheme 3.2: *Chemical copolymerization of EDOT monomer on G1PPT*

In the morning, 20 mL of water was introduced in the glassware and sonicated for about 15 minutes for the star-copolymer to be washed, then was centrifuged for about 30 min to separate the particles from water and the water was disposed. The same procedure was repeated twice with acetone except from the sonication step. Then the star-copolymer was allowed to dry at ambient air overnight. The following day the sample was collected and kept in a closed vial.

3.2.3 Synthesis of N, N-diisopropylnaphthalene diimide (NDI)

Just like for the functionalization of G1PPI, prior to the synthesis of NDI, a 250 mL 2-neck round bottom flask was washed, rinsed then dried for two (2) hours in order to remove all moisture. Then the glassware was cleaned with nitrogen (N_2) gas.

2.25 g (8.3900 mmol) of 1, 4, 5, 8- naphthalene tetracarboxylic dianhydride (NTCDA) was introduced in a 2-neck round bottom flask containing 25 mL of N, N-dimethylformamide.

Then two equivalences that is, 1.42 mL (0.9919 mol) of isopropylamine were added and the mixture was stirred at 110 ^{o}C overnight.

Scheme 3.3: *Synthesis of N, N-diisopropylnaphthalene diimide*

Due to its high boiling point, DMF couldn't be evaporated so a pump was used to filter the synthesized NDI. NDI was subsequently put in ice-cold water for 5 min and filtered again. This was done not only to purify the material but mostly to ensure the high crystallinity of the yellow-canary prepared NDI. NDI was then characterized by FTIR, UV-Vis Spectroscopy, Fluorescence, Cyclic Voltammetry (CV), Square Wave Voltammetry (SWV), HRSEM and XRD

3.2.4 Preparation of the Bulk Heterojunction active layer: G1PPT-co-PEDOT: NDI

0.01 M of G1PPT-co-PEDOT was prepared by dissolving 0.06930 g of the star-copolymer in 10 mL of DMSO and sonicated for 1 Hr. On the other hand, 0.01 M of N,N-diisopropylnaphthalene diimide was also prepared by dissolving 0.0350 g of NDI in 10 mL of DMSO for about 3 Hrs; this longer dissolution time is due to the poor solubility of NDI in DMSO.

Then the four different ratio of our bulk heterojunction active layer G1PPT-co-PEDOT were prepared. This was done by mixing:

- 1 mL of G1PPT-co-PEDOT with 1 mL of NDI → 1:1 layer
- 1 mL of G1PPT-co-PEDOT with 2 mL of NDI → 1:2 layer
- 1 mL of G1PPT-co-PEDOT with 3 mL of NDI → 1:3 layer
- 1 mL of G1PPT-co-PEDOT with 4 mL of NDI → 1:4 layer

3.3 Fabrication of the Photovoltaic BHJ solar cell: Spin-coating

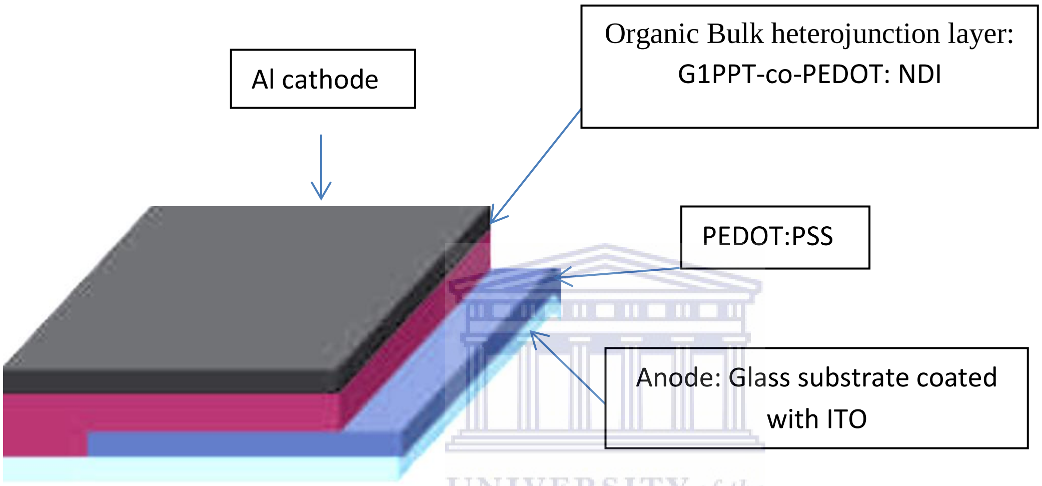

Scheme 3.4: *Fabricated organic BHJ photovoltaic cell of G1PPT-co-PEDOT: NDI*

In order to fabricate the BHJ solar cell, a 1cm by 6 cm ITO coated glass substrate was cut into 1 cm by 1 cm square pieces. The pieces of ITO coated glass substrates were then cleaned in acetone, ethanol and isopropanol consecutively to ensure complete removal of all impurities from the ITO coated glass substrates and were allowed to dry for five (5) min. Then they were placed at the centre of the spin-coater (Chemet Technology equipment) and 1 mL of PEDOT:PSS was spin-coated on the surface of the ITO coated glass surface then allowed to completely dry before 500 μL the active layer of G1PPT-co-PEDOT was also spin-coated on top of the PEDOT:PSS layer and allow to completely dry. The spin-coating parameters being used in this procedure were 9 s at 500 rpm speed followed by 15 s at 1500 rpm speed. Thereafter the 200 nm of aluminium will electrodeposited as the cathode material.

3.4 Supporting Electrolytes

0.1 M $LiClO_4^-$ in water was prepared as a supporting electrolyte for the voltammetric studies of G1PPT, by dissolving 0.53195 g of $LiClO_4^-$ powder in 50 mL of water.

0.1 M of Bu_4NPF_6 was prepared as supporting electrolyte for the voltammetric studies of NDI by dissolving 1.93715 g of Bu_4NPF_6 in 50 mL of DCM and 50 mL of DMF.

0.1 M $LiClO_4^-$and 0.1 M of Bu_4NPF_6 were prepared as supporting electrolytes for the voltammetric studies of G1PPT-co-PEDOT by dissolving 0.53195 g of $LiClO_4^-$ powder in 50 mL of acetonitrile and by dissolving 3.8743 g of Bu_4NPF_6 in 100 mL of acetonitrile respectively.

3.5 Instrumentation

3.5.1 Optical studies

Ultraviolet-visible (UV-Vis) absorption measurements were made using a quartz cuvette in a Nicolet Evolution 100 UV–visible spectrometer (Thermo Electron, UK). The measurements for most of the samples were carried between 200 – 1100 nm using both D_2 (Deuterium) and W (tungsten) lamps. Also, to ensure good absorbance peaks while avoiding noise, the samples were sufficiently diluted.

Fluorescence properties of G1PPT, G1PPT-co-PEDOT and NDI samples were studied using Horiba NanoLog™ - TRIAX (USA), with double grating excitation and emission monochromators at a slit width of 5 nm.

3.5.2 Fourrier-Transform Infrared spectroscopy (FT-IR)

FTIR spectra were recorded in the range 4000 - 300 cm^{-1} using a PerkinElmer model Spectrum 100 series.

3.5.3 XRD

X-ray diffraction (XRD) for the phase identification of the crystalline structures of G1PPT, G1PPT-co-PEDOT and NDI was performed by using a Bruker AXS D8 Advance diffractometer (voltage 40 KV; current 40 mA). The XRD spectra were recorded in the range 10-70 degrees. All three samples were analysed as prepared.

3.5.4 HRSEM

High Resolution Scanning electron microscopy was used to characterize the surface morphology of G1PPT, G1PPT-co-PEDOT and NDI, and to determine elemental composition and/or atomic percentage of the samples. The images were recorded using a Zeiss Auriga HRSEM analyser using the secondary electron (SE) mode with interchangeable accelerating voltages of 25 kV, and a maximum resolution of 20 μm. The chemical composition of the sample was obtained by energy dispersive x-ray spectroscopy (EDX) which was coupled to the HRSEM machine. The HRSEM/EDX samples were prepared by placing solid nanomaterial onto a carbon adhesive mounted on aluminium stubs.

3.5.5 Cyclic Voltammetry and Square Wave Voltammetry

The cyclic voltammetry measurements were performed using a BAS 100W electrochemical workstation and automated electrochemical potentiostat from Bio Analytical Systems, Lafayette, USA. The voltammograms were recorded with a computer interfaced to a BAS 100W electrochemical workstation. A 10 mL electrochemical cell with a conventional three electrode set up was used. The three electrodes consisted of either gold or platinum disk working electrodes depending on the sample analysed, an Ag/AgCl (saturated 3 M NaCl) reference electrode and a platinum wire as the auxiliary electrode. Therefore, all potentials in this study are quoted with respect to Ag/AgCl (3 M NaCl). The three electrodes and the corresponding three electrode cell configuration are shown in scheme 3.5 below.

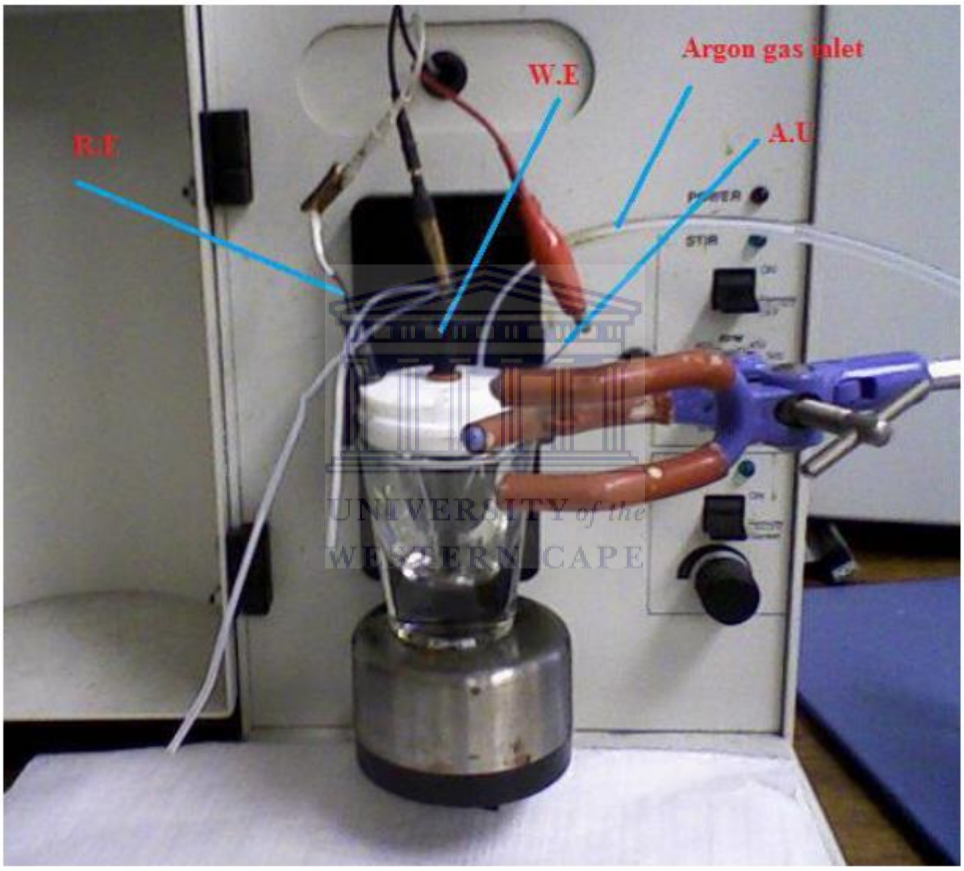

Scheme 3.5: *Cyclic Voltammetry experimental set-up*

For G1PPT electrochemical analyses, 10 mg of G1PPT was dissolved in 1mL of chloroform, of which 5 µL was drop-coated on a gold electrode and allowed to dry. Then the electrode was immersed in the electrochemical cell following the configuration presented in scheme 3.5 above. The sample was swept over a potential range between -900 - 1250 mV in 0.1 M $LiClO_4^-$. Same procedure was applied to G1PPT-co-PEDOT with the differences that here the solvent in which G1PPT-co-PEDOT was dissolved is DMSO and the potential range was -1000 – 1000 mV in acetonitrile (0.1 M LiClO^{4-}). In the case of the acceptor material, 1 mL of 0.1 mM NDI was run in solution using the same electrochemical cell configuration but this time with a Pt working electrode and potential was swept between (-1600) – (-500) mV.

Prior to all experiments (CV and SWV), Au and Pt electrode surfaces were cleaned by polishing consecutively with aqueous slurries of 1.0, 0.3, and 0.05 μm alumina powders on a microcloth pad (Bühler), gently rinsed with deionized water then ultra-sonicated in ethanol and then in distilled water for 5 min respectively each in order to remove residuals. The Pt auxiliary electrode was cleaned by burning in a flame for several minutes and the Ag/AgCl electrode was cleaned by rinsing with distilled water. 0.1 M $LiClO_4^-$ in water, 0.1 M $LiClO_4^-$ in acetonitrile and 0.1 M Bu_4NPF_6 in dichloromethane were used as the supporting electrolytes for all voltammetric measurements of G1PPT, G1PPT-co-PEDOT and NDI respectively. All experimental solutions were purged with high-purity argon gas for 15 –25 min and blanketed with argon atmosphere during measurements. The experiments were carried out at room temperature.

CHAPTER FOUR

Results and Discussion

4.1 Characterization of G1PPT

4.1.1 Fourrier Transform Infrared spectroscopy of G1PPT (FT-IR)

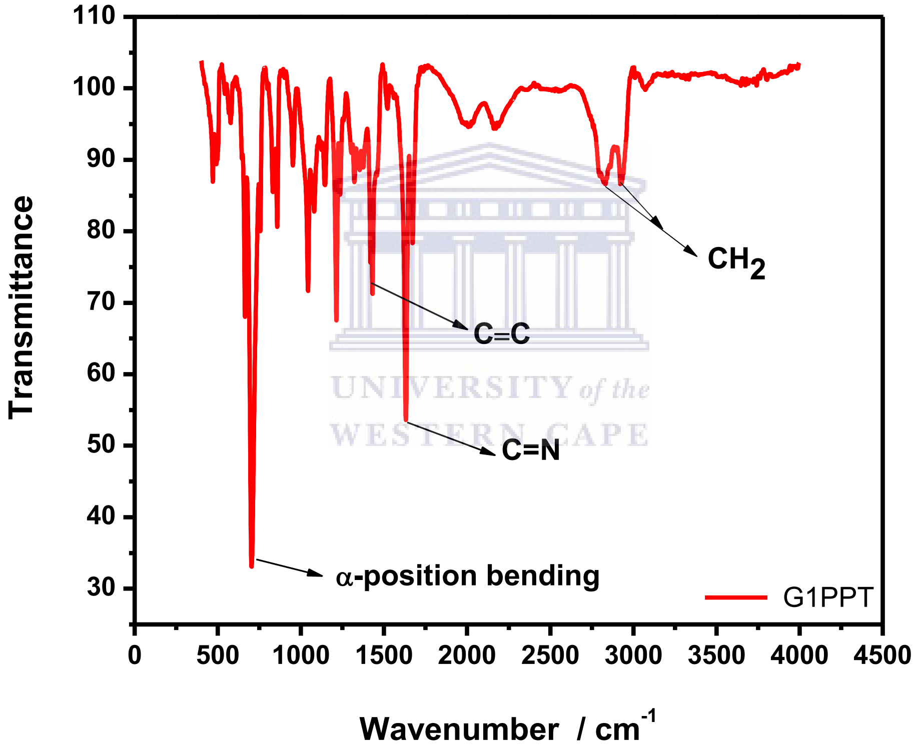

Figure 4.1: *FT-IR Spectrum of G1PPT*

G1PPT was characterized using FT-IR spectroscopy to confirm the functionalization of the dendrimer. Indeed, in the spectrum of the functionalized dendrimer, (see figure 4.1 above), several characteristic peaks at 475, 705, 833, 845, 1037, 1075, 1217, 1319, 1435, 1629, 1679, 2830, 2938 cm^{-1} for G1PPT were observed. In the spectrum of the G1PPT, out-of-plane bending of C-H bond located at the α-position to the thiophene ring was observed at 705 cm^{-}

[1]. At 1435 cm^{-1}, the medium-weak multiple bands account for the C=C stretching in the 5-membered aromatic ring of thiophene. The sharp band at 1629 cm^{-1} is attributed to the C=N bond stretching vibration present in the dendrimer moiety. The bands at 2830 and 2938 cm^{-1} in G1PPT indicate the presence of the CH_2 stretchings in the dendrimer moiety.

4.1.2 UV-Vis Spectroscopy of G1PPT

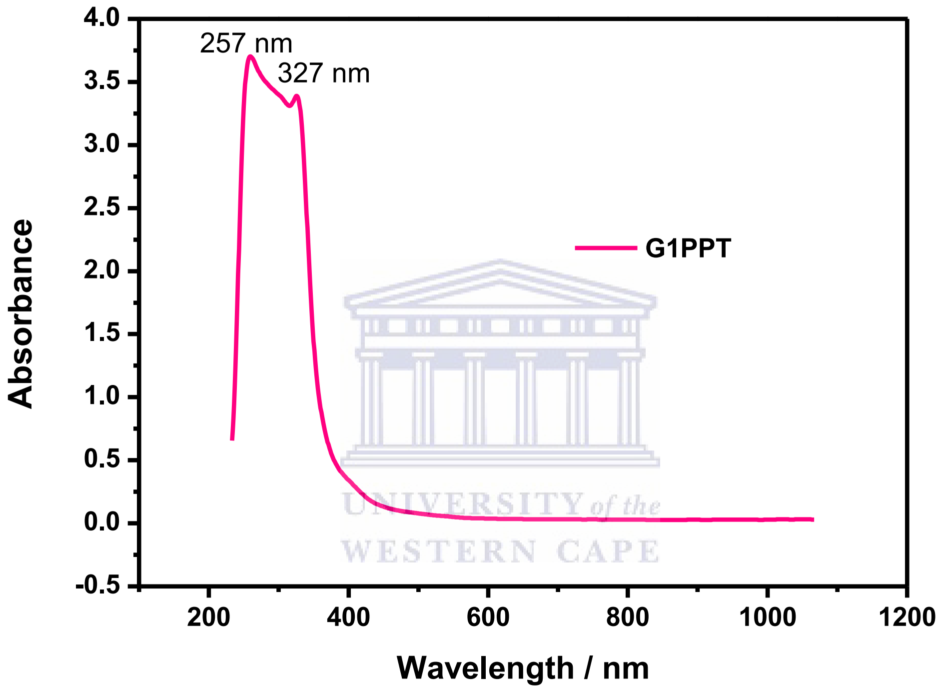

Figure 4.2: *UV-Vis Spectrum of G1PPT*

When exposing a sample material to a beam of light in the UV-Vis region, one or more electrons are getting excited from the lower energy band or valence band to the higher energy band or conduction band. The interaction between those two bands as well as the band gap, which is the energy separation between valence and conduction band determine the optical properties of the material. The UV-Vis spectrum of G1PPT in figure 4.2 above shows two distinct absorption peaks at 257 nm and 327 nm. These two peaks are characteristics of the absorbance of the two chromophores C-S-C and C=N respectively, present in the functionalized dendrimer whose transitions are respectively n-π^* and π-π^* with band gap energies of 4.83 eV and 3.79 eV. The band gap energies were calculated using the following equation:

$$\boldsymbol{E = \frac{hc}{\lambda}}$$

Where, E is the band gap energy, h = 4.135667516*10^{-15}eV s is the Planck's constant, c = 3*10^8 m s^{-1} is the speed of light, λ is the experimental absorption peak wavelength.

4.1.3 Electrochemical behaviour of G1PPT

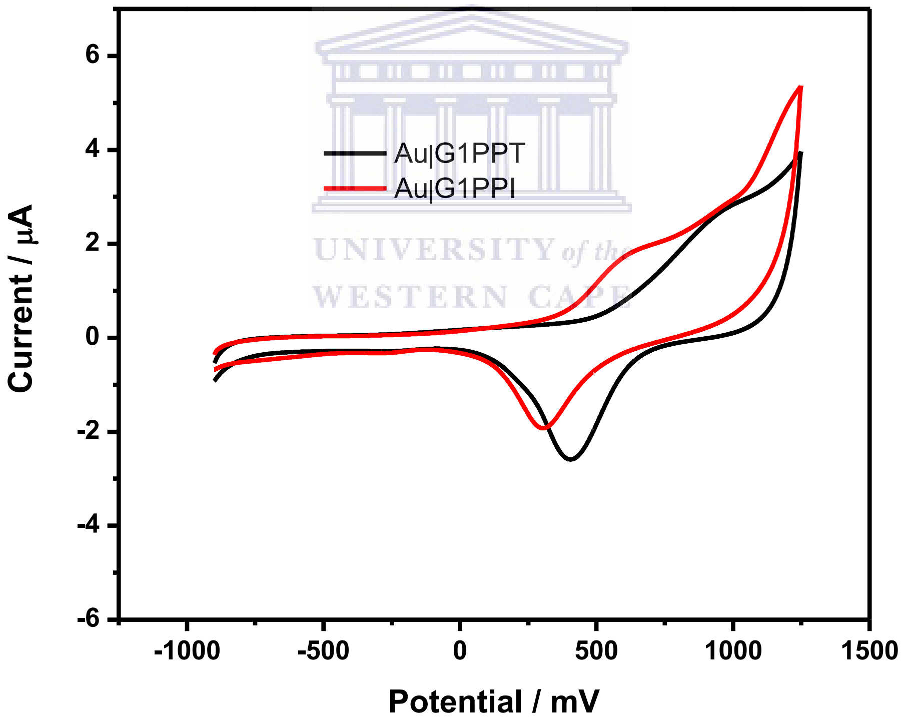

Figure 4.3: *Cyclic voltammogram of Au|G1PPT and Au|G1PPI in 0.1 M* $LiClO_4^-$

G1PPT was further studied using cyclic voltammetry sweep technique. Figure 4.3 above represents the cyclic voltammogramms of G1PPT, the functionalized dendrimer and G1PPI the starting material and the potential was swept between - 900 mV and 1250 mV at a scan rate of 50 mV s^{-1}. As it can be seen on the graph the oxidation peaks of G1PPI and G1PPT are at 603 mV and 862 mV respectively whereas the reduction peaks are at 306 mV and 400 mV respectively. It can also be observed from the graph that the onset potential of oxidation of G1PPI is before that of G1PPT which can allow us to say that there has been a change in the structure of the dendrimer and thus that the functionalization was successful. It also allows us to be able to state that G1PPT is more stable than G1PPI. On the other hand the onset potential of reduction of G1PPT is before that of G1PPI and we can thus conclude that G1PPT reduces easily compare to G1PPI.

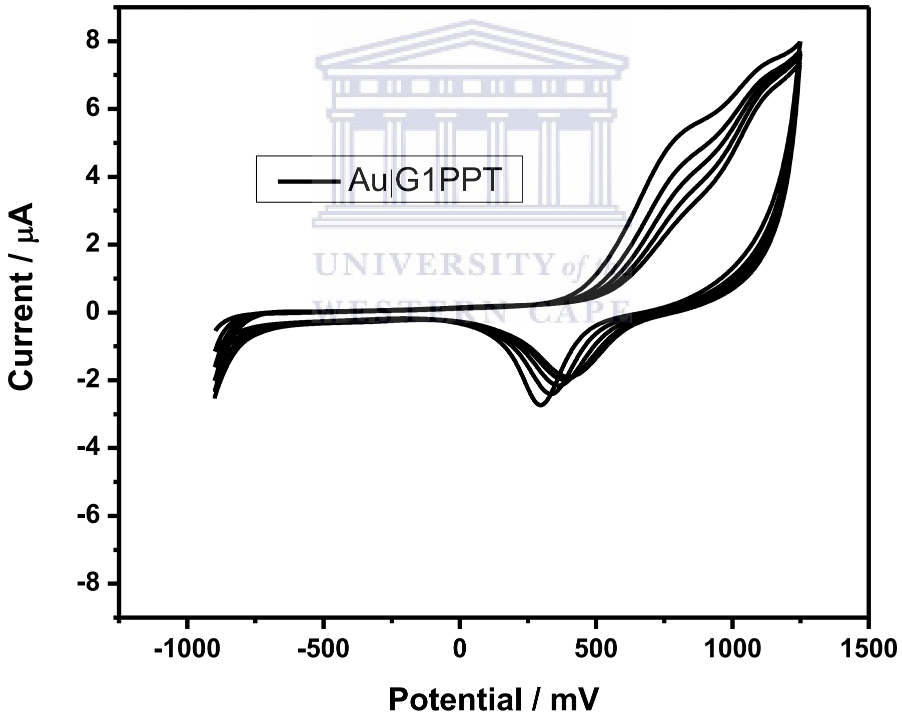

Figure 4.4: *Cyclic voltammogram of Au|G1PPT over five (5) cycles*

The oxidation and reduction peaks of G1PPT were confirmed by running the cyclic voltammetry of the material under the same parameters except that this time the sweeping was over five (5) cycles, see figure 4.4. The consistence in the appearance of the oxidation and reduction peaks of G1PPT therefore proved its electrochemical behaviour. And the peaks are as a result of the oxidation and reduction of the sulphur atom in the thiophene ring.

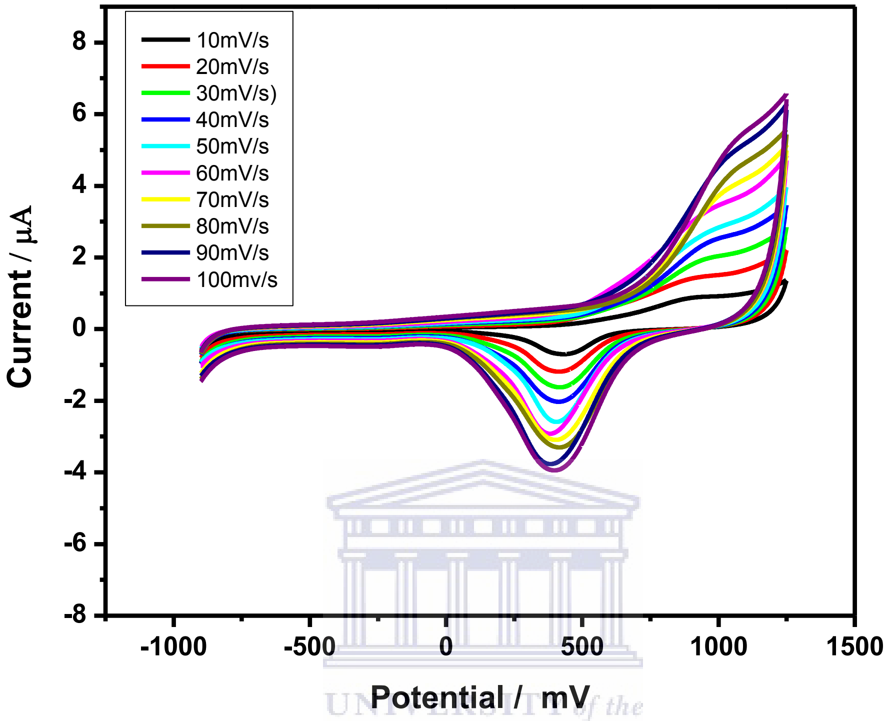

Figure.4.5: *Cyclic voltammetry of Au|G1PPT in 0.1 M LiClO$_4^-$ at different scan rates*

The figure 4.5 above represents the cyclic voltammogram of G1PPT at different scan rates varying from 10 mVs^{-1} to 100 mVs^{-1} and it shows that as the scan rate increases the current intensity also increases therefore proving that as the scan rate is increased, more electric field is generated.

4.1.4 XRD of G1PPT

Figure 4.6 below of G1PPT's diffraction paXRD studiesttern from Powder shows that G1PPT is amorphous as it is expected for all polymers and dendrimers.

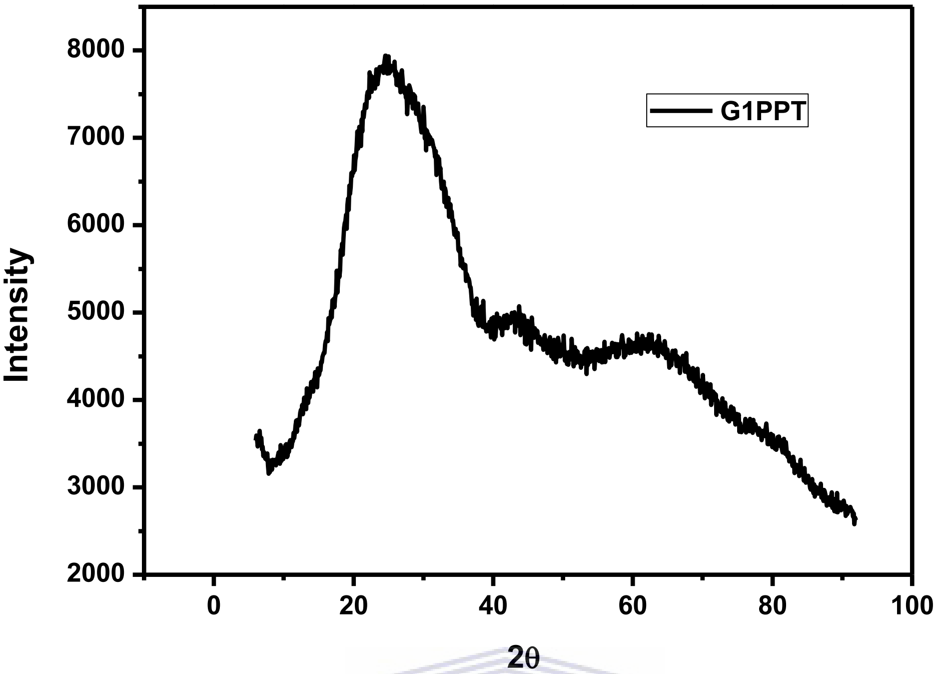

Figure.4.6: *Powder XRD diffraction pattern of G1PPT*

4.1.5 HRSEM of G1PPT

Figure 4.7 below represents the high resolution scanning electron micrograph of G1PPT. The images depicted shows that G1PPT at the nanometer scale has rough globular shape where atoms are aggregated; these images therefore also confirm their amorphous nature.

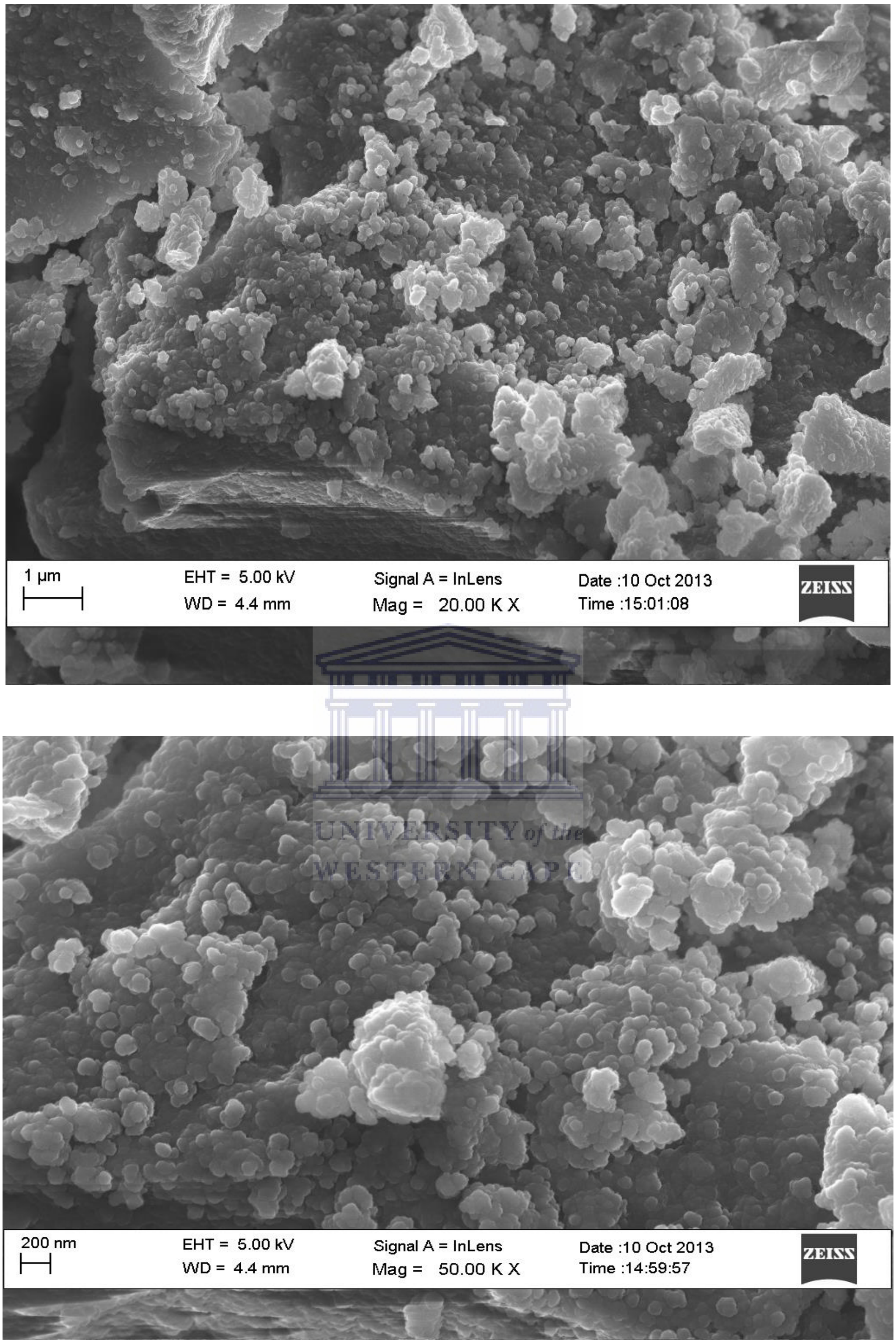

Figure 4.7: *HRSEM images of G1PPT*

4.2 Characterization of G1PPT-co-PEDOT

4.2.1 Fourrier Transform Infrared Spectroscopy of G1PPT-co-PEDOT (FT-IR)

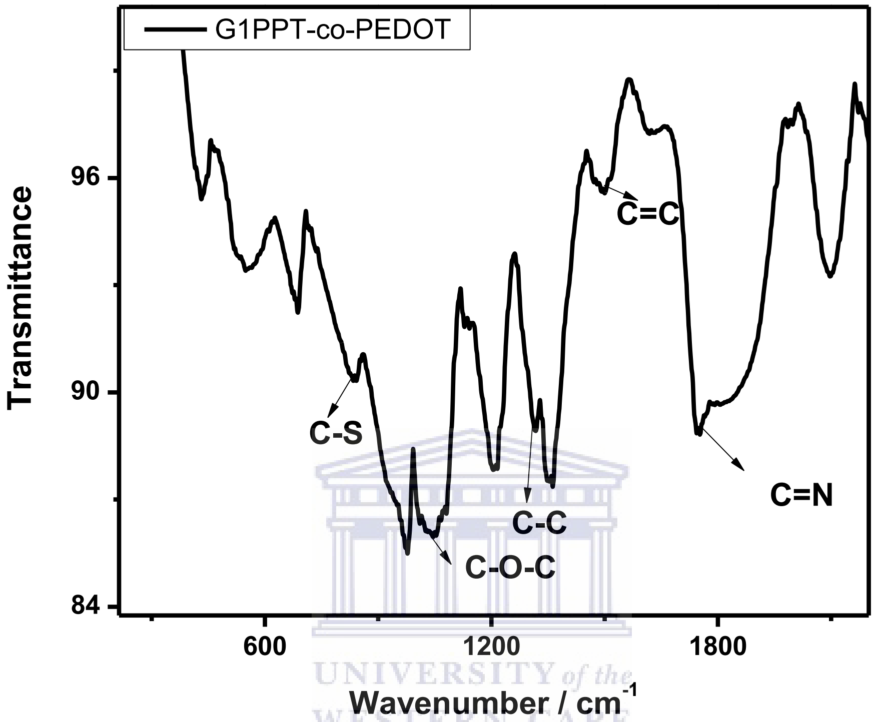

Figure 4.8: *FT-IR spectrum of G1PPT-co-PEDOT*

FT-IR spectrum (figure 4.8) of chemically synthesized G1PPT-co-PEDOT shows a peak at 1747 cm^{-1} corresponding to C=N stretchings in the dendrimer moiety. Strechings at 1504 and 1310 cm^{-1} are assigned to C=c and C-C bonds respectively. At 1050 cm^{-1} is the band due to C-O-C stretching and finally the band at 833 cm^{-1} is due to C-S stretchings in the thiophene ring.

4.2.2 UV-Vis spectroscopy of G1PPT-co-PEDOT

Figure 4.9 below represents the UV-Vis spectrum of G1PPT-co-PEDOT with reference to PEDOT (A) and G1PPT-co-PEDOT with reference to PEDOT and G1PPT (B). As it can be observed and as it is well known polymers in general have a broad absorption peak over a wide spectrum range. So it was highly expected to observe absorption over a wide range. PEDOT spectrum shows a sharp peak at 258 nm assigned to the absorption by C-S chromophore present in the polymer, followed by a broad peak between 400 nm and 600 nm. G1PPT-co-PEDOT on the other hand has a new peak at 357 nm which is accounted for the C-N chromophore present in the dendrimer part of the star copolymer. This peak was already identified when characterizing G1PPT using UV-Vis spectroscopy and this therefore also confirms G1PPT-co-PEDOT was synthesized. The wavelength at which G1PPT-co-PEDOT absorbance is maximal was estimated to be 550 nm which gives rise to an energy band gap of 2.25 eV. This thus confirms that copolymerization of PEDOT to the dendrimer reduced the band gap from 3.79 eV for G1PPT to 2.25 eV for G1PPT-co-PEDOT.

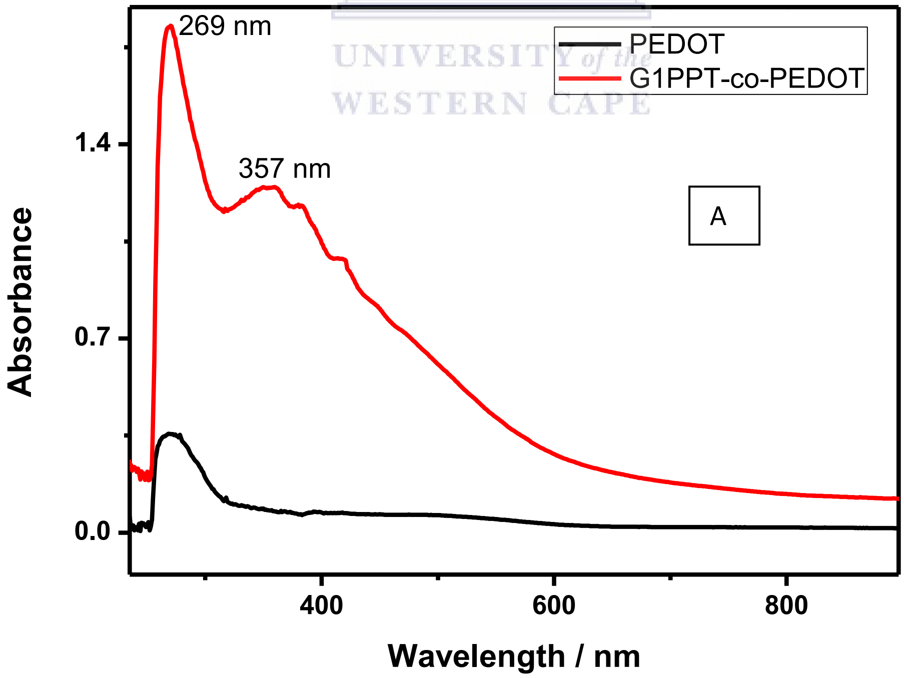

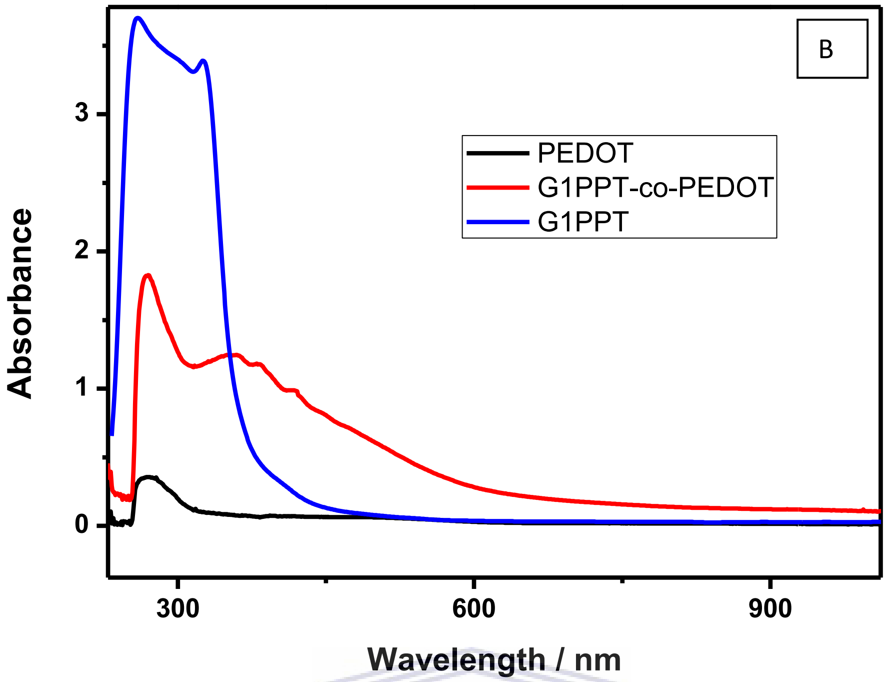

Figure 4.9: *UV-Vis spectra of (A) G1PPT-co-PEDOT and PEDOT and (B) G1PPT-co-PEDOT, G1PPT and PEDOT*

4.2.3 Fluorescence of G1PPT-co-PEDOT

Figure 4.10 below represents the emission spectrum of G1PPT-co-PEDOT. The donor was excited at 480 nm which is the wavelength at which the polymer absorbs light and we observe an emission at 560 nm which corresponds therefore to the relapse of one electron from excited state back to its original ground state.

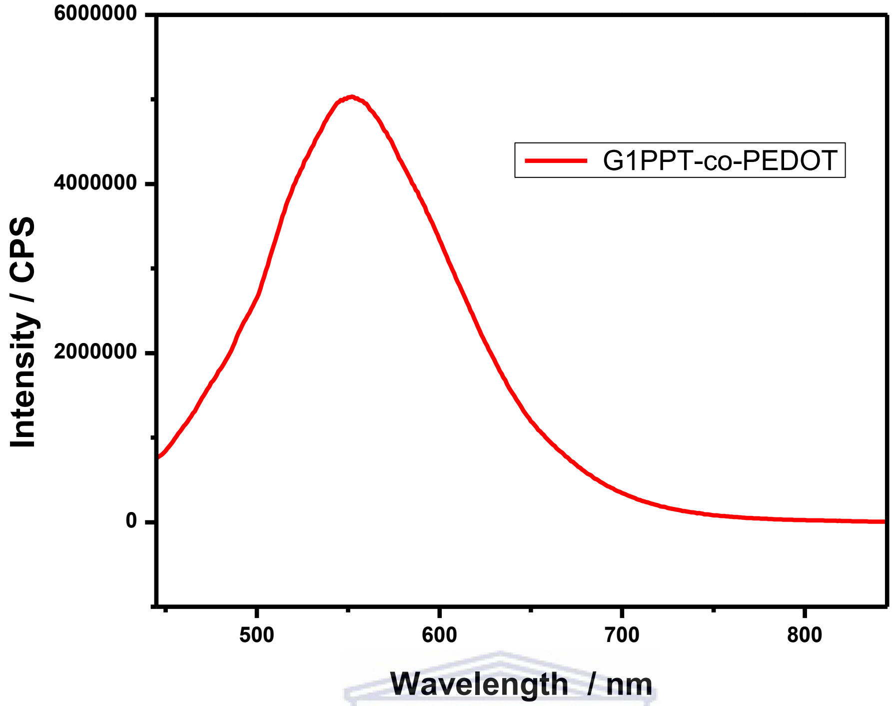

Figure 4.10: *Fluorescence of G1PPT-co-PEDOT*

4.2.4 Electrochemical behaviour of G1PPT-co-PEDOT

a- Cyclic voltammetry of G1PPT-co-PEDOT

Figure 4.11 below shows the cyclic voltammogram of chemically prepared G1PPT-co-PEDOT drop-coated on an Au electrode. On the graph (figure 4.12), two distinct oxidation peaks i_{pa1} and i_{pa2} at 595 mV and -148 mV and two distinct reduction peaks i_{pc1} and i_{pc2} at -51 mV and -503 mV can be observed. The persistence of those peaks when sweeping over the potential range at 100 mV s^{-1} during five cycles therefore confirmed the obtained peaks.

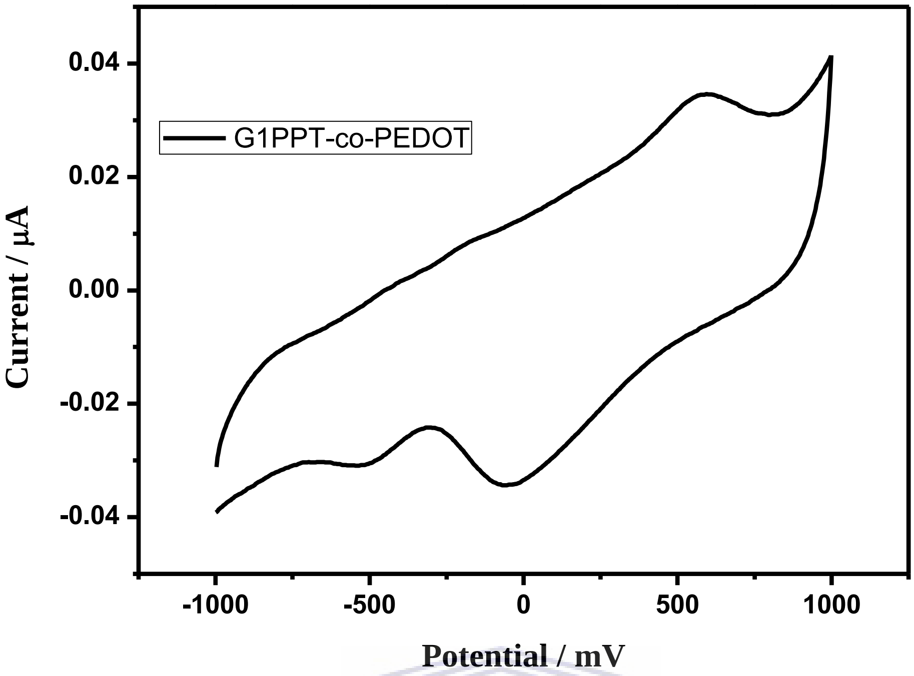

Figure 4.11: *Cyclic voltammetry of G1PPT-co-PEDOT at 100 mV s^{-1}*

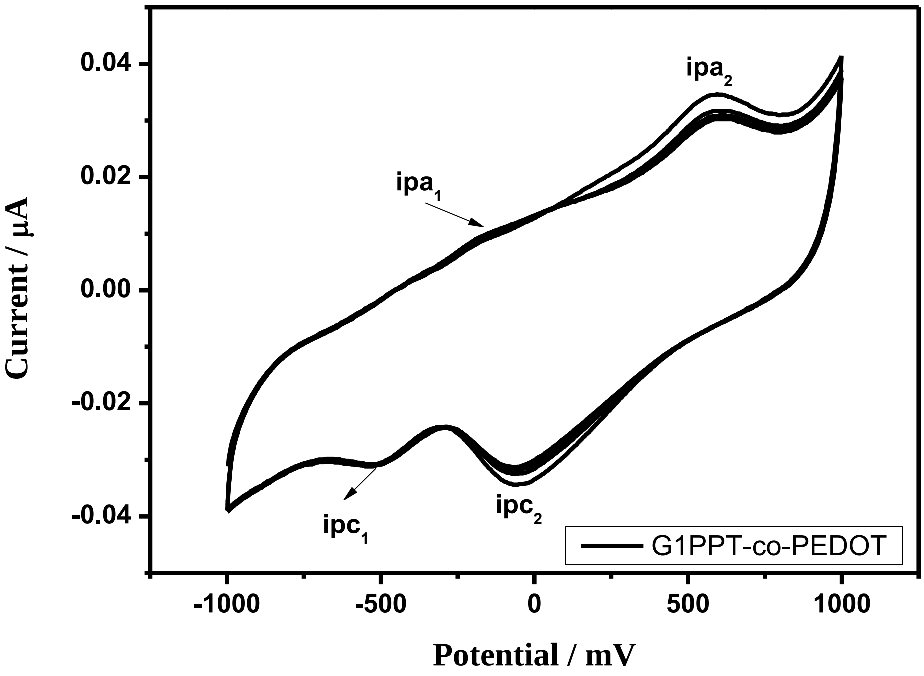

Figure 4.12: *Cyclic voltammetry of G1PPT-co-PEDOT over 5 cycles at 100 mV s^{-1}*

The redox mechanism of the copolymer, depicted in scheme 4.1 below, is as a result of ion transport in and out of the film corresponding to the insertion and removal of an ion in the electrolyte. The anodic and cathodic waves could therefore be explained by incorporation of a counter ion. The ClO_4^- anion incorporates into the copolymer matrix and interacts with the oxidation site of the polymer as counter ion. The electronic rearrangement of the redox reaction process (oxidation and reduction process) involving the removal and incorporation of the counter ion forms a conducting polycation in the presence of the charge-balancing anion as shown in scheme 4.1 .The first redox couple (ipa_1 and ipc_1) can be attributed to the introduction and release of the Li^+ cation while the other redox couple (ipa_2 and ipc_2) is associated to the insertion and release of the ClO_4^- anions respectively (Olowu *et al.*, 2011).

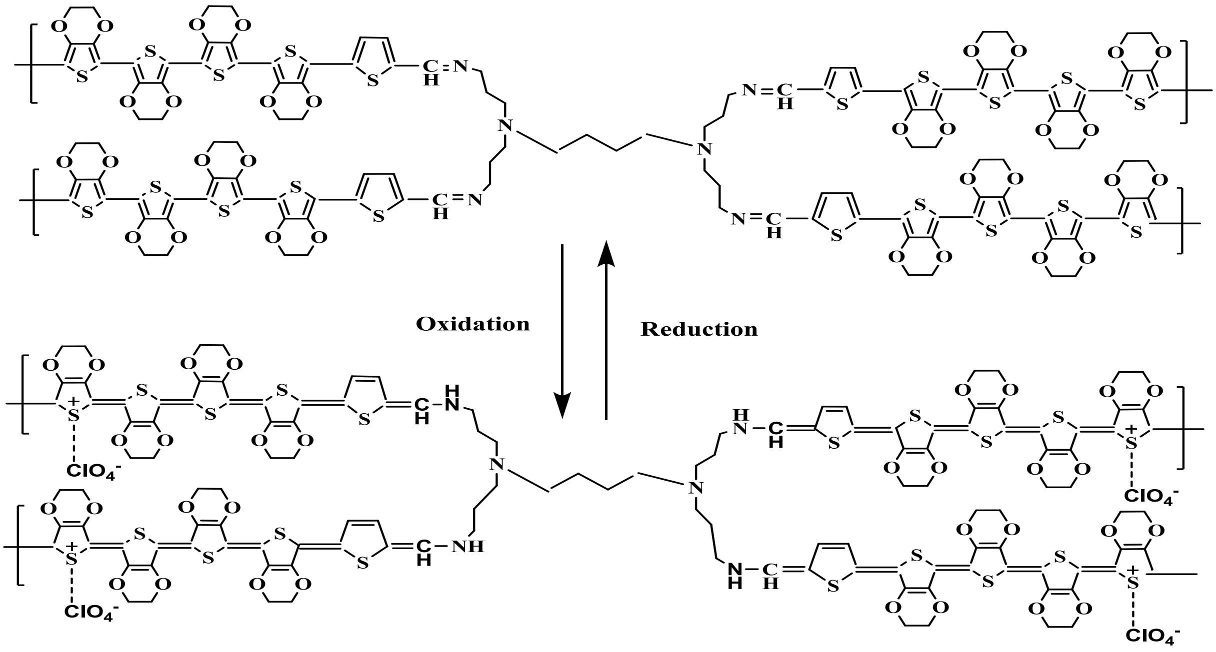

Scheme 4.1: *Redox mechanism of G1PPT-co-PEDOT*

In order to calculate the LUMO level of G1PPT-co-PEDOT, we used the same method used by Dong *et al*., (2009) whereby from the cyclic voltammogram we determined E_{red} onset potential and we use the equation expressed below. On the other hand, to calculate the HOMO level, we made use of the band gap value E_g obtained from the UV-Vis absorption properties of NDI, whereby we subtracted the calculated LUMO value from $E_{g.}$ See table 4.3 below.

Table 4.1: Summary of HOMO, LUMO and E_g values of G1PPT-co-PEDOT

Scan Rate / mV s^{-1}	100
E_{pa} / V	0.595
E_{pc} / V	-0.051
ΔE_p / mV	646
$E_{red,\ \mathrm{onset}}$ / V	-0.769
E_g / eV	2.256
LUMO / eV	-4.031
HOMO / eV	-6.287

Where,

LUMO = - ($E_{red,\ onset}$+ 4.8) eV, and

HOMO = - (E_g - LUMO) eV

4.2.5 HRSEM and EDX of G1PPT-co-PEDOT

G1PPT images presented amorphous globular aggregates both at micrometer and nanometer level, but in the case of G1PPT-co-PEDOT; we observed some amorphous packed sheets with some growth observed at the micrometer level (Figure 4.13). This growth can be associated to polymer growing at the surface of the dendrimer.

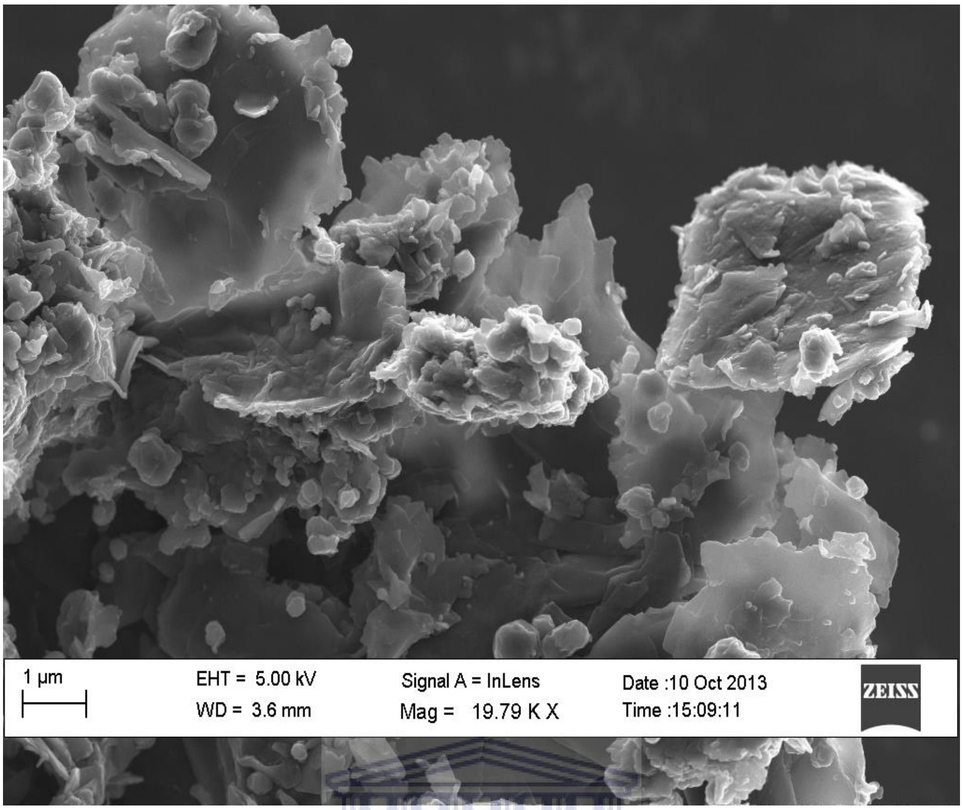
1 µm
EHT = 5.00 kV
WD = 3.6 mm
Signal A = InLens
Mag = 19.79 K X
Date :10 Oct 2013
Time :15:09:11
ZEISS

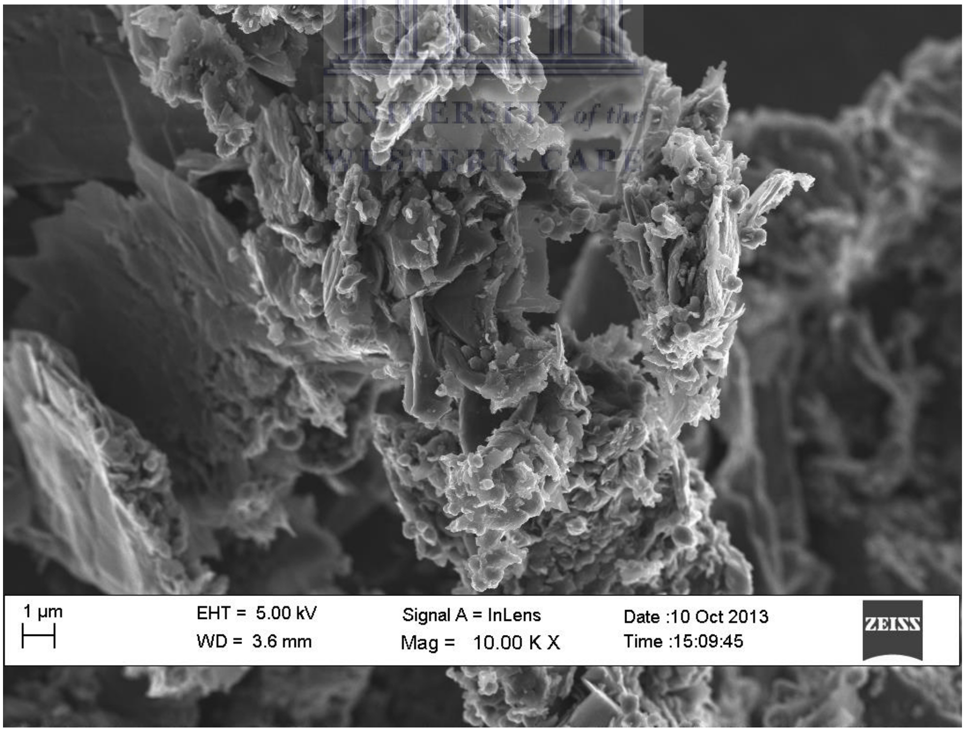
1 µm
EHT = 5.00 kV
WD = 3.6 mm
Signal A = InLens
Mag = 10.00 K X
Date :10 Oct 2013
Time :15:09:45
ZEISS

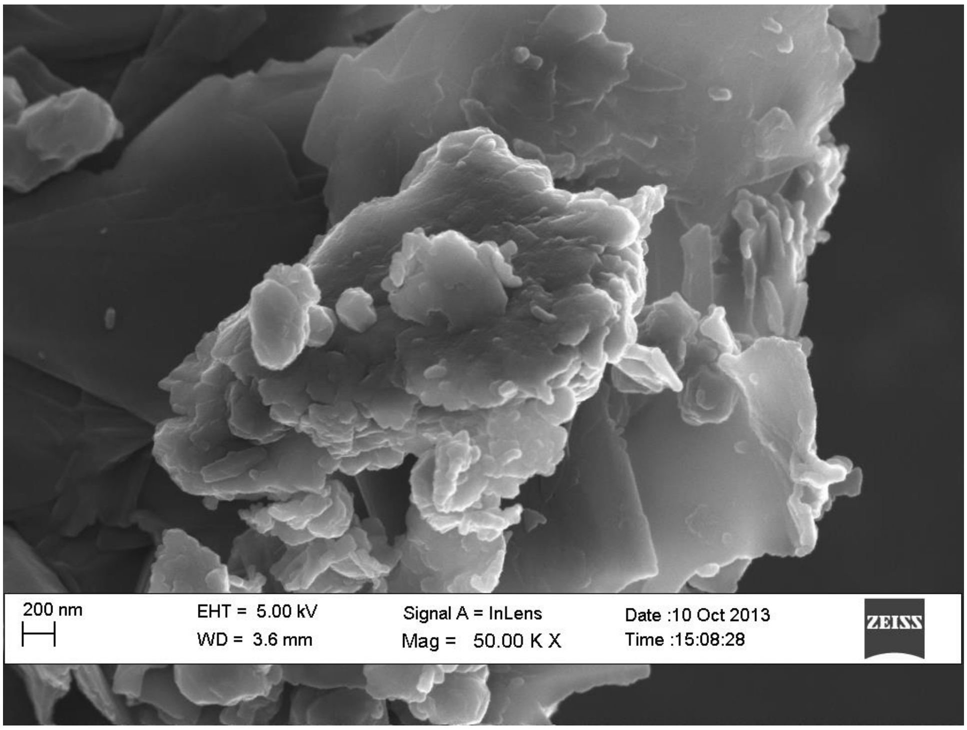

Figure 4.13: *HRSEM images of G1PPT-co-PEDOT*

Figure 4.14 below shows the elemental composition of G1PPT-co-PEDOT which proves that all the atoms expected to be found in the chemical formula of G1PPT-co-PEDOT are present.

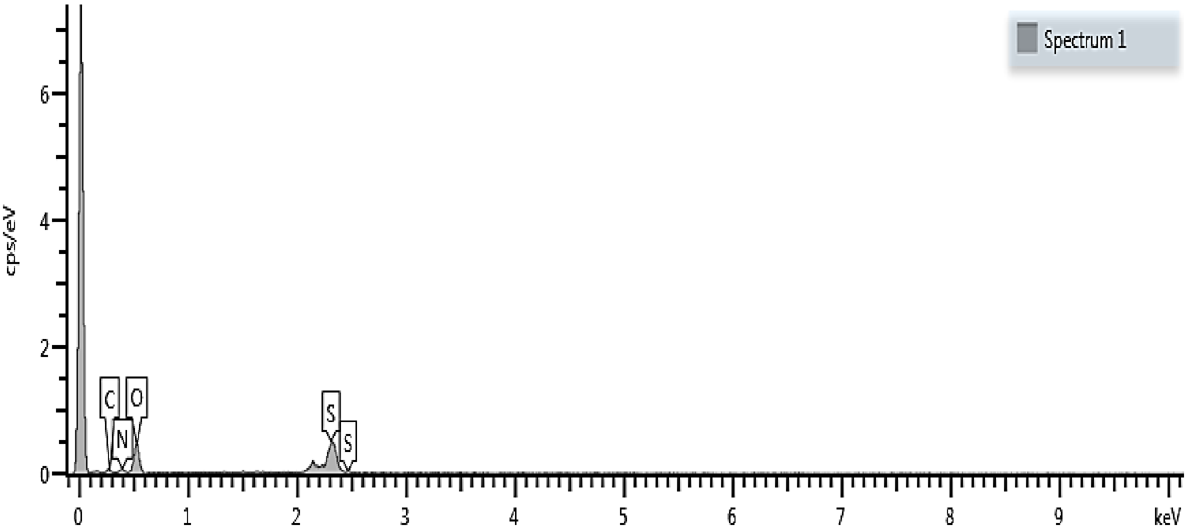

Figure 4.14*: Elemental composition of G1PPT-co-PEDOT*

4.2.6 XRD of G1PPT-co-PEDOT

Figure 4.15 below represents the powder XRD diffraction pattern of G1PPT-co-PEDOT. The diffraction pattern of G1PPT showed that it was amorphous and the same result was obtained for the diffraction pattern of PEDOT. It was therefore expected that G1PPT-co-PEDOT would be highly amorphous as expected for polymers which is confirmed by these XRD results.

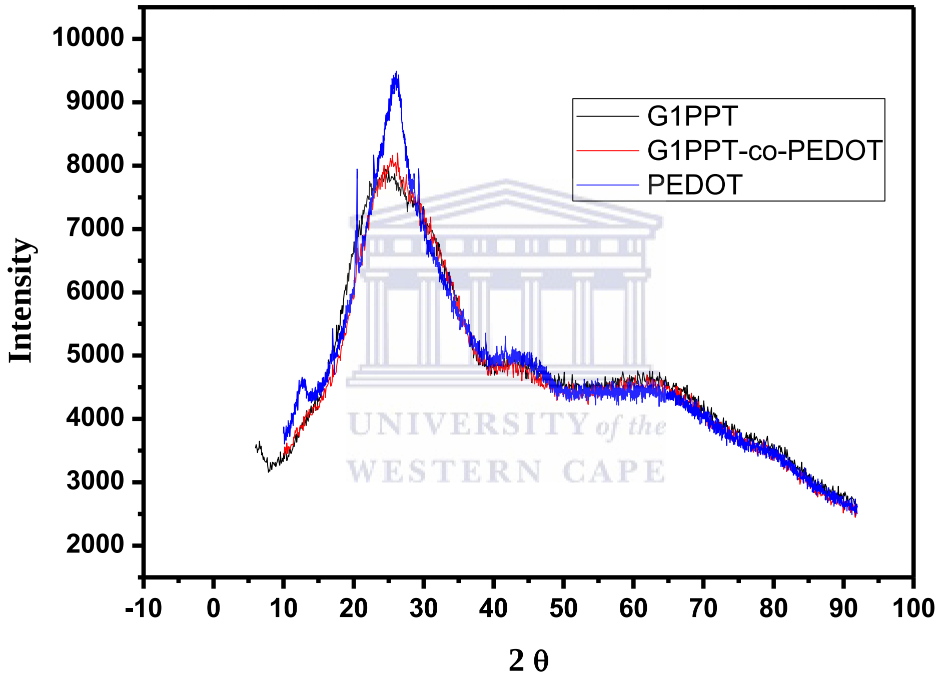

Figure.4.15: *Diffraction pattern of G1PPT, PEDOT and G1PPT-co-PEDOT*

4.3 Characterization of N, N-diidopropylnaphthalnediimide (NDI)

4.3.1 Fourrier Transform Infrared spectroscopy of NDI (FT-IR)

Figure 4.16 below represents the FT-IR spectrum of NDI characterized by bands at 735, 767, 887, 1072, 1142, 1247, 1325, 1653, 1698, 2932 and 2978 cm^{-1} among which the bands at

2932 and 2978 cm^{-1} correspond to the C-H stretchings, and the bands at 1698, 1653 and 1325 cm^{-1} are due to C=O, C-N and C=C stretchings respectively.

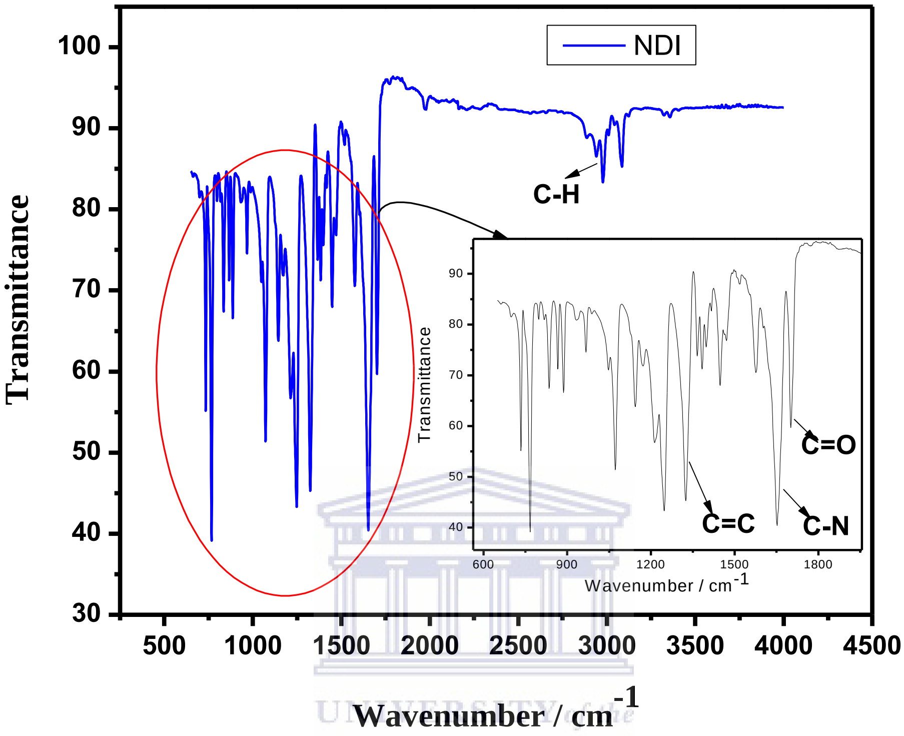

Figure 4.16: *FTIR spectrum of NDI*

4.3.2 UV-Vis Spectroscopy of NDI

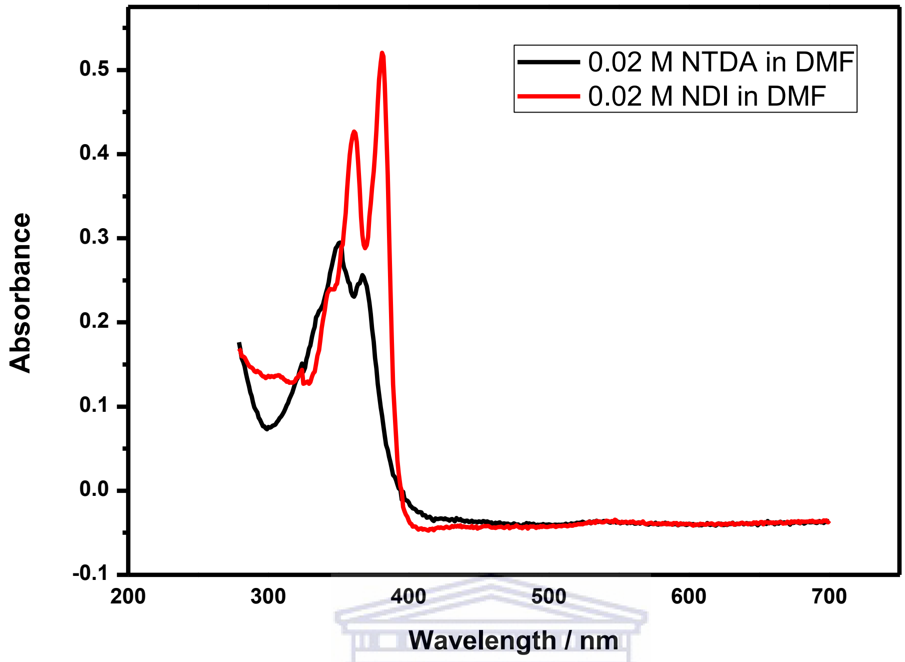

Figure.4.17: *UV-Vis Spectra of NTCDA and NDI in N, N-dimethylformamide*

Once NDI was synthesized and analysed using FT-IR spectroscopy, the next step was the optical analysis of our acceptor material. Because the acceptor starting material NTCDA was only soluble in DMF, we had to study both NTCDA and NDI optical properties in DMF in order to check if there was a difference in their absorbance properties and therefore conclude that a new material was synthesized. So as can be seen on figure 4.17 above, for the same concentration of NTCDA and NDI, 0.02 M in DMF we observe a shift in absorption peaks. Indeed, with NTCDA there are two main peaks at 350 nm and 367 nm with a small shoulder at 335 nm and those peaks can be assigned to C-O, C=O and C=C bonds respectively; whereas with NDI, there is a wavelength shift for all absorption peaks. The shoulder observed at 335 nm for NTCDA is now found at 344 nm for NDI; and instead of the two peaks at 350 nm and 367 nm, we now have two stronger peaks at 360 nm and 380 nm.

These optical properties of NDI were confirmed when analysed in DCM as shown in figure 4.18 below. Indeed, we observed the same peaks already found when NDI was studied in DMF which are in agreement with the work reported by Bhosale *et al.*, (Bhosale *et al.*, 2008). And we were now able to assign the peaks to the different chromophores in NDI. The two peaks at 380 nm and 360 nm are characteristics of the absorbance of the chromophores C=O and C=C whose peaks are results of $\pi-\pi*$ transitions. Also the small peak at 344 nm could be as a result of n - σ* transition within the C-N chromophore with band gap energies of 3.27 eV, 3.45 eV and 3.61 eV respectively calculated using the same equation as for the optical analysis of G1PPT.

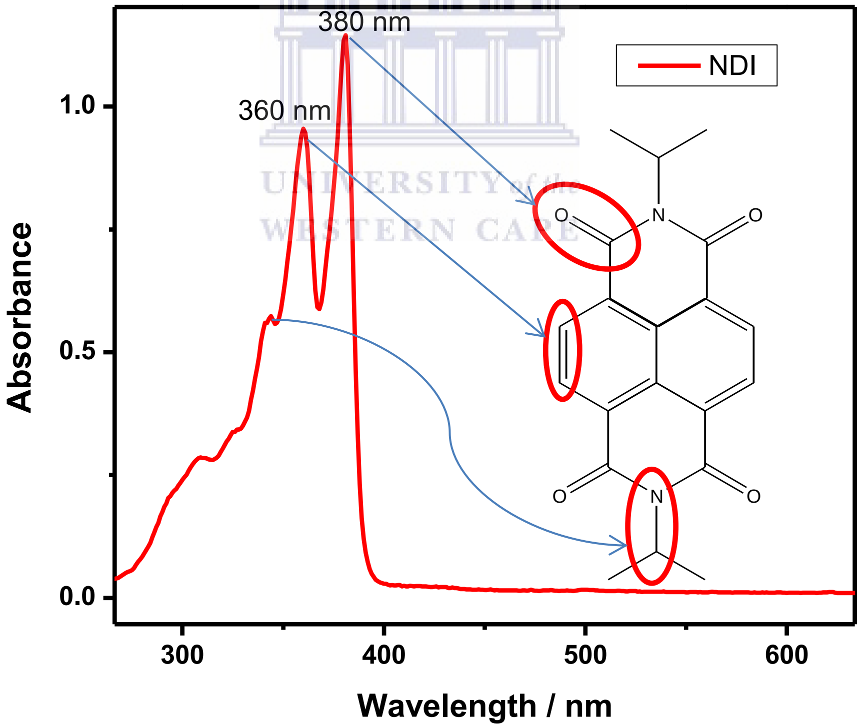

Figure 4.18: *UV-Vis spectrum of NDI in dichloromethane*

Then, NDI optical properties were studied in other solvents; the main reason being that there was no specific knowledge on which solvents will be suitable for both donor and acceptor material for the fabrication of the bulk heterojunction layer. Among the various solvents, chloroform was used based on the fact the donor starting material G1PPT dissolves in chloroform. Light absorption properties of NDI were also studied in DMSO, based on the fact that the donor G1PPT-co-PEDOT could only be soluble in DMSO. The main observation which can be made is that, the absorption properties of NDI studied at same concentrations are very low in DMSO as can be seen from looking at figure 4.19 A, B and C below. For absorbance values of 2.11 and 2.20 for the peaks at 360 nm and 380 nm respectively of 0.1 M NDI in both DCM and chloroform, we observe absorbance values of 0.48 and 0.51 only for the same concentration in DMSO.

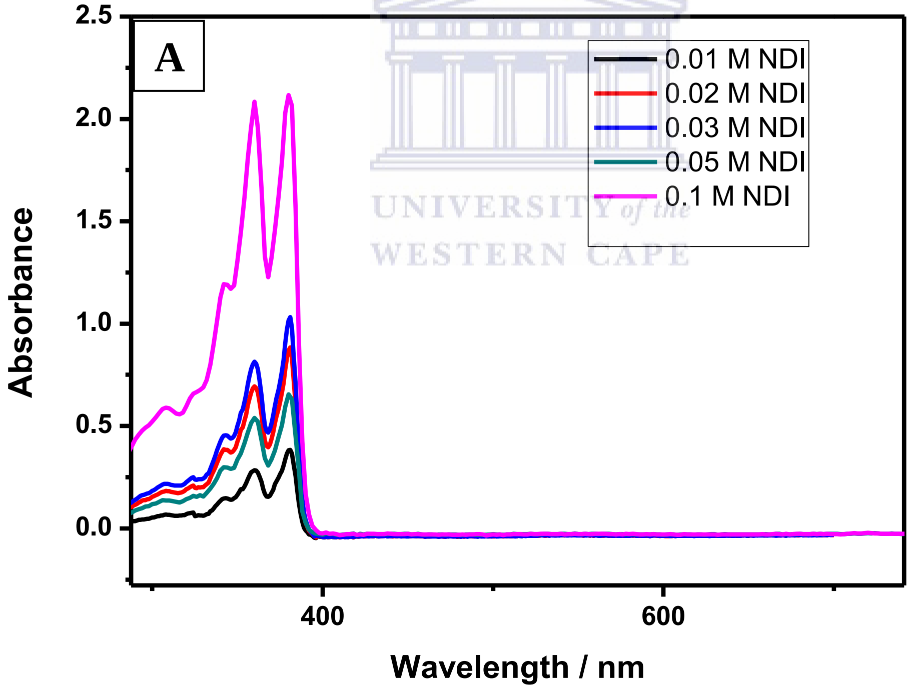

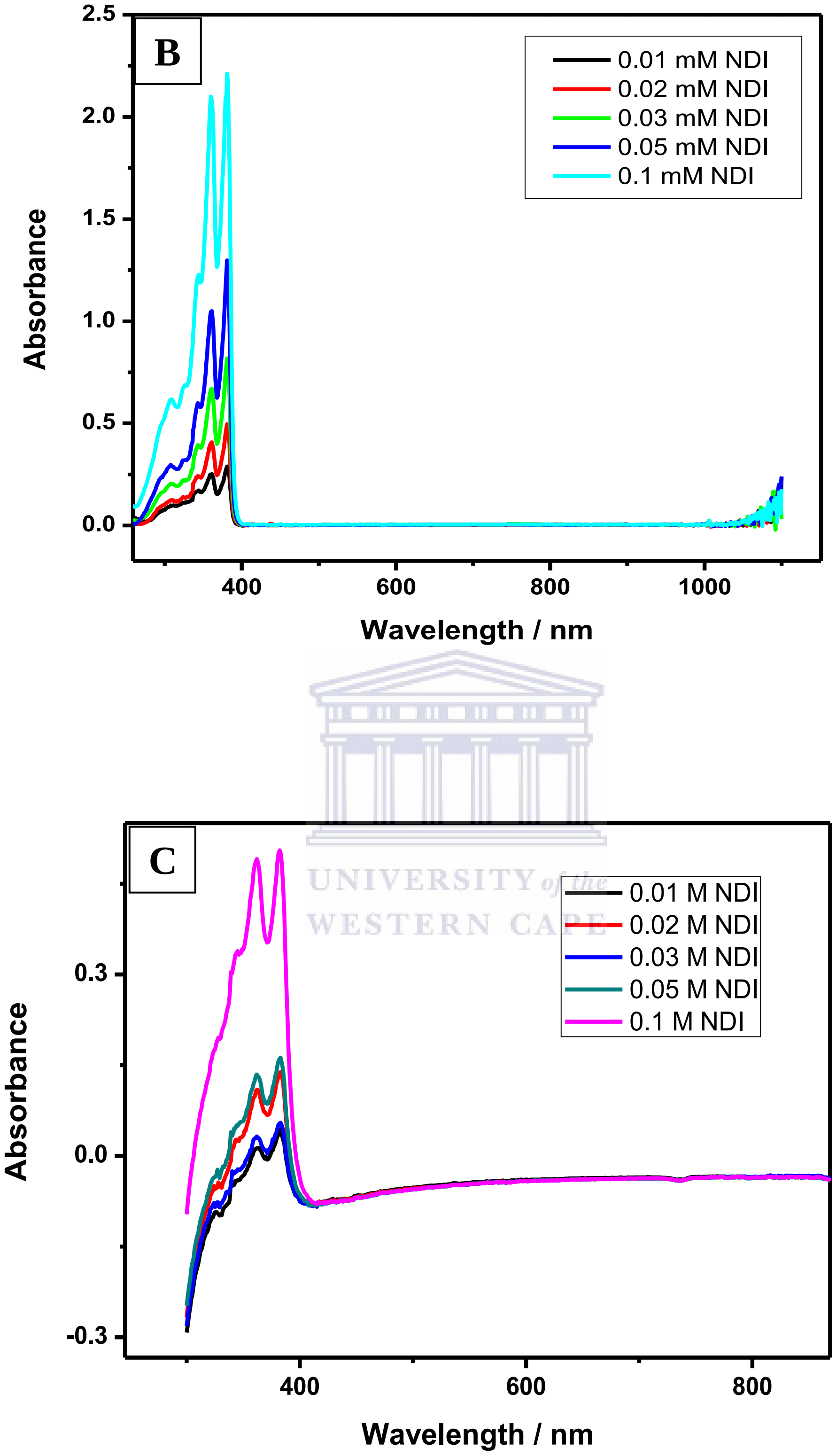

Figure.4.19: *UV-Vis Spectra of NDI in (A) DCM, (B) CHCl$_3$ and (C) DMSO at different concentrations*

4.3.3 Fluorescence Spectroscopy of NDI

Photoluminescence also referred to as fluorescence as it is well known, arises as a result of a relaxation of one or more excited electrons from higher energy conduction band to lower energy valence band. As such, it is expected from most of the materials which are able to absorb photons and jump from valence band to conduction band, to also be able to lose that energy and therefore decay back to the valence band and by doing such, those materials emit some light. To study the photoluminescence properties of NDI, we excited it a 360 nm and we observed three (3) distinct emission peaks at 390 nm, 408 nm and 433 nm as represented on figure 4.20 below. Also, Figure 4.21 below represents the normalized spectra of absorption (for an emitting wavelength of 408 nm) and emission spectra of NDI.

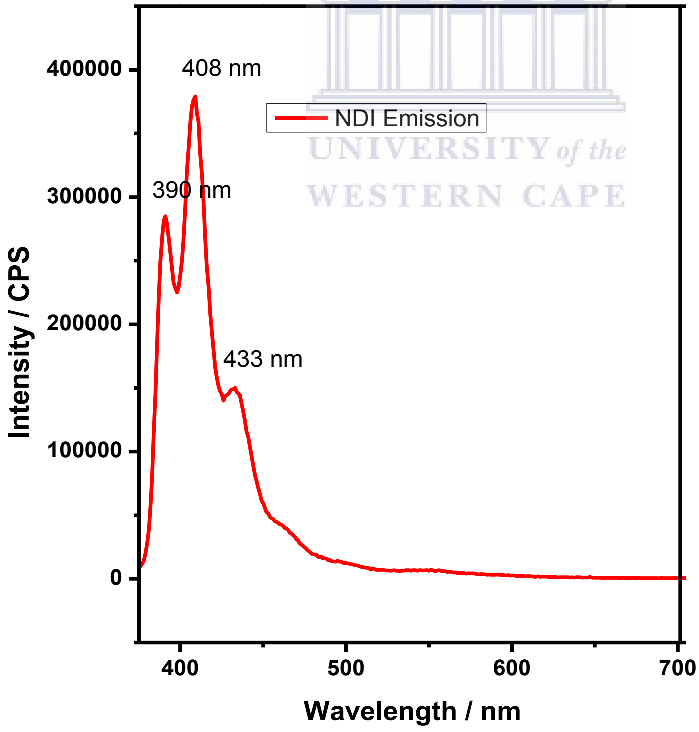

Figure 4.20: *Fluorescence Spectrum of NDI in DMSO*

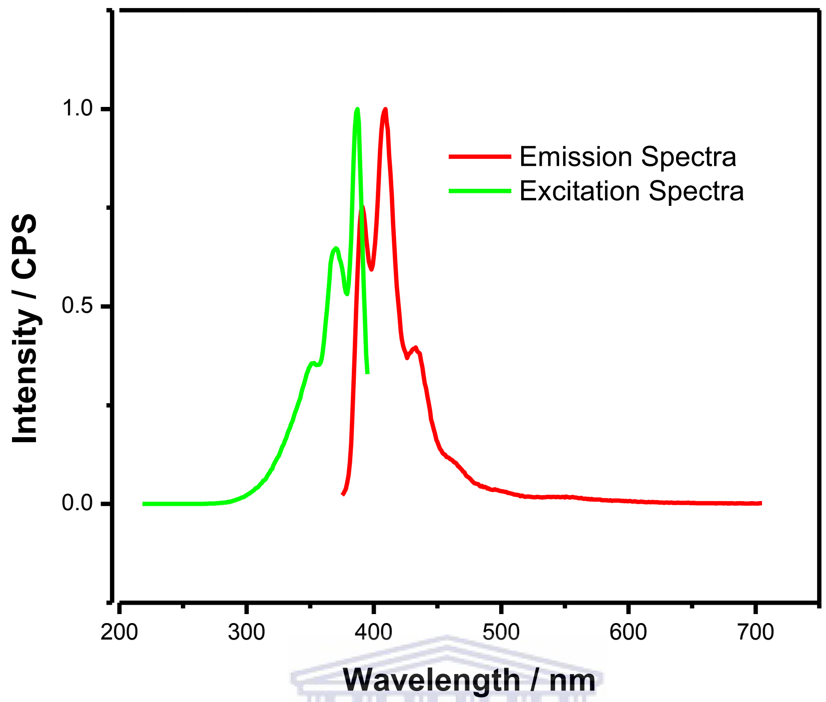

Figure 4.21: *Normalized Emission and Excitation spectra of NDI in DMSO*

4.3.4 Electrochemical behaviour of NDI

a- Cyclic Voltammetry of NDI

When studying the electrochemical properties of NDI, it is was with the aim of investigating if NDI was able to successfully undergo a redox reaction and how many electrons were gained and lost during the mechanism. It was also a way to be able to determine the HOMO and LUMO levels of the acceptor material. Indeed, figure 4.22 below presents the voltammogram of 1 mM NDI in DCM (0.1 M Bu_4NPF_6) within a potential range of (-1600) – (-500) mV with respect to the bare Pt electrode as a baseline, with a scan rate of 100 mVs^{-1}. It was observed that NDI undergoes two distinct one-electron transfer processes corresponding to the reduction of NDI into NDI^- and of NDI^- to the dianion NDI^{2-} giving rise to the two redox couples NDI/NDI^- and NDI^-/NDI^{2-}

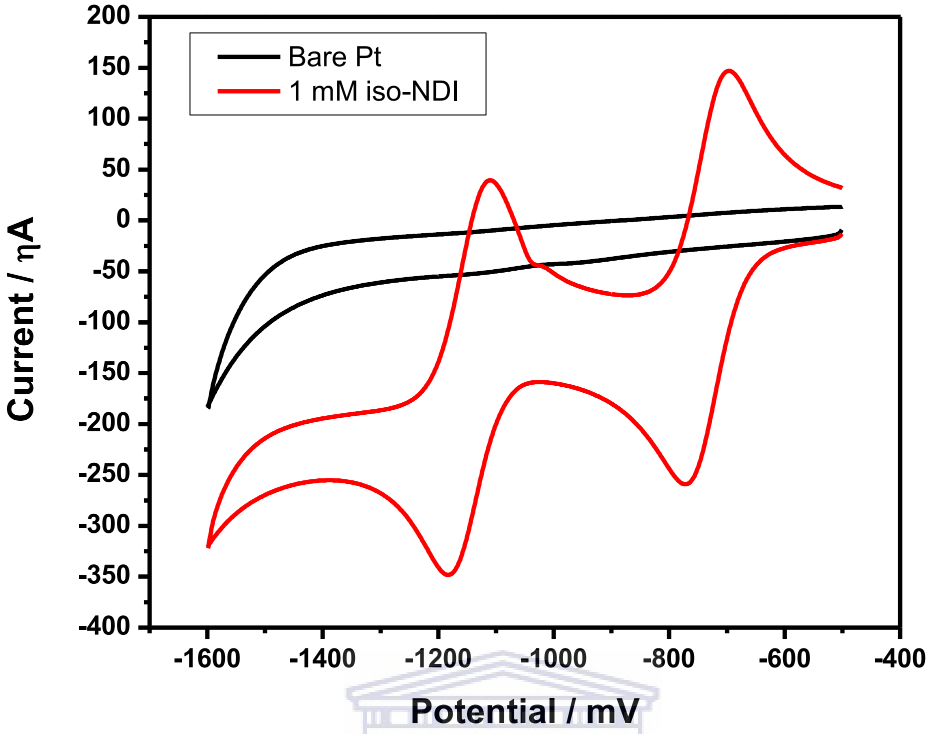

Figure.4 22: *Cyclic voltammetry of Pt bare electrode and 1mM NDI in* CH_2Cl_2 *(0.1 M* Bu_4NPF_6*)*

The following redox mechanism represents the electron transfer going on during cyclic voltammetry.

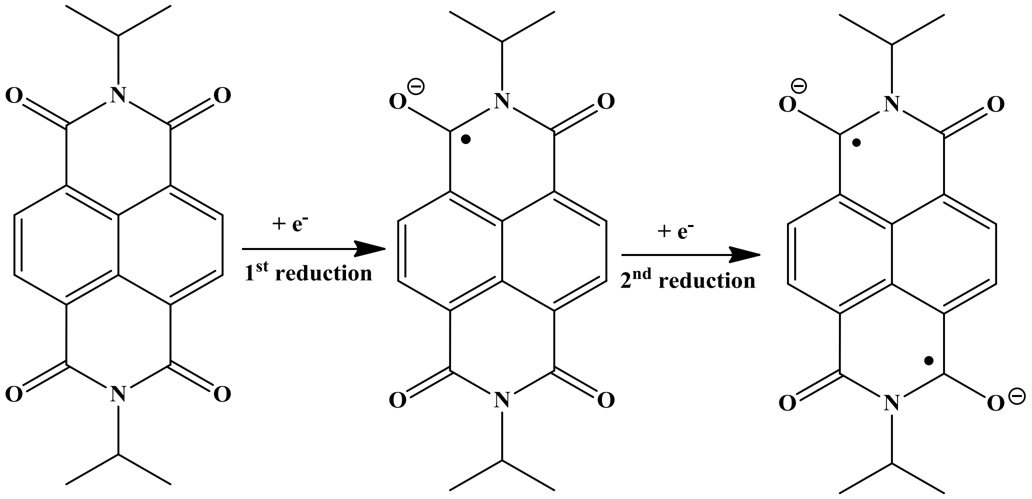

Scheme 4.2: *Reduction mechanism of NDI to* NDI^{-} *and from* NDI^{-} *to the dianion* NDI^{2-}

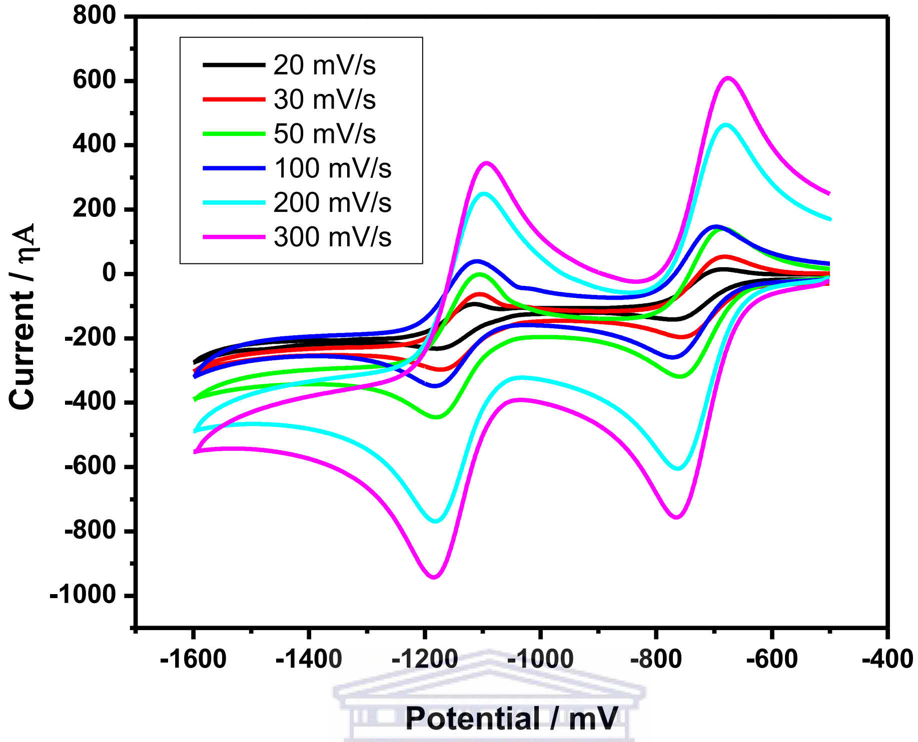

Figure 4.23: *Cyclic voltammetry of NDI at different scan rates*

Above, in figure 4.23 are the cyclic voltammograms of NDI at different scan rates and below is the table summarizing the oxidation and reduction peaks, as well as the change in potential, ΔE_p and the formal potential $E^{o'}$. From the table, we can see that the change in potential for first and second redox couples is ΔE_p ~ 59 mV at low scan rates which therefore enables us to confirm the idea that NDI undergoes two distinct reversible one-electron processes. Whereas at scan rates higher or equal to 100 mV s^{-1}, $\Delta E_p > 60$ mV and allows us to conclude that at those potentials the redox reactions are quasi-reversible.

Table 4.2: Summary of oxidation and reduction potentials, ΔE_p and $E^{o'}$ of 1 mM NDI in CH_2Cl_2 (0.1 M Bu_4NPF_6) at different scan rates.

Scan rate / mV s^{-1}		E_p^{ox} / mV	E_p^{red} / mV	ΔE_p / mV	$E^{o'}$ / mV
20	1st	-693	-752	59	-722.5
	2nd	-1110	-1170	60	-1144.5
30	1st	-690	-749	59	-716.5
	2nd	-1106	-1166	60	-1136
50	1st	-694	-753	59	-718.5
	2nd	-1108	-1168	60	-1141
100	1st	-699	-767	68	-731
	2nd	-1108	-1180	72	-1144
200	1st	-680	-760	80	-720
	2nd	-1096	-1180	84	-1138
300	1st	-694	-762	68	-728
	2nd	-1094	-1180	86	-1138

The reversible electron transfer properties of NDI at lower scan rates were also confirmed by plotting change in potential ΔE_p versus log of scan rate, $\log \upsilon$ whereby we were able to observe that for scan rates between 20-50 mV s^{-1} the graph is linear, see figure 4.24 below.

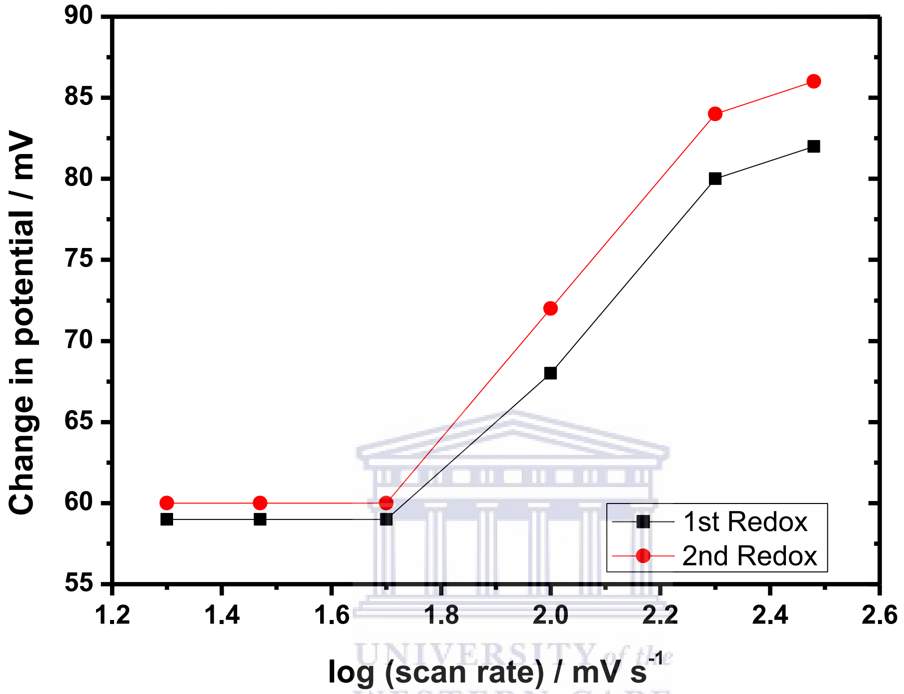

Figure 4.24: *Plot of ΔE_p versus $\log \upsilon$ for first and second redox couples of NDI*

Also from Table 4.2 above, we were also able to draw the graph depicted in figure 4.25 representing formal potentials versus scan rate and we found that, as the values were predicting the half-wave potential is independent on the scan as it is expected for reversible systems.

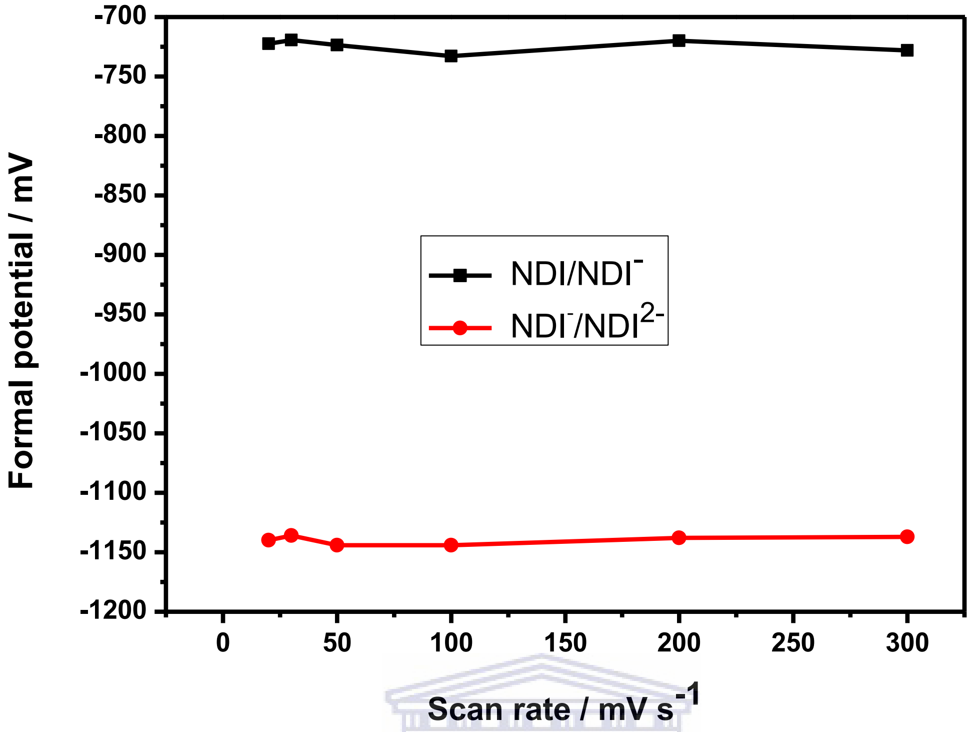

Figure 4.25: *Formal potential values versus scan rates of NDI*

Table 4.3: Summary of oxidation and reduction peak currents of NDI versus square root of scan rate

Scan rate / mV s^{-1}	**(Scan rate)$^{1/2}$ / $mV^{1/2}$ $s^{-1/2}$**		**I_p^{ox} / ηA**	**I_p^{red} / ηA**
20	4.47	1st	6.17	-135
		2nd	-101.75	-222.20
30	5.47	1st	-52.87	-196.17
		2nd	-61.28	-296.83
50	7.07	1st	146	-256.36
		2nd	-1.10	-343.52
100	10	1st	146	-316.55
		2nd	39.40	-444.18
200	14.14	1st	462	-606.06
		2nd	234.50	-766.90
300	17.32	1st	617	-746.14
		2nd	348.60	-941.23

A plot of peak current versus root of scan rate (Figure 4.26) shows that the anodic or oxidation peak currents increase with scan rate whereas the cathodic or reduction peak currents decrease for both redox couples.

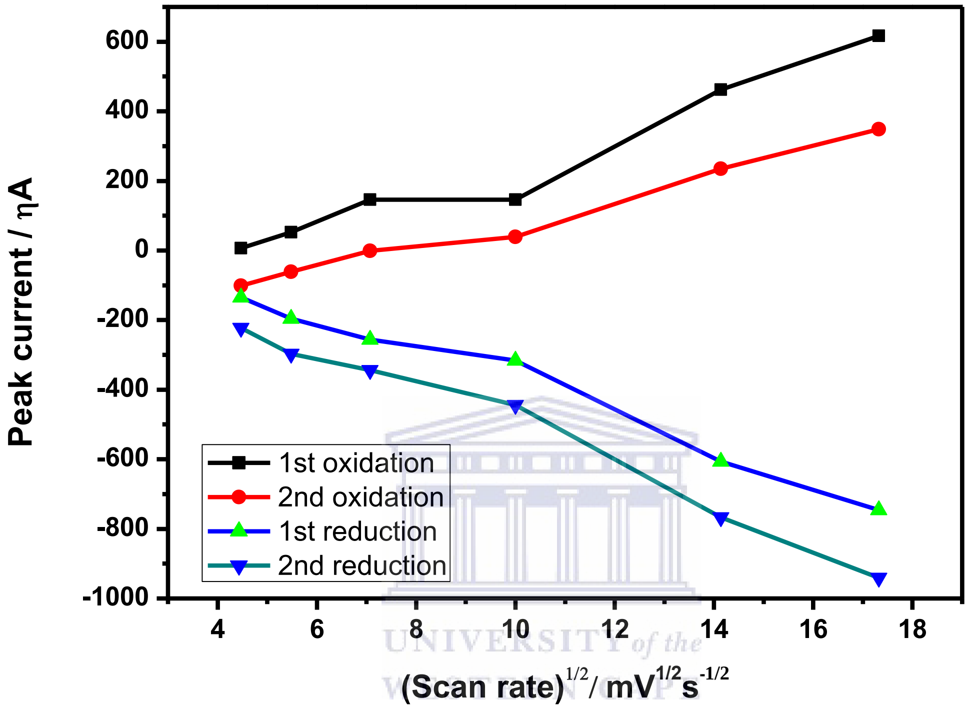

Figure 4.26: *Peak current, I_p vs square root, $(\upsilon)^{1/2}$ of scan rates of NDI*

In order to calculate the LUMO level of NDI, we applied the same method used by Dong *et al.*, 2009 whereby from the cyclic voltammogram we determined E_{red} onset potential. On the other hand, to calculate the HOMO level, we made use of the band gap E_g obtained from the UV-Vis absorption properties of NDI, whereby we subtracted the calculated LUMO value from E_g. See Table 4.4 below.

Table 4.4: Summary of HOMO, LUMO and E_g values of NDI

Scan Rate / mV s^{-1}	100
E_{pa} / V	-0.693
E_{pc} / V	-0.752
ΔE_p / mV	59
E_{red} onset / V	-0.498
E_g / eV	3.27
LUMO / eV	-4.302
HOMO / eV	-7.572

Where,

LUMO = - (E_{red} onset + 4.8) eV,

HOMO = - (E_g - LUMO) eV

b- O-Square Wave Voltammetry of NDI

OSWV of NDI was swept from -500 mV to -1600 mV back and forth and figure 4.27 below therefore represents the forward (A) (oxidation) and reverse (B) (reduction) square wave voltammograms of NDI which enables us to confirm the two oxidation and two reduction peaks obtained from the NDI's CV.

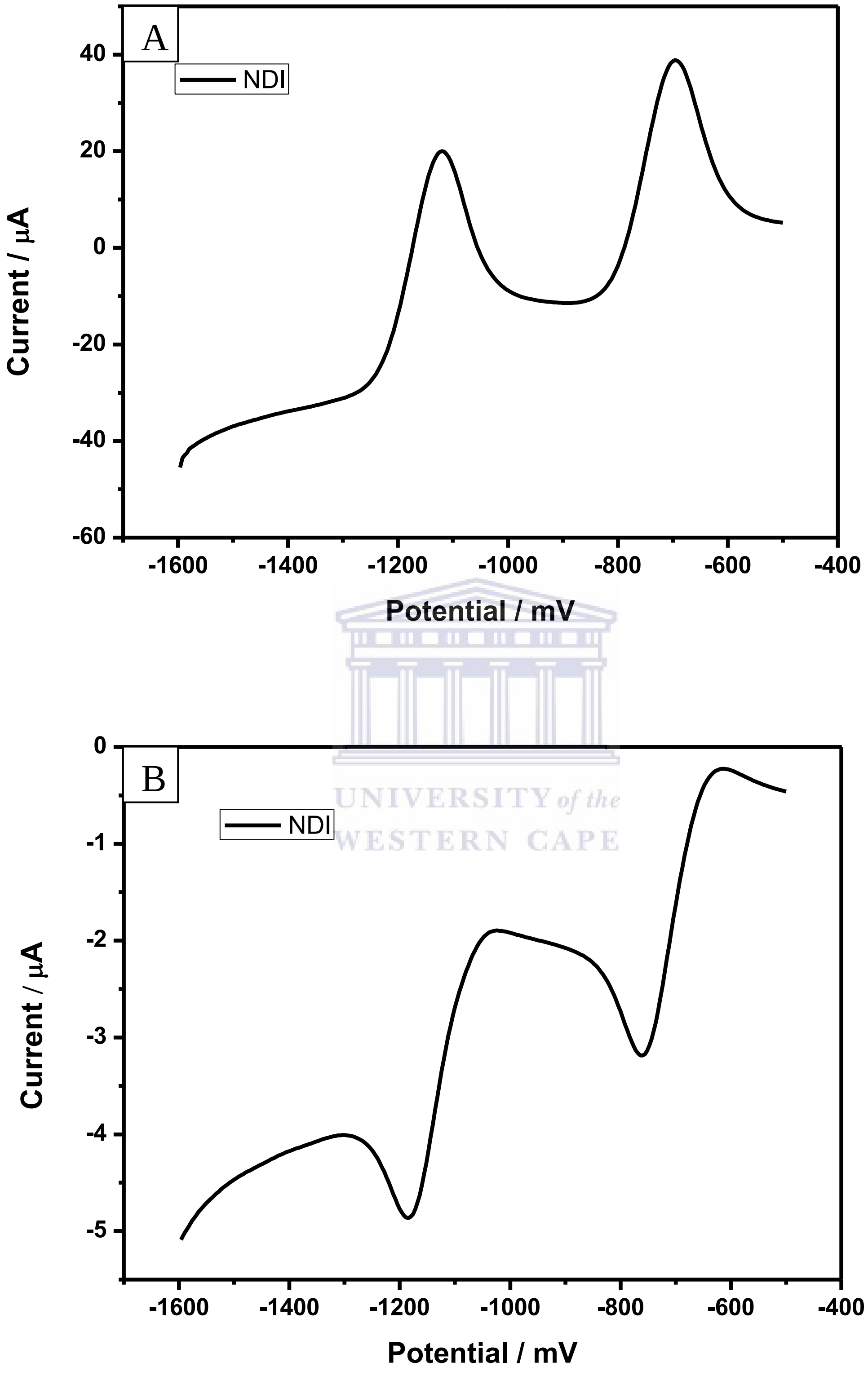

***Figure. 4.27:* *(A)* *Forward and* *(B)* *reverse OSWV of 1 mM NDI in* CH_2Cl_2 *(0.1 M* Bu_4NPF_6*)*

4.3.5 HRSEM and EDX of NDI

The HRSEM images of NDI (Figure 4.28) show highly pure rectangular shapes in the micrometer range. These images prove of the highly crystalline nature of the prepared NDI; which will be further confirmed by Single crystal XRD diffraction pattern.

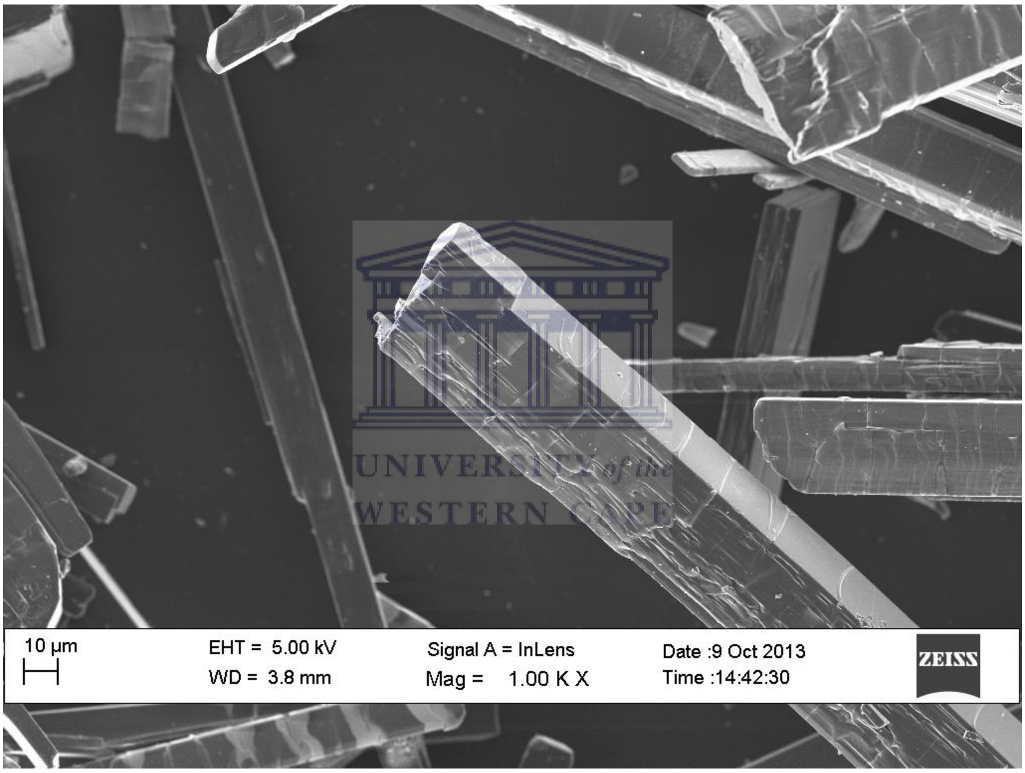

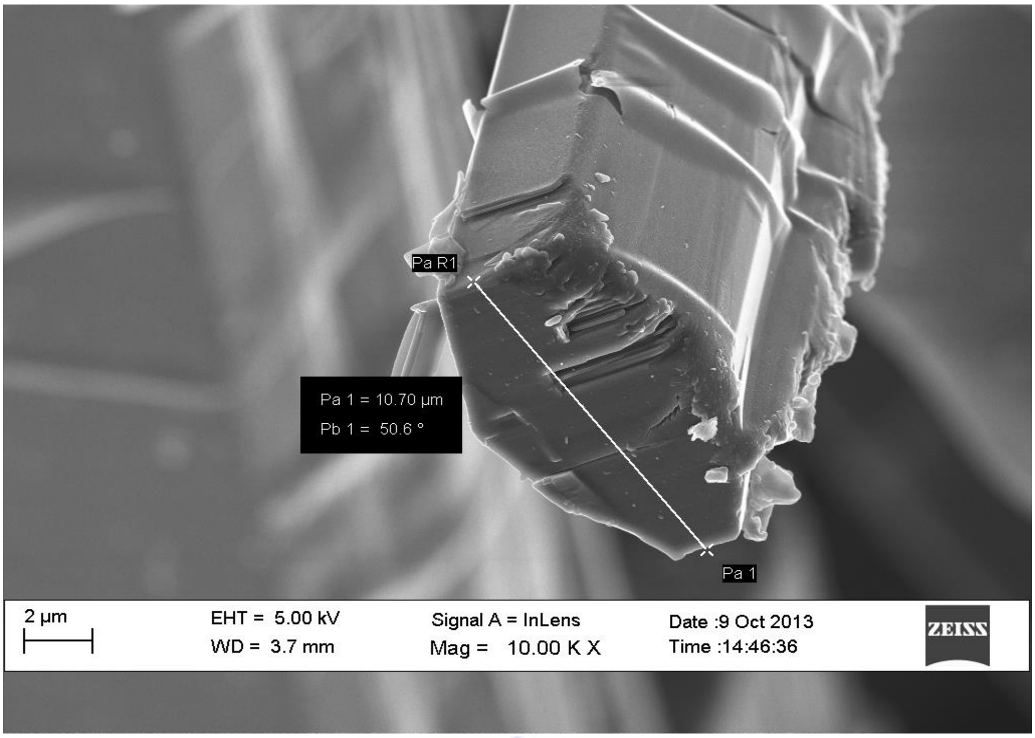

Figure 4.28: HRSEM images of NDI

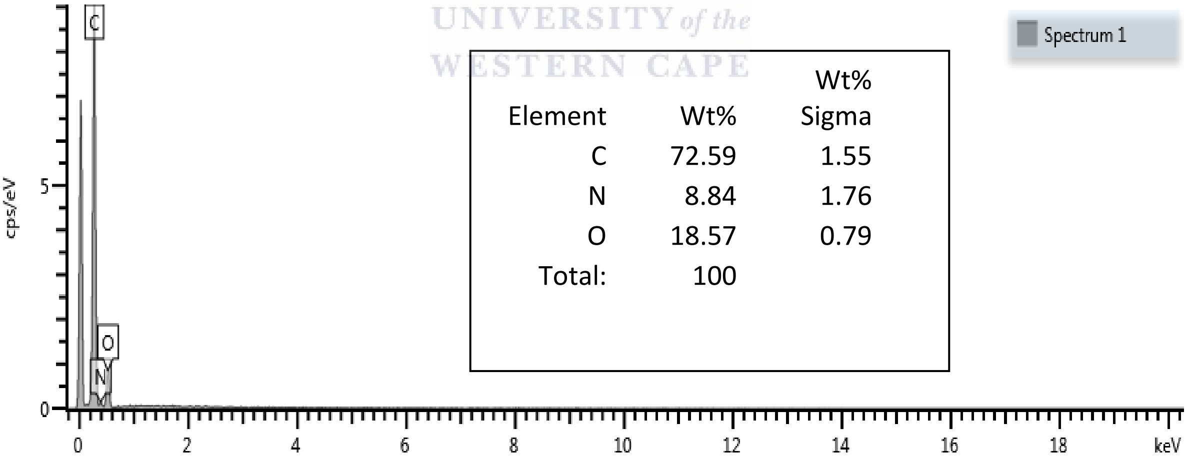

Element	Wt%	Wt% Sigma
C	72.59	1.55
N	8.84	1.76
O	18.57	0.79
Total:	100	

Figure 4.29: Chemical Composition spectrum of NDI

Based on the molecular formula of NDI and from a theoretical assumption, the percentage of each atom with respect to other atoms in the molecule was supposed to be as follows: N: C = 1: 10; N: O = 1: 2 and C: O = 1:5. From the EDX results (Figure 4.29) we obtained the following ratios N: C = 1: 8, N: O = 1: 2 and C: O = 1:4. Our main focus in this EDX result is the ratio N: O = 1:2 which therefore confirms that NDI was really synthesized.

4.3.6 XRD of NDI

Figure 4.30 below presents the diffraction pattern of NDI which shows and therefore confirms that the synthesized acceptor has a highly crystalline pattern as it was expected based on the HRSEM images.

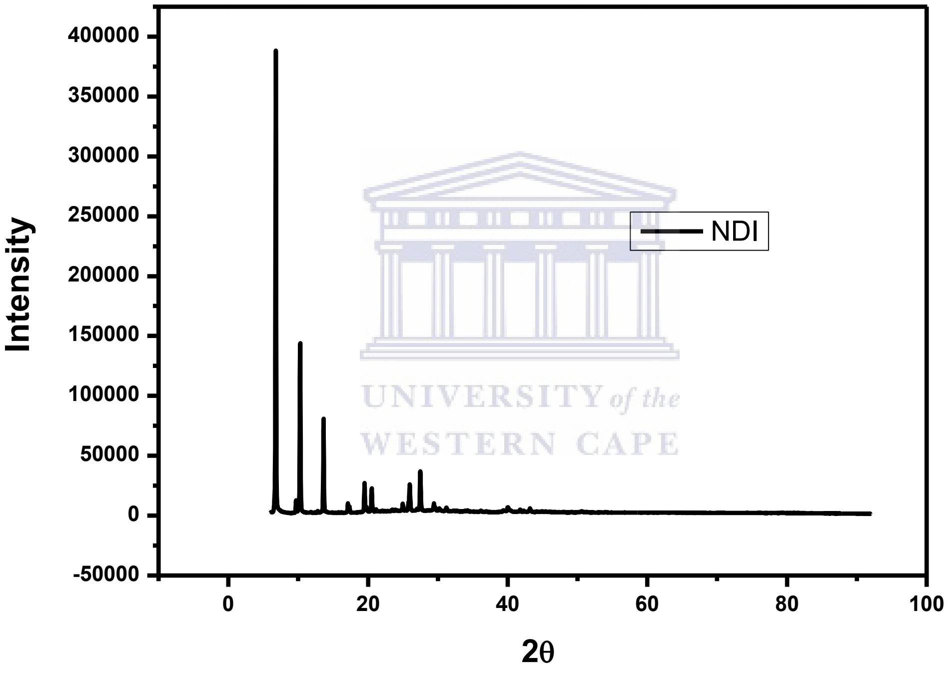

Figure 4.30: *Diffraction Pattern of NDI*

CHAPTER FIVE

Organic Bulk Heterojunction Cell Photovoltaic Properties

5.1 UV-Vis Properties of the BHJ layer: G1PPT-co-PEDOT:NDI

Figure below illustrates the UV-Vis absorption spectra of the blended organic bulk heterojunction active layer G1PPT-co-PEDOT:NDI at different ratios. As the ratio of the blend was going from 1:1 to 1:4, the absorption properties of NDI is increasing as a result of an increase of the NDI volume content in the blend. But it was observed that the absorbance of the donor G1PPT-co-PEDOT was instead decreasing from ratio 1:1 to ratio 1:3 and at ratio 1:4 the absorbance is higher.

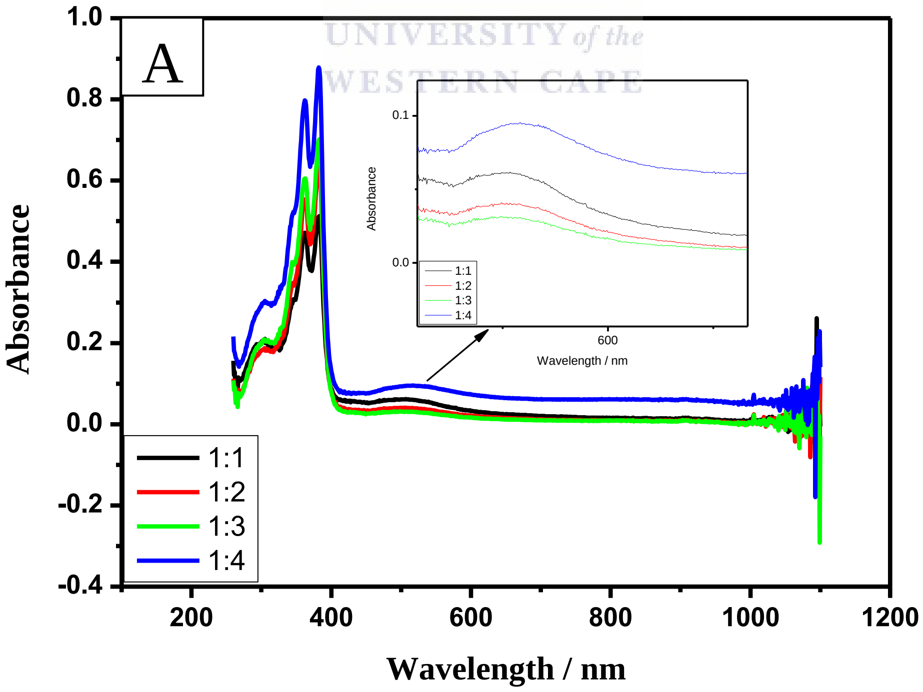

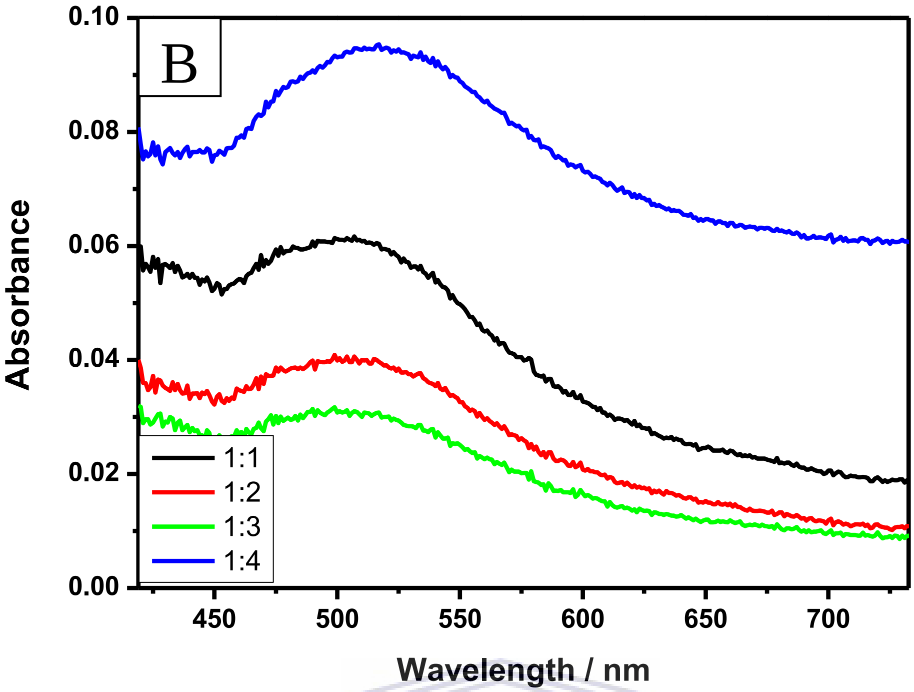

Figure 5.1: *UV-Vis Spectra of (A) BHJ Donor-Acceptor layer at different ratios (B) donor component part of Donor-Acceptor layer at different ratios*

5.2 Fluorescence properties of the BHJ layer: G1PPT-co-PEDOT:NDI

Fluorescence is the emission of light as a result of the relapse of one or more electrons from their excited state back to the ground state. When G1PPT-co-PEDOT was excited at 480 nm, an emission at 593 nm was observed with a very intense peak. But, when the same concentration of the blend acceptor- donor, G1PPT-co-PEDOT:NDI was excited at the same wavelength, approximately 35% quenching in emission peak height intensity of G1PPT-co-PEDOT was observed (Figure 5.2). This could be explained by the fact that in the mixture acceptor – donor, there is an electron-transfer occurring from the donor to the acceptor; as a result, there are fewer electrons available in the donor to relapse from excited state to ground state. This therefore confirms that G1PPT-co-PEDOT acts as the electron donor and NDI as an electron acceptor.

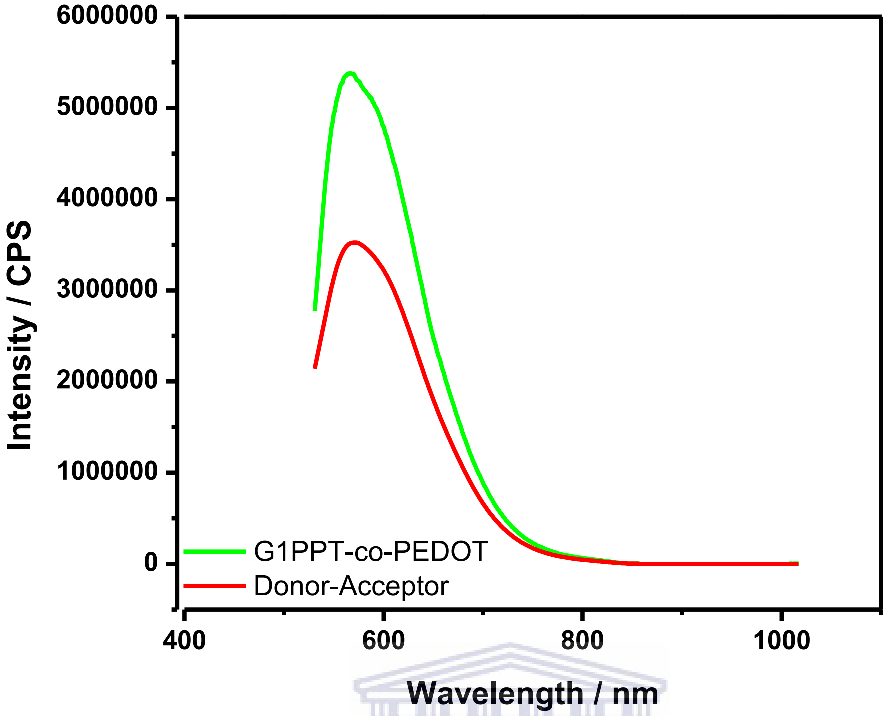

***Figure 5.2**: Fluorescence spectra of G1PPT-co-PEDOT and Donor-Acceptor*

Similarly, the different ratios of blend were excited at the same wavelength and it was observed that there is about 82% quenching in emission peak intensity from ratio 1:1 to ratio1:4 (Figure 5.3). This was highly expected because from ratio 1:1 to ratio 1:4 the amount of acceptor NDI is increasing therefore implying that more electrons can be accepted from the donor. This thus shows that the ratio 1:4 will provide the best organic bulk heterojunction active layer.

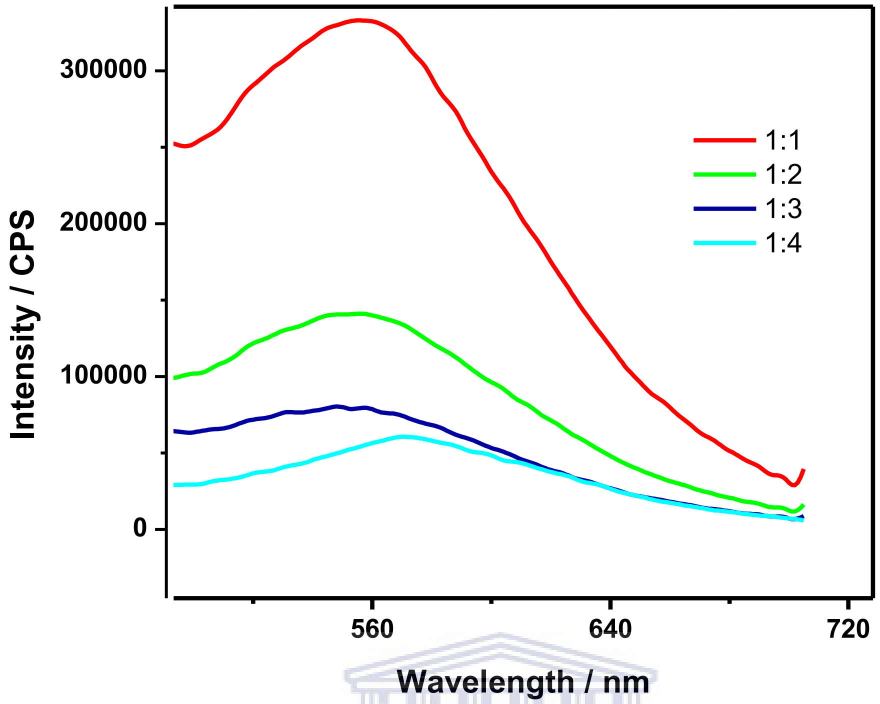

Figure 5.3: *Emission spectra of different ratio of blend donor-acceptor*

5.3 Energy diagram of G1PPT-co-PEDOT:NDI

Based on the data obtained from the UV-Vis spectra and cyclic voltammetry analyses of G1PPT-co-PEDOT and NDI, the HOMO, LUMO and energy bang gap E_g of each donor and acceptor material were determined. From these values the energy diagram (Figure 5.4) was designed. From the diagram the energy separation, ΔE_g between the HOMO of the donor and the LUMO of the acceptor was calculated to be 1.985 eV and the offset between the LUMO of the donor and the LUMO of the acceptor is 0.3 eV which is the ideal offset energy difference between an acceptor and a donor.

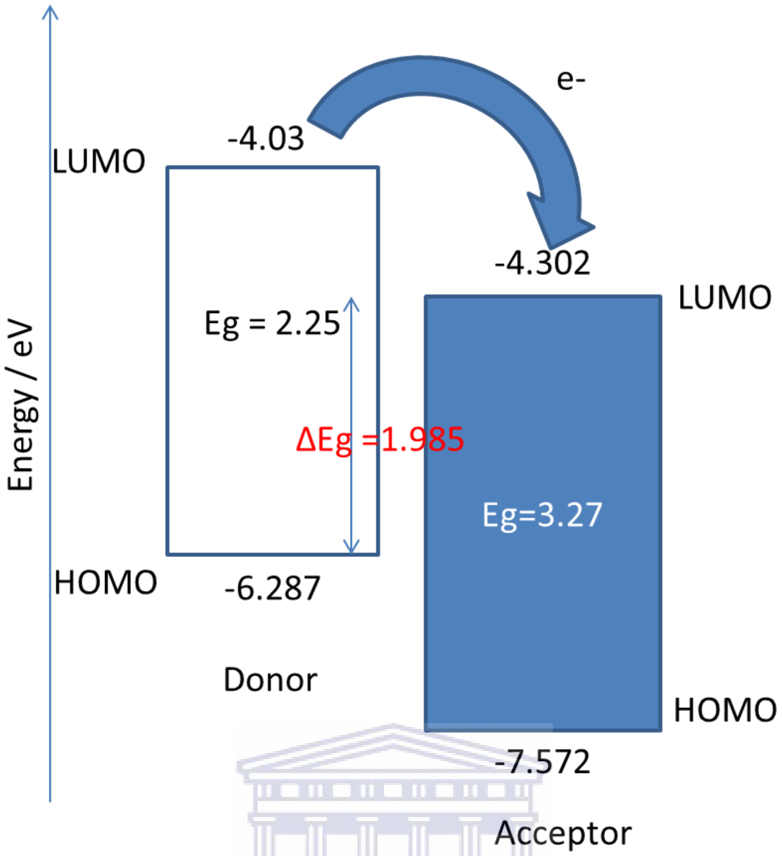

Figure 5.4: *Energy diagram of donor G1PPT-co-PEDOT and acceptor NDI*

CHAPTER SIX

Conclusion and Recommendations

6.1 Conclusion

In this study we explored the potential application of a newly developed organic bulk heterojunction active layer into solar energy conversion based on cyclic voltammetry and UV-Vis spectroscopy. Both donor, G1PPT-co-PEDOT and acceptor, NDI materials were successfully chemically synthesized via condensation reactions. Synthesis of G1PPT-co-PEDOT started by the functionalization of the stating material generation 1 poly(propyleneimine) tetramine dendrimer G1PPI into generation 1 poly(propylenethiophenoimine), G1PPT by reacting 0.3863 g (1.2205 mmol) of G1PPI with 472.55 µL (4.8821 mmol) of 2-thiophene carbaldehyde in methanol for 48 hours under N_2 gas; followed by the copolymerization of G1PPT with ethylenedioxythiophene (EDOT) monomer. This was done by mixing 495 mg (0.71424 mmol) of G1PPT with 318 µL (2.8570 mmol) of the monomer EDOT in 10 mL of chloroform and in the presence of 29.75 mL of 0.1 M $(NH_4)_2S_2O_8$ as oxidant and the mixture was allowed to stir for 2 hours at room temperature. The synthesis of these two materials was thus confirmed by means of FT-IR spectroscopy, UV-Vis spectroscopy and EDX techniques. HRSEM and XRD analyses enable us to study the morphology and the crystallinity of the prepared materials respectively and showed that G1PPT-co-PEDOT is characterized by globular shapes with PEDOT growing out of the dendrimer structure and is amorphous in nature whereas the acceptor material is characterized by highly pure yellow canary-like needles which are strongly crystalline.

On the other hand based on the cyclic voltammetry and UV-Vis spectroscopy results, HOMO, LUMO and energy band gaps E_g of both donor and acceptor materials were found to be -4.031, -6.287 and 2.256 eV for the donor and -4.302, -7.572 and 3.27 eV for the acceptor respectively. These values allow us to draw the BHJ layer energy diagram and the energy separation, ΔE_g between the HOMO of the donor and the LUMO of the acceptor was calculated to be 1.985 eV and the offset between the LUMO of the donor and the LUMO of the acceptor is 0.3 eV which is the ideal offset energy difference between an acceptor and a donor. Finally, the studies of the fluorescence properties of the fabricated organic bulk heterojunction blend G1PPT-co-PEDOT:NDI revealed that there was a quenching in its emission peak intensity relative to the emission peak intensity of the donor G1PPT-co-PEDOT alone. It therefore shows that there was an electron charge transfer from the donor G1PPT-co-PEDOT to the acceptor NDI. Also, blending of the organic BHJ at different ratio of donor to acceptor volume, revealed that the higher is the OBHJ content in acceptor material, the more will be the fluorescent quenching; thus the higher is the number of electrons transferred from the donor to the acceptor. This leads us to the conclusion that an organic bulk heterojunction layer based on a blend of G1PPT-co-PEDOT with NDI could be a suitable active layer for application in OPVs.

6.2 Recommendations

Future work with respect to this project will include:

- Study conductivity properties of both donor and acceptor materials.
- Investigation of the power conversion efficiency.

BIBIOGRAPHY

Ahmed, A.; Ren, G.; Kim, F.S.; Hollenbeck, E.C.; Jenekhe, S.A. Design of New Electron Acceptor Materials for Organic Photovoltaics: Synthesis, Electron Transport,Photophysics, and Photovoltaic Properties of Oligothiophene-Functionalized Naphthalene Diimides. Chemistry of Materials 2011, 23, 4563–4577.

Akcelrud, L. Electroluminescent polymers. *Journal of Progress in Polymer Sciences* 2003, 28, 875-962.

Andric, G.; Boas, J. F.; Bond, A.M.; Fallon, G.D.; Ghiggino, K.P.; Hogan, C.F.; Hutchison, J.A.; Lee, M.A.-P.; Langford, S.J.; Pilbrow, J.R.; Troup, G.J.; Woodward C.P. Spectroscopy of naphthalene diimides and their anion radicals. *Australian Journal of chemistry* 2004, 57, 1011–1019.

Anthopoulos, T.D.; Markham, J.P.J.; Namdas, E.B.; Samuel, D.W.; Lo, S.-C.; Burn, P.L. Highly efficient single-layer dendrimer light-emitting diodes with balanced charge transport. *Applied Physics Letters* 2003, 82, 4824.

Assender, H.; Brakhouse, A. Photovoltaic Polymer Materials. *Photochemistry and Photophysics of Polymer Materials*, Edited by Norman S. Allen 2010, John Wiley & Sons, Inc. 271-307. Online October 2013

Bernède, J.C.; Godoy, A.; Cattin, L.; Diaz, F.R.; Morsli, M.; del Valle, M.A. Organic Solar Cells Performances Improvement Induced by Interface Buffer Layers. *Solar energy*. Edited by Radu D. Rugescu, INTECH, Croatia, February 2010, 223-266. ISBN: 978-953-307-052-0, InTech, Available from: http://www.intechopen.com/books/solar-energy/organic-solarcells- Online March 2013.

Bhosale, S.V.; Jani, C.H.; Langford, S.J. Chemistry of Naphthalene diimides. *Chemistry Society Review* 2008, 37, 331-342.

Brabec, C.J. Organic photovoltaics: technology and market. *Solar Energy Materials & Solar Cells* 2004, 83, 273-292.

Brennan, J.F.; Romwr T.J.; Lees, R.S.; Tercyak, A.M.; Kramer, J.R.; Feld M.S. Determination of human coronary artery composition by Raman spectroscopy. *Circulation* 1997, 96, 99-105.

Chamberlain, G.A. Organic solar cells: A review. *Solar Cells* 1983, 8, 47–83.

Chen, L.-M.; Hong, Z.; Li, G.; Yang, Y. Recent Progress in Polymer Solar Cells: Manipulation of Polymer: Fullerene Morphology and the Formation of Efficient Inverted Polymer Solar Cells. *Advanced Materials* 2009, 21, 1434-1449.

Dimitrakopoulos, C.D. and Mascaro, D.J. Organic thin-film transistors: A review of recent advances. *IBM Journal of Research and Development* 2001, 45, 11–27.

Dong, B.; Xu, J.; Zheng, L.; Hou, J. Electrodeposition of conductive poly(3-methoxythiophene) in ionic liquid microemulsions. *Journal of Electroanalytical Chemistry* 2009, 628, 60-66.

Erten, S.; Posokhov, Y.; Alp, S. The study of the solubility of naphthalene diimides with various bulky flanking substituents in different solvents by UV–vis spectroscopy. *Dyes and Pigments* 2005, 64, 171–178.

Fallon, G.D.; Lee, M.A.-P.; Langford S.J.; Nichols, P.J. *Organic Letters* 2004, 6, 655–658.

Forrest, R.S. The limits to organic photovoltaic cell efficiency. *Materials Research bulletin* 2005, 28-32.

Green, M. A.; Emery, K.; King D. L.; Hishikawa, Y. and Warta, W. Solar cell efficiency tables (Version 28). *Progress in Photovoltaics*: *Research and Application* 2006, 14, 455-461.

Green, M.A.; Emery, K.; Hishikawa, Y.; Warta, W. Solar cell efficiency tables (Version 35). *Progress in Photovoltaics: Research and Applications* 2010, 18, 144-150.

Gregg, B.A. and. Hanna, M.C. Comparing organic to inorganic photovoltaic cells: Theory, experiment, and simulation. *Journal of Applied Physical* 2003, 93, 3605–3614.

Gregg, B.A. Excitonic solar cells. *Journal of Physical Chemistry* B 2003, 107, 4688-4698.

Guinier, A. *X-Ray Diffraction: In Crystals, Imperfect Crystals, and Amorphous Bodies.* Canada Ltd, 1994.

Gunes, S.; Neugebauer, H. Sariciftci, N.S. Conjugated polymer-based organic solar cells. *Chemical Reviews* 2007, 107, 1324-1338.

Hallam, S. Infrared Absorption Spectroscopy - Theoretical Principles. University Biosciences Online Learning, 2010. May 25, 2013.

http://teaching.shu.ac.uk/hwb/chemistry/tutorials/molspec/irspec1.htm.

Hansen, J. G.; Feeder, N.; Hailton, D. G.; Gunter, M. J.; Becherand, J.; Sanders, J. K. M. Macrocyclization and Molecular Interlocking via Mitsunobu Alkylation: Highlighting the Role of C−H···O Interactions in Templating. *Organic Letters* 2000, 2, 449–452.

Haugeneder, A.; Neges, M.; Kallinger, C.; Spirkl, W.; Lemmer, U.; Feldmann, J.; Scherf, U.; Harth, E.; Gügel, A. and Müllen, K. Exciton diffusion and dissociation in conjugated polymer/fullerene blends and heterostructures. *Physical Review* B 1999, 15346–15351.

Hoppe, H. and Sariciftci, N. S. Morphology of polymer/fullerene bulk heterojunction solar cells. *Journal of Material Chemistry* 2006, 16, 45-61.

Hoppe, H. and Sariciftci, N.S. Organic solar cells: An overview. *Journal of Materials Research* 2004, 19, 1924–1945.

Hummelen, J. C.; Knight, B. W.; LePeq, F.; Wudl, F.; Yao, J.; Wilkins, C. L. Preparation and Characterization of Fulleroid and Methanofullerene Derivatives. *Jounal of Organic Chemistry* 1995, 60, 532-538.

Hünig, S.; Grob, J.; Lier E.F.; Quast, H. Liebigs Annalen der Chemie 1973, 339–358.

Katz, H.E.; Lovinger, A.J.; Kloc, C.; Siegrist, T.; Li, W.; Lin, Y.-Y.; Dodabalapur, A. A soluble and air-stable organic semiconductor with high electron mobility. *Nature* 2000, 404, 478–481.

Kerp, H.R.; Donker, H.; Koehorst, R.B.M.; Schaafsma, T.J. and van Faassen, E.E. Exciton transport in organic dye layers for photovoltaic applications. *Chemical Physics Letters* 1998, 298, 302-308.

Kim, M.-S. Understanding Organic Photovoltaic Cells: Electrode, Nanostructure, Reliability, and Performance. *A dissertation submitted in partial fulfillment of the requirements for the degree of Doctor of Philosophy (Materials Science and Engineering)* 2009. Online, 22 March 2013.

Kittel, C. Introduction to Solid State Physics. Eighth Edition, John Wiley & Sons Ltd., Chichester, 2005.

Knupfer, M. Exciton binding energies in organic semiconductors. *Journal of Applied Physics A: Material Sciences & Processing* 2003, 77, 623-626.

Kopidakis,N.; Mitchell, W. J.; van de Lagemaat, J.; Ginley, D. S.; Rumbles, G.; Shaheenb, S. E. Bulk heterojunction organic photovoltaic devices using dendrimers. National Renewable Energy Laboratories 2005. Online March 2013.

Kopidakis,N.; Mitchell, W. J.; van de Lagemaat, J.; Ginley, D.S.; Rumbles, G.; Shaheenb, S.E. Bulk heterojunction organic photovoltaic devices based on phenyl-cored thiophene dendrimers. Applied Physics Letters 2006, 89, 103524-1 – 103524-3.

Li, G.; Shrotriya, V.; Huang, J.S.; Yao, Y.; Moriarty, T.; Emery, K. and Yang, Y. High-efficiency solution processable polymer photovoltaic cells by self-organization of polymer blends. *Nature Materials* 2005, 4, 864-868.

Lichtman, J.W.; Conchello, J.A. Fluorescence microscopy. *Nature Methods* 2005, 2, 910 - 919.

Lyman, C.E.; Newbury, D.E.; Goldstein, J.I.; Williams, D.B.; Romig, A.D.J.; Armstrong, J.T.; Echlin P.; Fiori C.E.; Joy D.C.; Lifshin, E.; Peters K. Scanning Electron Microscopy, X-Ray Microanalysis and Analytical Electron Microscopy. A Laboratory Workbook, *Plenum Press*: New York, 1990

Marks, R.N.; Halls, J.J.M.; Bradley, D.D.C.; Friend, R.H.; Holmes, A.B. The photovoltaic response in poly(p-phenylene vinylene) thin-film devices. *Journal of Physics: Condensed Matter* 1994, 6, 1379 – 1394.

Miller, L.L.; Duan, R.G.; Tully, D.C.; Tomalia, D.A. Electrically conducting polymers. *Journal of the American Chemistry Society* 1997, 119, 1005-1010.

Mozer, A.; Sariciftci, N.S. Conjugated polymer photovoltaic devices and materials. *Chimie* 2006, 9, 568-577.

Mukhopadhyay, P.; Iwashita, Y.; Shirakawa, M.; Kawano, S.; Fujita N.; Shinkai, S. Spontaneous Colorimetric Sensing of the Positional Isomers of Dihydroxynaphthalene in a 1D Organogel Matrix. *Journal of Angewandte. Chemie – International Edition* 2006, 45, 1592–1595.

Nalwa, H.S. Handbook of Organic Electronics and Photonics. *American Scientific Publishers* 2008, Valencia, CA.

Olowu, R. A.; Ndangili, P. M.; Baleg, A. A.; Ikpo, C. O.; Njomo, N.; Baker, P.; Iwuoha, E. Spectroelectrochemical Dynamics of Dendritic Poly (Propylene imine)-Polythiophene Star Copolymer Aptameric 17β-Estradiol Biosensor. *International Journal of Electrochemical Science* 2011, 6. 1686 – 1708.

Onsager, L. Initial recombination of ions. *Physical Review* 1938, 54, 554-557.

Padinger, F.; Rittberger, R.S.; Sariciftci, N.S. Effects of postproduction treatment on plastic solar cells. *Journal of Advanced Functional Materials* 2003, 13, 85-88.

Park, S.H.; Roy, A.; Beaupre, S.; Cho, S.; Coates, N.; Moon, J.S.; Moses, D.; Leclerc, M.; Lee, K.; Heeger, A.J. Bulk heterojunction solar cells with internal quantum efficiency approaching 100%. *Nature Photonics* 2009, 3, 297-303.

Peumans, P.; Yakimov, A. and Forrest, S.R. Small molecular weight organic thin-film photodetectors and solar cells. *Journal of Applied Physics* 2003, 93, 3693–3723.

Priceton Instruments. Raman spectroscopy basics. www.piacton.com. Online March 16, 2013

Primary Photoexcitations in Conjugated Polymers: Molecular Exciton versus Semiconductor Band Model; edited by Sariciftci, N.S. *World Scientific Publishing Company* 1997, Singapore.

Reese, M.O.; Nardes, A.M.; Rupert, B.L.; Larsen, R.E.; Olson, D.C.; Lloyd, M.T.; Shaheen, S.E.; Ginley, D.S.; Rumbles, G.; Kopidakis, N. Photoinduced Degradation of Polymer and Polymer–Fullerene Active Layers: Experiment and Theory. *Journal of Advanced Functional Materials* 2010, 20, 3476-3483.

Roncali, J. Conjugated poly(thiophenes): synthesis, functionalization and applications. *Chemical Reviews* 1992, 92, 711-738.

Savanije, T.J.; Warman, J.M.; Goossens A. Visible light sensitisation of titanium dioxide using a phenylenevinylene polymer. *Chemical Physical Letters* 1998, 287, 148.

Shafiee, S.; Topal E. When will fossil fuel reserves be diminished? *Energy Policy 2009*, 37, 181–189.

Shaheen, S.E.; Brabec, C.J.; Sariciftci, N.S; Padinger, F.; Fromherz, T. and Hummelen, J.C. 2.5% efficient organic plastic solar cells. *Applied Physics Letters* 2001, 78, 841-843.

Shinar, R.; Shinar, J. Organic Electronics in Sensors and Biotechnology. McGraw-Hill 2009, New York.

Shirakawa, H. Die Entdeckung der Polyacetylenefilme – der Beginn des Zeitalters leitfähiger Polymere (Nobel – Aufsatz). Angew. Chem. 2001, 113, 2642-2628.

Snaith, H.J.; Gratzel, M. Enhanced charge mobility in a molecular hole transporter via addition of redox inactive ionic dopant: Implication to dye-sensitized solar cells. *Applied Physics Letters* 2006, 89, 262114 - 262114-3.

Sonar, P.; Lim, J.P.F.; Chan, K.L. Organic non-fullerene acceptors for organic photovoltaics. *Journal of Energy Environmental Sciences* 2011, 4, 1558-1574

Spanggaard, H; Krebs, F.C. A brief history of the Development of Organic and Polymeric Photovoltaics. *Solar Energy Materials & Solar Cells* 2004, 83, 125–146

Stewart, W.W. Lucifer dyes—highly fluorescent dyes for biological tracing. *Nature* 1981, 292, 17–21.

Tang, C.W. 2-Layer Organic Photovoltaic Cell. *Applied Physical Letters* 1986, 48, 183-185.

Taylor, D.L.; Salmon, E.D., Basic fluorescence microscopy, in Methods in Cell Biology: Living Cell in Culture. Edited by J. L. Wang and D. L. Taylor. *Academic Press:* San Diego, California, USA. 1989, 207–237.

Thompson, B.C. and Frechet, J.M. Polymer–Fullerene Composite Solar Cells. *Journal of Angewandte Chemie - International Edition* 2008, 47, 58-77.

Weisstein, E.W., Math World: Fraunhofer Diffraction. http://scienceworld.wolfram.com/physics/FraunhoferDiffraction.html URL, 2005.

Wienk, M.M.; Kroon, J.M.; Verhees, W.J.; Knol, J.J.; Hummelen, C.; Hal, P.A.; Janssen, R.A. Efficient methano[70]fullerene/MDMO-PPV bulk heterojunction photovoltaic cells. *Journal of Angewandte Chemie - International Edition*. 2003, 42, 3371-3375.

Wöhrle, D. and Meissner, D. Organic solar cells. *Advanced Materials* 1991, 3, 129-138.

Wudl, F. The chemical properties of buckminsterfullerene (C_{60}) and the birth and infancy of fulleroids. *Accounts of Chemical Research* 1992, 25, 157-161.

Wurthner, F.; Ahmed, S.; Thalacker, C.; De baerdemaeker, T. Core-Substituted Naphthalene Bisimides: New Fluorophors with Tunable Emission Wavelength for FRET Studies. *Chemistry–A European Journal* 2002, 8, 4742–4750.

Yang, X.N.; Loos, J.; Veenstra, S.C.; Verhees, W.J.H.; Wienk, M.M.; Kroon, J.M.; Michels, M.A.J. and Janssen, R.A.J. Nanoscale Morphology of High-Performance Polymer Solar Cells. *Nano Letters* 2005, 5, 579-583.

Yu, G.; Wang, J.; McElvain, J.; Heeger, A.J. (). Large-area, full-color image sensors made with semiconducting polymers. *Journal of Advanced Materials* 1998, 10, 1431-1434.

Yuan, Zh.; Li, J.; Xiao, Y.; Li, Zh.; Qian, X. Core-Perfluoroalkylated Perylene Diimides and Naphthalene Diimides: Versatile Synthesis, Solubility, Electrochemistry, and Optical Properties. *Journal of Organic Chemistry* 2010, 75, 3007-3016.

Yumusak, C.; Egbe, D.A.M. Organic Bulk Heterojunction Solar Cells Based on Poly(p-Phenylene-Vinylene) Derivatives. *Solar Cells – New Aspects and Solutions 2011*. Edited by Prof. Leonid A. Kosyachenko. ISBN 978-953-307-761-1. Available from:

http://cdn.intechopen.com/pdfs/22574/InTech-Organic_bulk_heterojunction_solar_cells_based_on_poly_p_phenylene_vinylene_derivatives.pdf